

University of Windsor

## Scholarship at UWindor

---

Electronic Theses and Dissertations

Theses, Dissertations, and Major Papers

---

2009

# Smooth and Rough Wall Open Channel Flow Including Effects of Seepage and Ice Cover

Md. Abdullah Al Faruque  
*University of Windsor*

Follow this and additional works at: <https://scholar.uwindsor.ca/etd>

---

### Recommended Citation

Faruque, Md. Abdullah Al, "Smooth and Rough Wall Open Channel Flow Including Effects of Seepage and Ice Cover" (2009). *Electronic Theses and Dissertations*. 403.  
<https://scholar.uwindsor.ca/etd/403>

This online database contains the full-text of PhD dissertations and Masters' theses of University of Windsor students from 1954 forward. These documents are made available for personal study and research purposes only, in accordance with the Canadian Copyright Act and the Creative Commons license—CC BY-NC-ND (Attribution, Non-Commercial, No Derivative Works). Under this license, works must always be attributed to the copyright holder (original author), cannot be used for any commercial purposes, and may not be altered. Any other use would require the permission of the copyright holder. Students may inquire about withdrawing their dissertation and/or thesis from this database. For additional inquiries, please contact the repository administrator via email ([scholarship@uwindsor.ca](mailto:scholarship@uwindsor.ca)) or by telephone at 519-253-3000ext. 3208.

**SMOOTH AND ROUGH WALL OPEN CHANNEL FLOW INCLUDING  
EFFECTS OF SEEPAGE AND ICE COVER**

**By**

**Md Abdullah Al Faruque**

**A Dissertation**

**Submitted to the Faculty of Graduate Studies**

**through the Department of Civil and Environmental Engineering**

**in Partial Fulfillment of the Requirements for**

**the Degree of Doctor of Philosophy at the**

**University of Windsor**

**Windsor, Ontario, Canada**

**2009**

**© 2009 Md Abdullah Al Faruque**

Smooth and Rough Wall Open Channel Flow Including Effects of Seepage and Ice Cover

by

Md Abdullah Al Faruque

APPROVED BY:

---

Dr. Amruthur S. Ramamurthy, External Examiner  
Concordia University

---

Dr. Gary Rankin  
Department of Mechanical Automotive & Mechanical Engineering

---

Dr. Niharendu Biswas  
Department of Civil and Environment Engineering

---

Dr. Rupp Carriveau  
Department of Civil and Environment Engineering

---

Dr. Ramaswami Balachandar, Advisor  
Department of Civil and Environment Engineering

---

Dr. Kemal Tepe, Chair of Defense  
Department of Electrical and Computer Engineering

14 August 2009

## **Author's Declaration of Originality**

I hereby certify that I am the sole author of this thesis and that no part of this thesis has been published or submitted for publication.

I certify that, to the best of my knowledge, my thesis does not infringe upon anyone's copyright nor violate any proprietary rights and that any ideas, techniques, quotations, or any other material from the work of other people included in my thesis, published or otherwise, are fully acknowledged in accordance with the standard referencing practices.

I declare that this is a true copy of my thesis, including any final revisions, as approved by my thesis committee and the Graduate Studies office, and that this thesis has not been submitted for a higher degree to any other University or Institution.

## **PERMISSION TO USE**

The author has permission to the University of Windsor Library to make this dissertation available for inspection due to scholarly research. The author has also agreed that permission of copying this dissertation for scholarly purpose can be granted by the supervising professor (Dr. Ram Balachandar) or, in his absence, by the head of the Department of Civil and Environment Engineering or the Dean of the Faculty of Engineering. Copying or publishing or use of this dissertation for any financial gain without the written permission of the Author is strictly prohibited. Due recognition to the author and the University of Windsor must be granted for any scholarly use of the material in the dissertation.

In order to copy or to make any use of the material in the dissertation, request must be made to the following address:

The Head  
Department of Civil and Environment Engineering  
University of Windsor  
401 Sunset Ave.  
Windsor, Ontario  
Canada N9B 3P4

## ABSTRACT

A comprehensive study was carried out to understand the effects of roughness, seepage and ice cover on the turbulence characteristics of flow in an open channel. To this end, tests were conducted with four different types of bed surface conditions. This includes the use of an impermeable smooth bed, impermeable rough bed, permeable sand bed and an impermeable bed with distributed roughness. Both suction and injection seepage tests were conducted covering a range of seepage rates. For the ice cover tests, two different cover conditions were used. The tests were conducted at two different Reynolds number ( $R_e = 47,500$  and  $31,000$ ).

The effect of bed roughness on the turbulence characteristics is seen to have penetrated through most of the flow depth, disputing the ‘wall similarity hypothesis’ initially proposed by Townsend (1976). The results show that the distributed roughness shows the greatest roughness effect. Although the same sand grain is used to create the different rough bed conditions, there are differences in turbulence characteristics, which is an indication that specific geometry of the roughness has an influence. Roughness increases the contribution of the extreme turbulent events which produces very large instantaneous Reynolds shear stress and can potentially influence the sediment transport, resuspension of pollutant from the bed and alter the nutrient composition, which eventually affects the sustainability of benthic organisms.

For the tests with seepage, injection increases the magnitude of the various turbulent characteristics and suction reduces the values in comparison to no-seepage condition. Effect of seepage on different turbulent characteristics is not restricted to the near-bed region but can be seen through out the flow depth. The results from the analysis

of turbulent bursting events clearly show a distinct effect of seepage well beyond the near-bed region.

The introduction of ice cover causes a change in mean velocity profile and increases total resistance of the channel. The magnitude of this change depends on both the bed and the cover roughness. The change in turbulent characteristics seems to be bound to the upper half of the flow and the changes can be significant with the rougher cover.

## **DEDICATION**

*This thesis is dedicated to ALLAH, All Mighty and Merciful.*

**Dedication also goes to my advisor, Dr. Ram Balachandar.**

**To my love “LUNA”**



## **ACKNOWLEDGEMENT**

I would like to extend my heartfelt appreciation to my advisor and mentor Dr. Ram Balachandar for his thoughtful advice, best guidance, inspiration, constant supervision and innovative ideas. Sincere thanks to your family for extensive love and support to my family.

I would like to extend my thanks to my advisory committee members: Dr. Nihar Biswas, Dr. Gary Rankin and Dr. Rupp Carriveau for their useful suggestions, careful review. I would also like to thank my external examiner Dr. A. S. Ramamurthy for his useful suggestions and comments.

My sincere thanks to Mr. Lucian Pop, Mr. Matt Louis and Late Mr. Richard Clark for their enthusiastic support and service to make, maintain and frequent modification of the experimental setup.

Sincere appreciation to all of the financial supports received from Natural sciences and engineering research council (NSERC), Ontario graduate scholarship in science and technology (OGSST) and University of Windsor Graduate scholarship.

Acknowledgement is undone without recognizing the contribution of my caring wife and mother-in-law to take care of my family and allowing me to make this program a success.

## TABLE OF CONTENTS

AUTHOR’S DECLARATION OF ORIGINALITY	iii
PERMISSION TO USE	iv
ABSTRACT	v
DEDICATION	vii
ACKNOWLEDGEMENTS	viii
LIST OF TABLES	xiii
LIST OF FIGURES	xiv
NOMENCLATURE	xxiv
1. INTRODUCTION	
1.1 Open Channel Flow	1
1.2 Effect of Seepage	2
1.3 Effect of Ice Cover	3
1.4 Objective and Scope	
1.4.1 Objectives	4
1.4.2 Scope	4
2. LITERATURE REVIEW	6
2.1 Open Channel Flow: Effect of Roughness	6
2.2 Effect of Seepage	9
2.2.1 Effect of Seepage on Bed Stability	10
2.2.2 Effect of Seepage on Bed Shear Stress	11

2.2.3	Effect of Seepage on Velocity Profile	13
2.2.4	Effect of Seepage on Turbulence Distribution	14
2.3	Effect of ice cover	16
2.4	Refinement in Objectives	22
3.	EXPERIMENTAL SETUP	
3.1	Open Channel Flume	24
3.2	Test Conditions to Study the Effect of Roughness	24
3.3	Test Conditions with the Introduction of Seepage	26
3.4	Test Conditions with Ice Cover	27
3.5	The Laser Doppler Anemometry	28
4.	ROUGHNESS EFFECTS ON TURBULENCE CHARACTERISTICS	35
4.1	Mean Velocity Profiles	
4.1.1	Outer Coordinates	35
4.1.2	Inner Coordinates	36
4.2	Turbulence Intensity	
4.2.1	Streamwise Turbulence Intensity	37
4.2.2	Vertical Turbulence Intensity	39
4.3	Reynolds Shear Stress	39
4.4	Shear Stress Correlation Coefficient	40
4.5	Higher-Order Moments	41
4.6	Vertical Flux of the Turbulent Kinetic Energy	45
4.7	Quadrant Analysis	46
4.8	Conclusions	50

5	SEEPAGE EFFECTS IN OPEN CHANNEL FLOW	67
5.1	Mean Velocity Profiles	
5.1.1	Outer Coordinates	67
5.1.2	Inner Coordinates	69
5.2	Bed Stability	69
5.3	Turbulence Intensity	
5.3.1	Streamwise Turbulence Intensity	71
5.3.2	Vertical Turbulence Intensity	72
5.4	Reynolds Shear Stress	72
5.5	Shear Stress Correlation Coefficient	73
5.6	Higher-Order Moments	73
5.7	Quadrant Analysis	76
5.8	Conclusions	79
6	ICE COVERED OPEN CHANNEL FLOW	104
6.1	Mean Velocity Profiles	
6.1.1	Outer Coordinates	104
6.1.2	Inner Coordinates	105
6.2	Turbulence Intensity	
6.2.1	Streamwise Turbulence Intensity	106
6.2.2	Vertical Turbulence Intensity	107
6.3	Reynolds Shear Stress	108
6.4	Conclusions	108
7	MAJOR CONCLUSIONS AND FUTURE RECOMMENDATIONS	133

REFERENCES	136
APPENDIX A: UNCERTAINTY ESTIMATES	144
VITA AUCTORIS	147

## LIST OF TABLES

Table 2.1:	Summary of results of previous seepage studies	23
Table 3.1:	Gradation measurements of the sand	29
Table 3.2:	Summary of test conditions to study the effect of roughness	29
Table 3.3:	Summary of test conditions with the introduction of seepage	30
Table 3.4:	Summary of test conditions with ice cover	31
Table 5.1:	Comparison of percentage change of near bed velocity and friction velocity	81
Table A.1:	Uncertainty estimates for tests over smooth bed	145
Table A.2:	Uncertainty estimates for tests over distributed roughness bed	145
Table A.3:	Uncertainty estimates for tests over continuous roughness bed	146
Table A.4:	Uncertainty estimates for tests over natural sand bed	146

## LIST OF FIGURES

Figure 3.1:	Schematic of the open channel flume and experimental setup	32
Figure 3.2:	Plan view of different fixed bed condition	32
Figure 3.3:	Section of natural sand bed	33
Figure 3.4:	Schematic of seepage zone setup	33
Figure 3.5:	Pictures of seepage console	
	a) Seepage console setup	34
	b) Perforated pipes	34
	c) Filter net	34
	d) Perforated plate	34
Figure 4.1:	Streamwise mean velocity profile for flow over different bed condition	54
Figure 4.2:	Mean velocity profile in inner coordinates for flow over different bed condition	55
Figure 4.3:	Streamwise turbulence intensity for flow over different bed condition	56
Figure 4.4:	Vertical turbulence intensity for flow over different bed condition	57
Figure 4.5:	Reynolds shear stress distribution for flow over different bed condition	58
Figure 4.6:	Distribution of correlation coefficient for flow over different bed condition	59

Figure 4.7:	Distribution of different velocity triple products for flow over different bed condition at $Re \sim 47,500$	60
Figure 4.8:	Distribution of different velocity triple products for flow over different bed condition at $Re \sim 31,000$	61
Figure 4.9:	Distribution of vertical flux of the turbulent kinetic energy for flow over different bed condition	62
Figure 4.10:	Contribution of different quadrant events to the Reynolds shear stress for flow over different bed condition with higher Reynolds number	63
Figure 4.11:	Contribution of different quadrant events to the Reynolds shear stress for flow over different bed condition with lower Reynolds number	64
Figure 4.12:	Ratio of different quadrant events to the Reynolds shear stress for flow over different bed condition	65
Figure 4.13:	Ratio of number of different quadrant events for flow over different bed condition	66
Figure 5.1:	Mean velocity profile in outer coordinates for,	
	a) Injection_450 GPM,	82
	b) Injection_720 GPM,	82
	c) Suction_450 GPM,	83
	d) Suction_720 GPM	83



Figure 5.2:	Mean velocity profile in inner coordinates for,	
	a) Injection_450 GPM,	84
	b) Injection_720 GPM,	84
	c) Suction_450 GPM,	85
	d) Suction_720 GPM.	85
Figure 5.3:	Streamwise turbulence intensity for,	
	a) Injection_450 GPM,	86
	b) Injection_720 GPM,	86
	c) Suction_450 GPM,	87
	d) Suction_720 GPM.	87
Figure 5.4:	Vertical turbulence intensity for,	
	a) Injection_450 GPM,	88
	b) Injection_720 GPM,	88
	c) Suction_450 GPM,	89
	d) Suction_720 GPM.	89
Figure 5.5:	Reynolds shear stress for,	
	a) Injection_450 GPM,	90
	b) Injection_720 GPM,	90
	c) Suction_450 GPM,	91
	d) Suction_720 GPM.	91

Figure 5.6:	Distribution of correlation coefficient for,	
	a) Injection_450 GPM,	92
	b) Injection_720 GPM,	92
	c) Suction_450 GPM,	93
	d) Suction_720 GPM.	93
Figure 5.7:	Distribution of different velocity triple product,	
	a) $u^3$ : Injection_450 GPM,	94
	b) $v^3$ : Injection_450 GPM,	94
	c) $u^3$ : Injection_720 GPM,	94
	d) $v^3$ : Injection_720 GPM	94
Figure 5.8:	Distribution of different velocity triple product,	
	a) $u^3$ : Suction_450 GPM,	95
	b) $v^3$ : Suction_450 GPM,	95
	c) $u^3$ : Suction_720 GPM,	95
	d) $v^3$ : Suction_720 GPM	95
Figure 5.9:	Distribution of different velocity triple product,	
	a) $D_v$ : Injection_450 GPM,	96
	b) $D_u$ : Injection_450 GPM,	96
	c) $D_v$ : Injection_720 GPM,	96
	d) $D_u$ : Injection_720 GPM	96

Figure 5.10:	Distribution of different velocity triple product,	
	a) $D_v$ : Suction_450 GPM,	97
	b) $D_u$ : Suction_450 GPM,	97
	c) $D_v$ : Suction_720 GPM,	97
	d) $D_u$ : Suction_720 GPM	97
Figure 5.11:	Contribution of different quadrant events to the Reynolds stress for lower flow rates and with introduction of injection.	98
Figure 5.12:	Contribution of different quadrant events to the Reynolds stress for higher flow rates and with introduction of injection	99
Figure 5.13:	Contribution of different quadrant events to the Reynolds stress for lower flow rates and with introduction of suction	100
Figure 5.14:	Contribution of different quadrant events to the Reynolds stress for higher flow rates and with introduction of suction	101
Figure 5.15:	Ratio of different quadrant events to the Reynolds stress for different flow rates and with introduction of injection	102
Figure 5.16:	Ratio of different quadrant events to the Reynolds stress for different flow rates and with introduction of suction	103
Figure 6.1:	Mean velocity profile in outer coordinates for flow over,	
	a) Smooth Bed: $Re \sim 47,500$ ,	111
	b) Smooth Bed: $Re \sim 31,000$	111
Figure 6.2:	Mean velocity profile in outer coordinates for flow over,	
	a) Distributed Roughness Bed: $Re \sim 47,500$ ,	112
	b) Distributed Roughness Bed: $Re \sim 31,000$	112

Figure 6.3:	Mean velocity profile in outer coordinates for flow over,	
	a) Continuous Roughness Bed: $R_e \sim 47,500$ ,	113
	b) Continuous Roughness Bed: $R_e \sim 31,000$	113
Figure 6.4:	Mean velocity profile in outer coordinates for flow over,	
	a) Natural Sand Bed: $R_e \sim 47,500$ ,	114
	b) Natural Sand Bed: $R_e \sim 31,000$	114
Figure 6.5:	Mean velocity profile in outer coordinates for flow	
	over different beds with,	
	a) Cover 1: $R_e \sim 47,500$ ,	115
	b) Cover 1: $R_e \sim 31,000$	115
Figure 6.6:	Mean velocity profile in outer coordinates for flow	
	over different beds with,	
	a) Cover 2: $R_e \sim 47,500$ ,	116
	b) Cover 2: $R_e \sim 31,000$	116
Figure 6.7:	Mean velocity profile in inner coordinates with Cover 1	
	and $R_e \sim 47,500$ for flow over,	
	a) Smooth Bed,	117
	b) Distributed Roughness Bed,	117
	c) Continuous Roughness Bed,	117
	d) Natural Sand Bed	117

Figure 6.8:	Mean velocity profile in inner coordinates with Cover 2	
	and $R_e \sim 47,500$ for flow over,	
	a) Smooth Bed,	118
	b) Distributed Roughness Bed,	118
	c) Continuous Roughness Bed,	118
	d) Natural Sand Bed	118

Figure 6.9:	Mean velocity profile in inner coordinates with Cover 1	
	and $R_e \sim 31,000$ for flow over,	
	a) Smooth Bed,	119
	b) Distributed Roughness Bed,	119
	c) Continuous Roughness Bed,	119
	d) Natural Sand Bed	119

Figure 6.10:	Mean velocity profile in inner coordinates with Cover 2	
	and $R_e \sim 31,000$ for flow over,	
	a) Smooth Bed,	120
	b) Distributed Roughness Bed,	120
	c) Continuous Roughness Bed,	120
	d) Natural Sand Bed	120

Figure 6.11:	Streamwise turbulence intensity for different cover conditions and $Re \sim 47,500$ for flow over,	
	a) Smooth Bed,	121
	b) Distributed Roughness Bed,	121
	c) Continuous Roughness Bed,	121
	d) Natural Sand Bed	121
Figure 6.12:	Streamwise turbulence intensity for different cover conditions and $Re \sim 31,000$ for flow over,	
	a) Smooth Bed,	122
	b) Distributed Roughness Bed,	122
	c) Continuous Roughness Bed,	122
	d) Natural Sand Bed	122
Figure 6.13:	Streamwise turbulence intensity for flow over different beds with,	
	a) Cover 1: $Re \sim 47,500$ ,	123
	b) Cover 1: $Re \sim 31,000$	123
Figure 6.14:	Streamwise turbulence intensity for flow over different beds with,	
	a) Cover 2: $Re \sim 47,500$ ,	124
	b) Cover 2: $Re \sim 31,000$	124

Figure 6.15:	Vertical turbulence intensity for different cover conditions and $R_e \sim 47,500$ for flow over,	
	a) Smooth Bed,	125
	b) Distributed Roughness Bed,	125
	c) Continuous Roughness Bed,	125
	d) Natural Sand Bed	125
Figure 6.16:	Vertical turbulence intensity for different cover conditions and $R_e \sim 31,000$ for flow over,	
	a) Smooth Bed,	126
	b) Distributed Roughness Bed,	126
	c) Continuous Roughness Bed,	126
	d) Natural Sand Bed	126
Figure 6.17:	Vertical turbulence intensity for flow over different beds with,	
	a) Cover 1: $R_e \sim 47,500$ ,	127
	b) Cover 1: $R_e \sim 31,000$	127
Figure 6.18:	Vertical turbulence intensity for flow over different beds with,	
	a) Cover 2: $R_e \sim 47,500$ ,	128
	b) Cover 2: $R_e \sim 31,000$	128

Figure 6.19: Reynolds shear stress for different cover conditions and $R_e \sim 47,500$ for flow over,	
a) Smooth Bed,	129
b) Distributed Roughness Bed,	129
c) Continuous Roughness Bed,	129
d) Natural Sand Bed	129

Figure 6.20: Reynolds shear stress for different cover conditions and $R_e \sim 31,000$ for flow over,	
a) Smooth Bed,	130
b) Distributed Roughness Bed,	130
c) Continuous Roughness Bed,	130
d) Natural Sand Bed	130

Figure 6.21: Reynolds shear stress for flow over different beds with,	
a) Cover 1: $R_e \sim 47,500$ ,	131
b) Cover 1: $R_e \sim 31,000$	131

Figure 6.22: Reynolds shear stress for flow over different beds with,	
a) Cover 2: $R_e \sim 47,500$ ,	132
b) Cover 2: $R_e \sim 31,000$	132



## NOMENCLATURE

### ACRONYMS

CFD = Computational Fluid Dynamics

GPM = Gallon per minute

INJ = injection

LDA = Laser Doppler Anemometer

PIV = Particle Image Velocimetry

SUC = Suction

### ENGLISH SYMBOLS

$b$  = width of the flume

$B$  = log-law parameter (= 5.0)

$C_f$  = friction coefficient

$C_z$  = coefficient of curvature

$d$  = depth of flow

$d_{50}$  = median size of sand

$d_N$  = diameter of sand,  $N\%$  of which is finer by weight ( $N = 5, 10, 16, 30, 60, 84, 95$ )

$F_r$  = flow Froude number

$g$  = acceleration due to gravity

$H$  = hole size

$N$  = number of samples

$Q_i$  = Reynolds shear stress contribution from a given quadrant ( $i = 1$  to  $4$ )

$R$  = correlation coefficient

$R_e$  = Reynolds number based on depth of flow

$u$  = streamwise turbulence intensity

$U$  = streamwise component of mean velocity

$U_{avg}$  = average streamwise velocity

$U_e$  = Maximum streamwise velocity

$U_\tau$  = friction velocity

$U^+$  = velocity in inner coordinate (velocity scaled by the friction velocity) =  $U/U_\tau$

$v$  = vertical or wall-normal turbulence intensity

$V$  = vertical component of mean velocity

$y$  = vertical or wall-normal distance

$y^+$  = depth in inner coordinates (or depth scaled by friction velocity) =  $y U_\tau / \nu$ .

## **GREEK SYMBOLS**

$\Delta U^+$  = roughness function

$\kappa$  = Von Karman constant

$\nu$  = kinematic viscosity of the fluid

$\sigma_g$  = geometric standard deviation of sand

$\sigma_o$  = error in beam-crossing angle (percent)

# CHAPTER 1

## INTRODUCTION

### 1.1 Open Channel Flow

Understanding the structure and dynamics of open channel flow which comprises of a sheared boundary layer like flow is of vital importance to the modeling of sediment transport and resuspension, bed formation, entrainment and the exchange of energy and momentum. Processes of special interest within the flow include the horizontal and vertical transfer of energy and momentum by turbulence. For example, in the case of some benthic organisms, nutrition/oxygen utilization rates are known to vary with flow conditions. Increasing current speed enhances transport of phytoplankton due to increased turbulent mixing. Although the mechanisms concerning the above mentioned phenomena have been studied in the past, they are not completely understood. Rashidi et al. (1990) indicate that even average particle volume fractions as low as  $10^{-4}$  lead to a significant modulation of turbulence. The shape, size and arrangement of bed particles also contribute to the modulation of turbulence. In contrast to the vast research on turbulent boundary layer and pipe flow, research in open channel turbulence has been limited. Since 1970, extensive experimental and theoretical turbulent flows over smooth surfaces have been completed (Grass, 1971; Nakagawa and Nezu, 1977; Nezu and Nakagawa, 1993; Tachie, 2001; Nezu, 2005; Balachandar and Bhuiyan, 2007; Afzal et al., 2009). Flow over a rough surface has significance in many engineering applications. However, as rightly pointed by Patel (1998), flow over rough surface continues to be the Achilles heel of turbulence research. The suggested use of turbulent boundary layer data for modeling open channel flow is debatable due to basic differences between the two;

influenced by the channel aspect ratio and the presence of the free surface (Roussinova et al., 2008). Formation and enhancement of secondary currents occur due to the presence of the free surface and the side walls of the open channel. Free surface also dampens the vertical velocity fluctuations.

## **1.2 Effect of Seepage**

Natural channels, rivers, and streams have beds formed by earthen permeable material and experience seepage flow through boundaries due to the difference between water levels in the channel and the adjoining ground-water level. If the free water surface in the channel is higher than the adjoining ground-water level, seepage flow is called ‘suction’. Whereas, if the free water surface in the channel is lower than the adjoining ground-water level, seepage flow occurs into the channel and is called ‘injection’. It has been noted that the hydrodynamic characteristics of a channel flow can be significantly altered by seepage flow (Rao and Sitaram, 1999). Although, in most cases, the magnitude of seepage flow is much less in comparison to the main flow, in certain cases the inflow seepage can be large enough to produce a ‘quick’ condition in the channel bed or the outflow seepage can be large enough to cause a loss of water of as high as 45% of the water supplied at the upstream section of a channel (Shukla and Mishra, 1994). In comparison with the number of studies conducted in the area of turbulent flows over impervious smooth and rough boundaries, very few studies about the interaction of the pervious bed and the turbulent flow have been carried out.

The permeable boundary enables mass and momentum transfer across the interface between the fluid and the porous media, which needs to be accounted for in

modeling such flows. The interaction between turbulent flow and a permeable boundary may result in changes in the velocity profile, turbulent intensity and boundary shear stress, as compared with those in relation to an impermeable boundary (Cheng and Chiew, 1998a). The variable intensity of seepage flow may cause variation in flow properties. Furthermore, porous bed can work as a sink or source for harmful toxicants and fine sediments.

Seepage can alter the flow boundary conditions and eventually affect sediment transport and can change scouring action in channels. The knowledge of the flow structure over the seepage zone is required for the accurate estimation of the boundary shear stress. The process of suction draws faster moving flow into contact with the bed for a bed-type river intake. This process of suction can cause local scour and the undesirable exposure of the intake structure due to increase in boundary shear stress (Maclean, 1991). Furthermore, excess sediment deposition can cause severe navigational problems and may need extensive dredging work to keep the flowing of goods through waterways uninterrupted.

### **1.3 Effect of Ice Cover**

Formation of ice-cover on a river or a channel during winter months is a common event in the northern hemisphere. The presence of an additional boundary almost doubles the wetted perimeter and the flow, in general, becomes asymmetric due to different roughness on the top and bottom boundaries. Flow properties like velocity profile, shear stress distribution and mixing properties change due to the ice-cover. Bed load alteration would occur due to change in bed shear stress and at the same time, suspended load

alteration would occur due to change in the turbulent diffusion. Exact understanding of how an ice-cover affects bed-form geometry and suspended load is very important for hydropower station operation, transport and fate of pollutants, or flood levels in frigid environments. General practice at present for estimating flow resistance in ice-covered alluvial channels is to assume either that the bed resistance coefficients do not change with the ice-cover presence or that the flow-resistance behavior of the bed can be determined by approximating an ice-covered flow as a composite of two non-interacting flow layers, with the lower layer of flow affecting the bed (Smith and Ettema, 1997). Neither assumption is sound for alluvial channels, which predominantly have dune formations and dune morphology is influenced by the full flow depth (Smith and Ettema, 1997; Balachandar et al., 2007).

## **1.4 Objectives and Scope**

### **1.4.1 Objectives**

The objective of this research is to further understand the extent of effect of roughness, the effect of seepage and ice cover on the bed stability and turbulence characteristics in an open channel flow. Understanding the effect of roughness, seepage and ice cover is important to the modeling of sediment transport, resuspension, entrainment, modulation of turbulence and the use of turbulent boundary layer data for modeling open channel flow. Wide range of permeable bed materials in natural environment necessitates the laboratory experiments on the influence of seepage of flow characteristics and bed stability. The present study also aims to understand the effect of ice cover on flow properties due to the presence of an additional boundary.

### **1.4.2 Scope**

To study the effect of roughness, four different types of bed surface conditions consisting of smooth, distributed roughness, continuous roughness, and natural sand bed were used. Two different Reynolds number were adopted for each bed surface. To understand the effect of the introduction of seepage on different turbulent characteristics in an open channel flow, various degrees of suction and injection are introduced. Two different types of ice cover are used to study the effects of ice cover on flow in open channel flow. The variables of interest include the mean velocity, turbulence intensity, Reynolds shear stress, shear stress correlation and higher-order moments. Particular attention is paid to mean velocity, turbulence intensity, Reynolds shear stress, shear stress correlation, higher-order moments and quadrant analysis. The nominal flow depth was maintained to 100 mm, resulting in a width-to-depth ratio of 11.

Relevant literature dealing with experimental and numerical analysis on various aspect of open channel flow is reviewed in Chapter 2. At the end of Chapter 2, the modified objectives of the study based on understanding from previous studies are re-stated. Description of the experimental details is provided in Chapter 3. An overview of the laser Doppler anemometer (LDA) system and a description of different flow systems are also provided in Chapter 3. Results and discussion of the effect of roughness and Reynolds number is presented in Chapter 4. Chapter 5 contains the description of test results with the introduction of seepage. Test results with the ice cover and related discussion is provided in Chapter 6. The major conclusions from the present research including the recommendation for future research are included in Chapter 7.

## CHAPTER 2

### LITERATURE REVIEW

The existing literature in open channel flow is first reviewed in the context of the effect of bed roughness. This is followed by reviewing the literature on effects of seepage and ice cover.

#### **2.1 Open Channel Flow: Effect of Roughness**

Kirkgöz and Ardiçhoğlu (1997) studied the flow progression from a developing state to a fully developed condition and noted that along the axis of a fully developed section, the boundary layer extends to the water surface if the aspect ratio  $b/d \geq 3$ . Near the free surface, they did not observe any dip in the velocity profile at the channel centerline even for channel with aspect ratio as low as  $b/d = 3$ . Tachie et al. (2003) showed that roughness effects on the velocity field were similar to those observed in a zero-pressure gradient turbulent boundary layer, even though the boundary layer in an open channel flow is influenced by the free surface. Nezu (2005) related the aspect ratio (width/depth ratio of flow,  $b/d$ ) to the formation of secondary currents and noted that the maximum velocity on the centerline occurred below the free surface for  $b/d < 5$  (velocity-dip phenomenon). Balachandar and Patel (2002) indicated that the streamwise mean velocity profiles follow the well-known logarithmic law for the smooth surface, and with an appropriate shift, for the rough surface. Tachie et al. (2000) observed that wall roughness led to higher turbulence levels in the outer region of the boundary layer. Tachie et al. (2003) noted that roughness enhances the levels of the turbulence intensities over most of the flow.



Kaftori et al. (1995) noted that the coherent wall structures are the dominant factor affecting particle motion near a solid boundary, as well as influencing deposition and entrainment. They also noted that the vortices generate high-speed regions relative to the fluid in the viscous layer, sweep along the wall, pushing particles out of the way. Dancy et al. (2000) reported that for locations above the roughness sublayer, the distributions of the second-order turbulent stresses are similar to the smooth-wall distributions. Tachie et al. (2003) noted that roughness enhances the levels of the Reynolds shear stress over most of the flow. Tachie et al. (2004) noted that surface roughness significantly enhances the levels of the Reynolds stresses in a way that depends on the specific geometry of the roughness elements. They also noted that, surface roughness enhances the level of the Reynolds stresses over most of the flow and suggest a stronger interaction between the inner and outer regions of the flow than would be implied by the wall similarity hypothesis.

Nezu (2005) predicted that the Reynolds shear stress ( $-\overline{uv}$ ) might become negative near the free surface if the flow becomes three-dimensional (when  $b/d \leq 5$ ). He emphasized the importance of the correlation coefficient of the Reynolds stress because it involved only turbulence quantities, without the need for estimating friction velocity. Correlation coefficient of the Reynolds stress indicates the degree of similarity of turbulence and could be defined as  $\left( R = \frac{-\overline{uv}}{u \times v} \right)$ . Here,  $u$  and  $v$  are the turbulence intensity in streamwise direction and normal to the bed, respectively. Nezu (2005) noted that the value of  $R$  increases monotonously with  $y/d$  in the wall region, decreases in the free-surface region and remains nearly constant, at about 0.4~0.5, in the intermediate region ( $0.1 \leq y/d \leq 0.6$ ). He also noted that the distribution of  $R$  is universal, i.e., it is

independent of the properties of mean flow and the wall roughness. Bigillon et al. (2006) noted that the Reynolds stress attains a maximum and decreases towards the bed in the wall region. They explained that in the case of smooth walls, this behavior was due to the viscous effects, while for rough walls it was due to the existence of a roughness sublayer where additional mechanisms for momentum extraction emerge. They noticed contradicting behavior of Reynolds stress with variation of Reynolds number and associated this to secondary currents due to a relatively lower value of aspect ratio.

Dancey et al. (2000) reported that the relative contributions of sweep and ejection events within the sublayer showed that sweep events provide the dominant contribution to the Reynolds shear stress within this region. Tachie et al. (2003) noted that triple correlations and turbulence diffusion were strongly modified by the surface roughness. Tachie et al. (2004) noted that surface roughness significantly enhances the levels of the turbulence kinetic energy, and turbulence diffusion in a way that depends on the specific geometry of the roughness elements. Balachandar and Bhuiyan (2007) showed that the triple products are sensitive to the wall condition and the effects are prevalent throughout the depth of flow. They noted that ejection events are dominant throughout the depth and also vary significantly with wall roughness. From a velocity quadrant decomposition, they also noted that the magnitudes of the extreme events are higher for the rough wall in comparison to smooth wall throughout the depth. This indicates that effect of bed roughness is not limited to the region close to the bed. Roussinova et al. (2008) showed from the quadrant analysis that the turbulent structures in the outer region of the open channel are similar to the structures noted in turbulent boundary layers, but only for the case where all turbulent events were included. They observed significant differences

between open channel flow and turbulent boundary when only the extreme events are considered.

The existing literature can be summarized as follows:

1. Bed roughness influences bed formation and turbulence characteristics.
2. There are conflicting opinions among researchers about the extent of the effect of bed roughness and aspect ratio on turbulence characteristics.
3. There are contradictory remarks regarding the magnitude of sweep and ejection type turbulent events, though these events play a major role in transport mechanisms.

## **2.2 Effect of Seepage**

The number of previous studies of flow over a porous boundary is much less compared to the flow over non-porous boundary, and more importantly, the outcome of these studies is not unanimous. An excellent review of seepage studies can be found in Lu et al. (2008). Summary of the results of previous studies provided in Table 2.1, provide a glimpse of conflicting opinion about the influence of seepage. For clarity, the available literature is classified into four groups dealing with effect of seepage on (i) bed stability, (ii) bed shear stress, (iii) velocity distribution and (iv) turbulence distribution.

### **2.2.1 Effect of Seepage on Bed Stability**

In an effort to study the influence of seepage on sediment motion, Watters and Rao (1971) studied the effect of seepage on the hydrodynamic drag and lift forces acting on a sediment particle. They used a strain gage dynamometer to measure the drag and lift forces on an instrumented sphere. Four different bed configurations made up of spheres were used and the instrumented sphere is one of many similar spheres in each case. They measured the drag force directly and concluded that injection tended to reduce the drag on bed particles irrespective of the bed configuration. They observed an unexpected negative lift force with injection for some specific bed configurations. Judging from the view point of drag forces only, they concluded that injection inhibits the motion of bed particles, while suction enhances the motion.

Rao and Sitaram (1999) studied the effects of seepage on the stability, mobility, and incipient motion of sand-bed particles. They noted that suction decreases the stability of bed particles and increases their mobility, whereas injection increases the stability of the particles when compared with no-seepage condition. They observed that suction can initiate the movement of bed particles that are otherwise at rest under no-seepage conditions but injection does not initiate the particle movement. They concluded from the above observation that when the bed is transporting or eroding initially, suction enhances the erosion rates while injection reduces the rates of erosion and even stop the movement of particles.

Richardson et al. (1985) noted that inflow seepage (injection) increases sediment transport albeit slightly but did not appear to enhance channel scour. They also noted that injection causes bed forms such as dunes to become longer, flatter, move more erratically

in the reach where inflow occurred and concluded that injection could significantly influence the channel hydraulics, bed form and bed roughness in the localized zone of inflow. To the contrary, Sarkar and Dey (2007) noted that the characteristic length scales of the scour geometry decrease with increase in injection velocity.

Simons and Richardson (1966) concluded that suction would tend to increase the effective weight of the bed particles and, therefore, increase the stability of the bed. Conversely, with injection, the effective weight of the bed particles decreases and thereby decreases the bed stability. They also noted that the injection could result in an increase in the sediment transport and change in the predicted bed form. Oldenziel and Brink (1974) also stated that injection reduces the apparent weight of the sand particles and eventually their stability. They concluded that suction always decreases the rate of sand transport whereas injection increases this rate. Willetts and Drossos (1975) observed the formation of a localized scour hole in the suction zone and a downstream dune due to vigorous localized suction.

The study of Harrison (1968) indicates that injection had a limited effect on the stream sediment transport rate, even for quick bed condition. He concluded that the decrease in effective grain density brought about by injection might be compensated entirely, or in part, by a decrease in the surface drag on the individual grains and an increase in form drag.

### **2.2.2 Effect of Seepage on Bed Shear Stress**

Rao et al. (1994) studied the effects of seepage on flow over a sand bed in a straight rectangular flume under both non-transporting and transporting sediment at a

constant concentration. Their experimental results revealed that seepage can cause an increase or decrease in bed shear stress in comparison with the value under no-seepage condition. They concluded that the increase or decrease in bed shear stress depends on the initial flow condition and the relative magnitude of seepage applied.

Rao and Sitaram (1999) concluded that bed-shear stresses at pseudo-incipient motion with suction or injection could be significantly higher or lower than the critical stresses under no-seepage conditions obtained from the Shields' curve. They also recommended that the conventional Shields' curve couldn't be used to predict bed-shear stresses of the particles at such pseudo-incipient motion conditions because the seepage effects are not accounted in the conventional Shields' curve.

Cheng and Chiew (1998a) noted that Reynolds shear stress increases significantly in the near-bed region due to injection. They also noted that with increasing relative injection velocity, the relative bed shear stress decreases. Their experimental data shows that the reduction becomes much gentler for a rough sediment bed, as compared with the previous study for a smooth permeable boundary. Cheng and Chiew (1998b) noted that the bed-shear stress is reduced sharply at the beginning of the seepage zone due to injection. The reduction becomes more apparent for injection intensity. However, towards the downstream end of the seepage zone, the bed-shear stress exhibits a gradual increase.

Prinos (1995) found that the bed shear stress in the suction region increased with increasing suction rate and the increase can be as high as eight times the bed shear stress with no suction.

### 2.2.3 Effect of Seepage on Velocity Profile

Watters and Rao (1971) commented that the bed of an alluvial channel alters the flow configuration and modifies the velocity profile near the channel bed. They concluded that a decrease in velocity near the bed contributes to a lower drag force in the presence of injection and an increase in velocity near the bed contributes to a higher drag force due to suction. However, Richardson et al. (1985) noted that the mean channel velocity increased with injection.

Maclean (1991) found that the friction velocity decreased with the increasing suction, indicating a reduction in the velocity gradient  $dU/dy$  in the logarithmic region. He observed a deceleration of the flow near the free surface and to satisfy continuity, the flow is drawn downwards. He also observed an acceleration near the bed as the faster moving fluid from above are drawn down and with increasing suction rates, the streamwise velocity near the bed is increased, resulting in the formation of a more uniform velocity profile. He noted that the logarithmic profile is an indication that the basic structure of the flow in this region is effectively unchanged. He also studied the effect suction on the vertical velocity ( $V$ ) and found that  $dV/dy$  was negative close to the bed due to the region of longitudinally accelerating flow. Since  $V$  is already negative at the bed due to suction, means that the magnitude of  $V$  will become more negative away from the bed. This trend would be prevalent until the upper limit of accelerating flow is reached and the magnitude  $V$  would decrease steadily as  $y$  increases above this. He also found that contrary to expectation, the vertical velocity was non-zero for zero suction rates and associated it with the disturbance over the cavity of the surface. He also found an inner boundary layer across which the shear stress changed rapidly, above which was

a logarithmic region in which the flow structure was effectively unaltered by the presence of suction. Chen and Chiew (2007) also observed a more negative vertical (downward) velocity very close to the bed at the leading edge of the suction zone.

Cheng and Chiew (1998a) noted that along the seepage zone, the mean streamwise velocity increases much more in the free surface region than that in the near-bed region due to injection. Cheng and Chiew (1998b) showed that the deviation of the measured velocity distribution from the logarithmic law of the wall increases with increasing ratio of the seepage velocity to the shear velocity due to introduction of injection. Chen and Chiew (2004) found a more uniform velocity distribution due to the increase in the near bed velocity and a reduction of velocity near the water surface subjected to bed suction. They also suggested that there are two regions in the suction zone, “transitional” region of rapidly readjusting velocity profile at the beginning of the suction zone and an “equilibrium” region where the change is more gradual. They also found that bed suction causes a significant increase in the shear velocity.

#### **2.2.4 Effect of Seepage on Turbulence Distribution**

Watters and Rao (1971) reviewed the effect of seepage on the channel boundary layer. They observed a reduction in the sublayer thickness due to suction. They pointed out that the suction effectively increases the hydrodynamic roughness. They also noted that in the presence of suction, there is a decrease in turbulence level, which eventually leads to lesser momentum exchange between fluid particles. This analysis contradicts recent observations that roughness increases turbulence levels in the flow (Tachie et al., 2003; Balachandar and Bhuiyan, 2007). In the presence of injection, they observed an



increase in sublayer thickness and noted an increase in turbulence level, which eventually leads to a greater momentum exchange between fluid particles. They noted that turbulence fluctuations were more intense for injection than for suction or without seepage.

Richardson et al. (1985) found that the injection increases turbulence along the interface and thought that the fluid shear and particle to particle momentum transfer between the main and seepage flow is responsible for this increase of turbulence. Cheng and Chiew (1998a) also noted that along the seepage zone, the turbulent intensities increase significantly in the near-bed region due to injection.

Prinos (1995) showed a considerable reduction in turbulence level and Reynolds stress with increasing suction rates. He commented that high suction rates tend to destroy the turbulence and there would be a probability of an inverse transition in the case of a long suction region. Chen and Chiew (2007) also found similar reduction of turbulence intensities and Reynolds shear stress due to suction and noted that the reduction is more significant with higher relative suction. They recognized that over the entire water depth, turbulence intensities and Reynolds shear stress decrease more rapidly near the bed than those near the free surface.

The existing literature can be summarized as follows:

1. Seepage can potentially change the bed formation in open channel flow. However, there are many thoughts about the extent of change.
2. There is conflicting opinion about the influence of the seepage (suction/injection) on bed stability.

3. Injection increases turbulent intensity near the bed and suction decreases the same. More clarification is required to check the increase/decrease of streamwise/vertical turbulence intensity and the affected portion of the depth.
4. Mean streamwise velocity increases much more in the surface layer than that in the near-bed region for injection, whereas, mean streamwise velocity increases in the near-bed region and reduces near the water surface for suction.
5. Reynolds shear stress increases significantly in the near-bed region due to injection and reduces in the presence of suction. Further, the extent of influence of seepage in the depth-wise direction needs to be studied.
6. Bed shear stress decreases due to injection and increases due to suction. However, the initial flow conditions and the magnitude of seepage can alter the results. More research is required in this direction.

### **2.3 Effect of Ice Cover**

Lau and Krishnappan (1981) developed a turbulent model and a numerical scheme to calculate the uniform two-dimensional flow in channels with and without ice-covers. They found that computed velocity and eddy viscosity distributions do not follow the conventional logarithmic and parabolic distributions for the whole depth of flow. They noted that for the open channel flow, the velocity distribution deviates slightly from the logarithmic profile for the top 25% of the flow, while the eddy viscosity distribution deviates from the parabolic distribution for the top half of the flow. They stated that in all cases, the equivalent ice-covered flows have larger flow depths and smaller bed shears

than the free-surface flows. The resulting eddy viscosity is smaller than the free-surface flow values.

Lau (1982) used a  $k$ - $\epsilon$  turbulence model to calculate the velocity distribution with floating covers and under uniform flow conditions. The resulting distributions were used to review the standard procedures for stream gauging ice-covered flows. Although the velocities at 0.2 and 0.8 of the depth may deviate significantly from the overall average velocity but it was found that the average of the velocities at 0.2 and 0.8 of the depth is indeed very nearly equal to the overall average velocity. The computed velocity distributions show that the velocity profiles deviate from the logarithmic distribution for about 40% of the flow depth.

Lau and Krishnappan (1985) conducted laboratory tests on bed form, frictional characteristics and sediment transport for equivalent free-surface and covered flows. They found that the sediment transport rates with a floating cover are much smaller than the free-surface flow values even though the changes in friction velocity are not large. They noted that the presence of a top cover does not have significant effect on the bed form characteristics. They also noted that the bed shear stress and the eddy viscosity are both smaller than the corresponding free surface flows.

Walker (1994) examined the variability of streamflow velocity adjustment coefficients computed from vertical velocity profiles measured at 13 stations located across the northern United States and found that nearly one-half of the adjustment coefficients at particular streamflow gauging stations demonstrated statistically significant differences on a measurement-by-measurement basis. He concluded that the

traditional 2 & 8 two-point method was inaccurate and recommended two different discharge-measurement procedures.

Parthasarathy and Muste (1994) conducted laboratory experiments of asymmetric turbulent channel flows to understand the changes in the flow due to ice cover as the roughness characteristics were changed and the implications of the flow behavior on the suspended sediment transport. The measurements confirmed the noncoincidence of the planes of maximum velocity and zero Reynolds stress, with the plane of zero Reynolds stress always located close to the smooth surface. They noted that significant diffusion of momentum and kinetic energy took place from the rough to the smooth surface. They also noted a decrease in the sediment suspension mechanism if the roughness of the cover was increased due to decreased vertical transfer of vertical velocity fluctuations near the bed.

Using profiles generated numerically, based on a two-power law description of vertical distribution of streamwise velocity, Teal et al. (1994) evaluated point-measurement methods for estimating the mean velocity of vertical distributions of streamwise velocity in ice-covered channels. They confirmed the accuracy of the two-point method (velocity measurements taken at 0.2 and 0.8 of flow depth and averaged to obtain an estimate of the mean) for estimating mean velocity in a stream-section vertical. Although they preferred the two-point method, they recommended using single-point method for very shallow streams.

Yoon et al. (1996) used a numerical model to simulate the flow in a channel with a free-floating ice cover. Application of the model to a hypothetical case of an ice cover on a dune-bed channel showed how the principal hydraulic parameters of an open

channel were affected by the growth of an ice cover during winter. The simulation resulted in a 16% increase of flow depth for an ice covered flow in comparison to open-water flow. They also observed that the flow near the dune bed remains essentially unchanged with the addition of the ice cover, but on the other hand, the effect of the cover was quite obvious in the top-half of the channel. The mean-velocity components and the turbulence parameters all vanished at the cover, whereas, with the exception of the normal-velocity component and the Reynolds shear stress, all other quantities remained finite at the free surface of an open channel.

Smith and Ettema (1997) conducted experiments to describe the influences of floating ice covers and bed-load transport in alluvial channels. The main findings were that ice covers increased flow depth, decreased bulk flow velocity, increased dune length, and significantly decreased bed-load transport rate. They commented that the particle friction factor increased with increasing cover roughness because ice cover affected it through two mechanisms. First, the cover presence and increasing cover roughness, reduced the bulk flow velocity, which tends to reduce the surface resistance of the bed. Second, the cover presence and increasing cover roughness reduce dune steepness, which reduced the sizes of the flow recirculation zones behind the dune crest.

Tan et al. (1999) conducted numerical-simulation to investigate the influence of ice-cover on the mixing and transport of a neutrally buoyant contaminant released from a point source located near a dune bed or the underside of a level ice cover in a straight reach of the channel. These conditions were selected to determine how an ice-covered presence influences near-field mixing. Their numerical results showed that for constant water discharge, the presence of the cover reduces the near-field mixing because it

redistributes the flow, increases flow depth, decreases bulk velocity, reduces maximum level of turbulence, and modifies the dune geometry. For the ice-covered flow, a contamination released near the bed or near the underside remains closer to those boundaries over a long distance than for a corresponding open-water flow. They noted that the ice-covered flow needed an additional two to three times the distance to attain fully mixed condition due to its reduced near-field mixing.

Helmiö (2001) aimed to describe the effect of ice cover on flow and determined how the resistance coefficients vary in winter condition in a natural river. He described different methods, and problems that arose in direct measurement of roughness of ice cover and specially problems in indirect measurement with the help of discharge, water level and thickness of ice cover. He carried out discharge, water level and ice measurements in River Pöntänenjoki (Western Finland), to compare the resistances during ice and open water flow conditions. He was surprised with the result as it indicated that total resistance coefficients of the channel were remarkably lower in winter than in summer and it directly contradicted the finding of Ashton (1986), who said that resistance of flow under ice cover is almost always higher than that during open channel flow.

Ettema (2002) reviewed alluvial channel responses to ice formation, and raises practical engineering issues. He pointed out that the interactions between the flow, the ice, and the loose bed act over a range of scales in space and time. The nub of the argument made in his review was that the interactions raised important issues that require further consideration in river-ice hydraulics.

The existing literature can be summarized as follows:

1. For equivalent ice-covered flow, the resulting eddy viscosity is smaller than the corresponding free-surface flow.
2. The equivalent ice-covered flows have larger flow depth in comparison to the free-surface flow.
3. There is conflicting opinion about effect of ice-cover on the bed-form characteristics.
4. Some researchers confirmed the accuracy of the practical two-point method (velocity measurements taken at 0.2 and 0.8 of flow depth are averaged to obtain an estimate of mean velocity), whereas, others concluded that the traditional two-point was inaccurate.
5. Sediment transport rates with a floating cover were found to be much smaller than the free surface flow.
6. There is conflicting opinion about the flow resistance under ice-cover.

## **2.4 Refinement in Objectives**

On the basis of our understanding on the different aspect of open channel flow from the above mentioned literature, the specific objectives of our study can be re-stated as:

1. To investigate the effect of surface roughness and Reynolds number on turbulence characteristics in open channel flow.
2. To investigate the effect of seepage on bed stability and turbulence characteristics in open channel flow.
3. To investigate the effect of ice cover on the bed friction and turbulence characteristics in open channel flow.
4. Analysis of the Reynolds stress, turbulent higher-order moments and quadrant decomposition for flow in open channels.
5. In conjunction with other studies simultaneously being carried out at the University of Windsor, to produce a database that can be used in the development and calibration of numerical models.



Table 2.1: Summary of results of previous seepage studies

Source	Sediment transport rate		Bed shear stress		Turbulence intensity	
	Suction	Injection	Suction	Injection	Suction	Injection
Walters and Rao (1971)	Increase	Decrease	-	-	Decrease	Increase
Oldenziel and Brink (1974)	Decrease	Increase	-	-	-	-
Willetts and Drossos (1975)	Increase	-	-	-	-	-
Richardson et al. (1985)	Decrease	Increase	-	-	-	-
Maclean and Willetts (1986)	-	-	Increase	-	-	-
Maclean (1991)	-	-	Increase	-	-	-
Ramakrishna Rao et al. (1994)	-	-	Increase/ Decrease	Increase/ Decrease	-	-
Antonia and Zhu (1995)	-	-	-	-	Decrease	Increase
Cheng and Chiew (1998a)	-	-	-	Decrease	-	-
Cheng and Chiew (1998b)	-	-	-	Decrease	-	-
Cheng and Chiew (1999)	-	Increase	-	Decrease	-	-
Rao and Sitaram (1999)	Increase	Decrease	Increase/ Decrease	Increase/ Decrease	Increase	Decrease
Krogstad and Kourakine (2000)	-	-	-	Decrease	-	Increase
Chen and Chiew (2004)	-	-	Increase		-	-
Chen and Chiew (2007)	-	-	-	-	Decrease	Increase
Simons and Richardson (1966)	Decrease	Increase	-	-	-	-

## CHAPTER 3

### EXPERIMENTAL SETUP

#### 3.1 Open Channel Flume

Experiments were carried out in a 9-m long rectangular open channel flume (cross-section 1100 mm x 920 mm) at the University of Windsor. A schematic of the open channel flume and the experimental setup is shown in Figure 3.1. The header tank upstream of the rectangular cross-section was 1.2 m square and 3.0 m deep. The nominal flow depth ( $d$ ) in the measurement region was 100 mm, resulting in a width-to-depth ratio ( $b/d$ ) of approximately 11. This value of the aspect ratio is considered to be large enough to minimize the effect of secondary currents and the flow can be considered to be nominally two-dimensional (Nezu, 2005). The water was recirculated by two 15-horsepower centrifugal pumps. The sidewalls and bottom of the flume were made of transparent tempered glass to facilitate velocity measurements using a laser Doppler anemometer (LDA). The flume is a permanent facility and the quality of flow has been confirmed in several previous studies (Faruque et al., 2006; Sarathi et al., 2008). The bottom slope of the flume was adjustable and for this study, it was kept horizontal and two constant discharges of 720 GPM (Gallon per minute) and 450 GPM were used.

#### 3.2 Test Conditions to Study the Effect of Roughness

Four different types of bed surface conditions were used in this study. The base case was a hydraulically smooth surface generated using a polished aluminum plate spanning the entire width of flume (Figure 3.2a). Three different types of rough surfaces

were used. Sand particles ( $d_{50} = 2.46$  mm,  $\sigma_g = \sqrt{d_{84} / d_{16}} = 1.24$ ) were used to create the rough surfaces. The gradation characteristics of the sand shown are in Table 3.1 and the bed can be classified to be composed of uniform particles.

To generate the first rough surface (designated as ‘distributed roughness’), 18-mm wide sand strips were glued to the smooth aluminum plate alternating with 18-mm wide smooth strips as shown in Figure 3.2b. The second roughness condition consisted of the same sand grains glued over the entire smooth surface as shown in Figure 3.2c (continuous roughness). Third rough surface was generated using 200-mm thick and 3.7 m long uniform sand bed as shown in Figure 3.3. The flow conditions were maintained in such a manner that there was no initiation of sand movement. However, a sand trap was provided at the downstream of the bed to prevent any accidental transport of sand particles into the pump/piping assembly.

Two different Reynolds numbers were used for each bed condition. The Reynolds numbers were chosen to maintain subcritical flow conditions (i.e., Froude numbers less than unity). Flow conditions correspond to values of Reynolds number,  $Re = U_{avg}d/\nu \approx 47,500$  &  $31,000$  and the corresponding Froude numbers are  $Fr = U_{avg}/(gd)^{0.5} \approx 0.40$  &  $0.24$  respectively. Here,  $U_{avg}$  is the average streamwise velocity,  $d$  is the depth of flow,  $g$  is the acceleration due to gravity and  $\nu$  is the kinematic viscosity of the fluid. In the test section, the measured variation of water surface elevation was less than 1 mm over a streamwise distance of 600 mm implying a negligible pressure gradient. Flow straighteners were used at the beginning and the end of flume to condition the flow. To ensure the presence of a turbulent boundary layer, a 3-mm diameter rod was used as a (Figure 3.1) trip upstream of the measurement region. The boundary layer shape factor

for the smooth bed which can be defined as the ratio of displacement to momentum thickness is found to be  $\approx 1.3$ , which is an indication of fully developed turbulent flow (Schlichting, 1979). The measurements for the distributed roughness were conducted on top of 60<sup>th</sup> sand strip. All the measurements were conducted along the centreline of the channel to minimize secondary flow effects. Preliminary tests were conducted to ensure a fully developed flow condition. The summary of the test conditions were presented in Table 3.2.

### **3.3 Test Conditions with the Introduction of Seepage**

Experiments were carried out in the open channel flume with the same sand described earlier. The setup of the seepage zone is schematically shown in Figure 3.4. The seepage zone subjected to suction or injection is 2.4 m long, 125-mm deep and spans the entire width of flume. The seepage zone was designed by introducing a seepage console to ensure uniform seepage velocity over the entire area. Fifteen identical perforated pipes were used to drain water into the flow field (injection) or out of the flow field (suction) uniformly. Perforation diameter of the pipe varied from  $\frac{3}{4}$  inch to  $\frac{3}{8}$  inch to produce uniform distribution. The maximum perforation diameter is at the center of the seepage console and reduced to minimum at the end of the seepage console. Outside the seepage console, all these fifteen perforated pipes were connected to a common feeder pipe and regulated with a valve. Two separate identical pumps with control valves were used to maintain the flow rate for suction/injection, which was monitored using a flow meter. The sand was placed on top of a filter net, which in turns, overlays a perforated plate. The picture of different phases of the construction of seepage console is shown in

Figure 3.5. The use of filter net (Figure 3.5 c) prevents the sediment particles from falling down. Water is allowed to seep through the perforated plate, filter net and sand layer to ensure uniform seepage flow within the granular materials.

Two different flow rates (450 GPM and 720 GPM) were used and the flow was maintained to be subcritical. Flow straighteners were used at the beginning and the end of flume to condition the flow. All the measurements were conducted along the centreline of the channel to minimize secondary flow effects. Although efforts were made to ensure uniform distribution of seepage flow throughout the bed, the velocity measurements were conducted in the middle of the seepage console. This follows the earlier measurement location choice by Cheng and Chiew (1998b), Richardson et al. (1985), Rao and Sitaram (1999). Preliminary tests were conducted to ensure a fully developed flow conditions. The summary of the test conditions are presented in Table 3.3.

### **3.4 Test Conditions with Ice Cover**

The experiments were also conducted on three different types of water surface conditions (open-water flow as a base case; Cover 1 and Cover 2 as simulated ice covered flow). Following the suggestions of Smith and Ettema (1997) extruded polystyrene foam panels were used to simulate Cover 1 and a wire mesh (23 gauge galvanized steel wire, 25600 meshes per m<sup>2</sup>) was stapled to the polystyrene foam bottom surface to simulate Cover 2. Cover 2 represents much rougher ice covered flow than Cover 1. The polystyrene foam panels were 2400 mm long and 1090mm wide and were connected to provide a continuous floating cover for the entire test bed. The bed

conditions remained the same as before. The summary of the test conditions are presented in Table 3.4.

### **3.5 The Laser Doppler Anemometry**

A commercial two-component fibre-optic LDA system (Dantec Inc.) powered by a 300-mW Argon-Ion laser was used for the velocity measurements. This system has been used in several previous studies and details are avoided for brevity (Faruque et al., 2006; Bey et al., 2007; Afzal et al., 2009). The optical elements include a Bragg cell, a 500-mm focusing lens and the beam spacing was 38 mm. 10,000 validated samples were acquired at each measurement location. The data rate varied from 4 Hz to 65 Hz. Prior to the measurement of each set of data, the side wall of the flume were cleaned to minimize extraneous light scattered from particles distributed throughout the illuminating beams. Prior to the start of the measurements, the water was filtered for several days and then seeded with hollow spheres (Mean particle size = 12 microns and Density = 1.13 g/cc). The configuration of the present two-component LDA system would not permit measurements very close to the wall, while one-component (streamwise velocity) measurements were made over the entire depth. The LDA probe was tilted  $2^\circ$  towards the bottom wall to capture near wall data for two-component velocity measurements. Kaftori et al. (1995) and Tachie (2001) have successfully adopted this procedure by tilting the probe by  $3^\circ$  and  $2^\circ$ , respectively, to allow data acquisition closer to the wall.

Table 3.1: Gradation measurements of the sand

$d_{50}$ (mm)	2.46
$d_{95}/d_5$	1.91
$d_{95}/d_{50}$	1.34
$d_{84}/d_{50}$	1.26
$\sigma_g = \sqrt{d_{84}/d_{16}}$	1.24
$C_z = d_{30}^2/(d_{60}d_{10})$	1.00

Table 3.2: Summary of test conditions to study the effect of roughness

Test	Bed Condition	d (mm)	$R_e$	$F_r$
1	Smooth bed	~ 100	~ 47,500	~ 0.40
2		~ 100	~ 31,000	~ 0.24
3	Distributed roughness	~ 100	~ 47,500	~ 0.40
4		~ 100	~ 31,000	~ 0.24
5	Continuous roughness	~ 100	~ 47,500	~ 0.40
6		~ 100	~ 31,000	~ 0.24
7	Natural sand bed	~ 100	~ 47,500	~ 0.40
8		~ 100	~ 31,000	~ 0.24

Table 3.3: Summary of test conditions with the introduction of seepage

Test	Flow condition	% Rate of Suction/Injection	$R_e$
1	No suction/injection	0	~ 31,000
2	Suction	5	~ 31,000
3		7	~ 31,000
4		9	~ 31,000
5		12	~ 31,000
6		14	~ 31,000
7		Injection	5
8	7		~ 31,000
9	9		~ 31,000
10	12		~ 31,000
11	14		~ 31,000
12	No suction/injection	0	~ 47,500
13	Suction	3	~ 47,500
14		5	~ 47,500
15		7	~ 47,500
16		9	~ 47,500
17	Injection	3	~ 47,500
18		5	~ 47,500
19		7	~ 47,500
20		9	~ 47,500



Table 3.4: Summary of test conditions with ice cover

Test	Bed	Cover	$Re$	$F_r$
1	Smooth	Open-water Flow	~ 47,500	0.40
2			~ 31,000	0.24
3		Cover 1	~ 47,500	0.40
4			~ 31,000	0.24
5		Cover 2 (rougher)	~ 47,500	0.40
6			~ 31,000	0.24
7	Distributed Roughness	Open-water Flow	~ 47,500	0.40
8			~ 31,000	0.24
9		Cover 1	~ 47,500	0.40
10			~ 31,000	0.24
11		Cover 2 (rougher)	~ 47,500	0.40
12			~ 31,000	0.24
13	Continuous Roughness	Open-water Flow	~ 47,500	0.40
14			~ 31,000	0.24
15		Cover 1	~ 47,500	0.40
16			~ 31,000	0.24
17		Cover 2 (rougher)	~ 47,500	0.40
18			~ 31,000	0.24
19	Natural Sand Bed	Open-water Flow	~ 47,500	0.40
20			~ 31,000	0.24
21		Cover 1	~ 47,500	0.40
22			~ 31,000	0.24
23		Cover 2 (rougher)	~ 47,500	0.40
24			~ 31,000	0.24

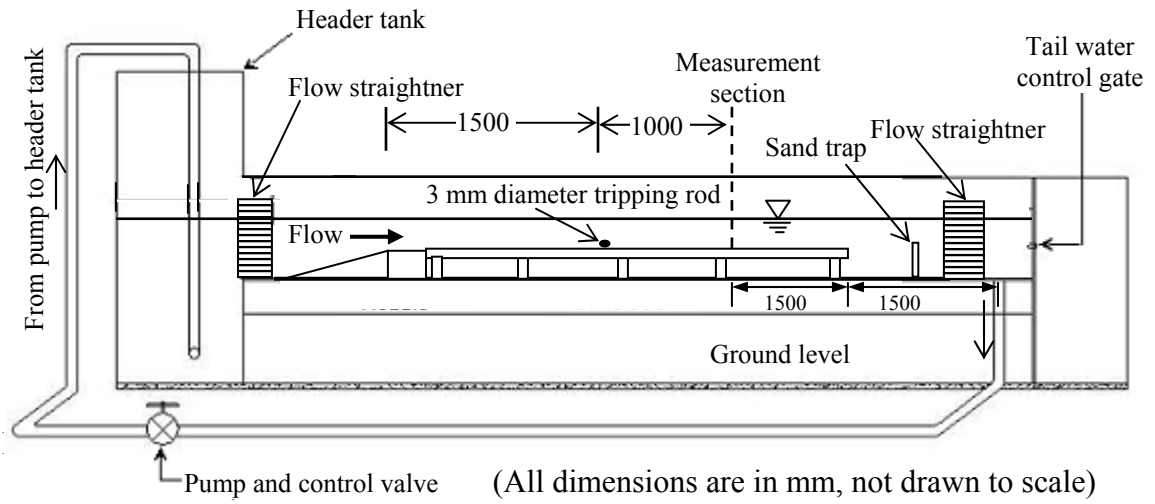


Figure 3.1: Schematic of the open channel flume and experimental setup.

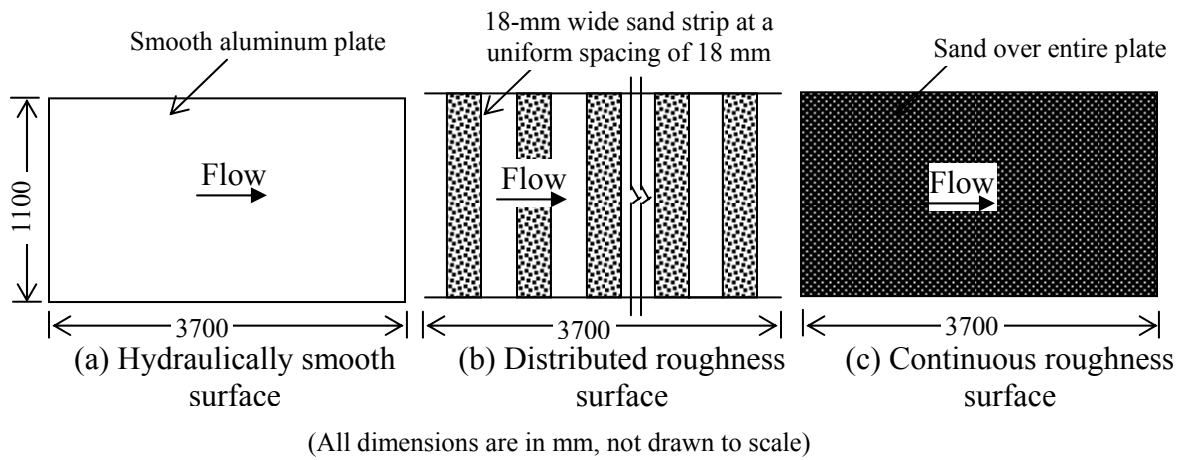
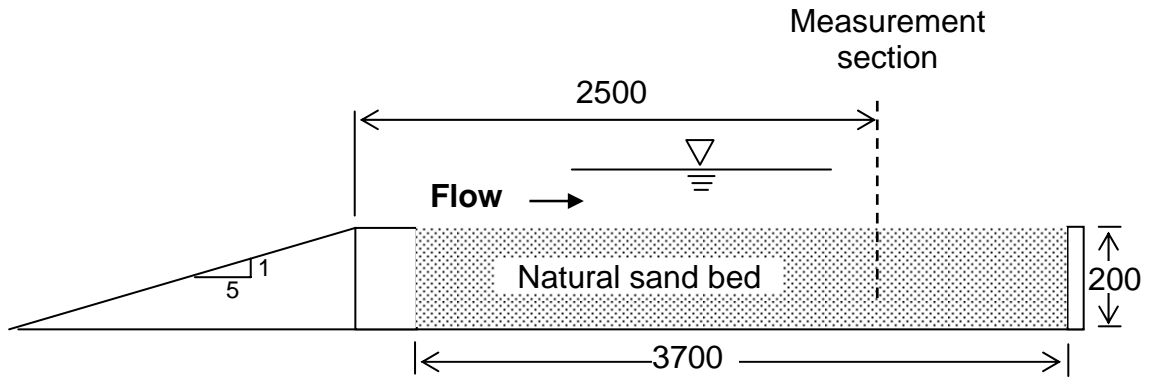
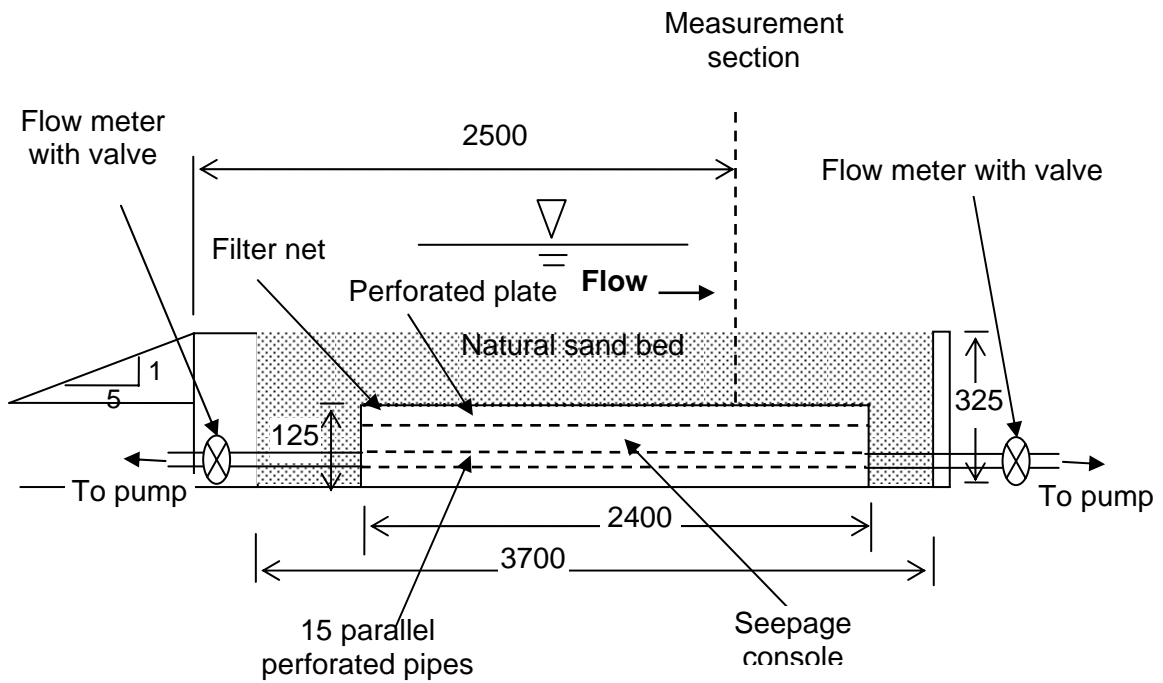


Figure 3.2: Plan view of different fixed bed condition.



(All dimensions are in mm, not drawn to scale)

Figure 3.3: Section of natural sand bed.



(All dimensions are in mm, not drawn to scale)

Figure 3.4: Schematic of seepage zone setup.

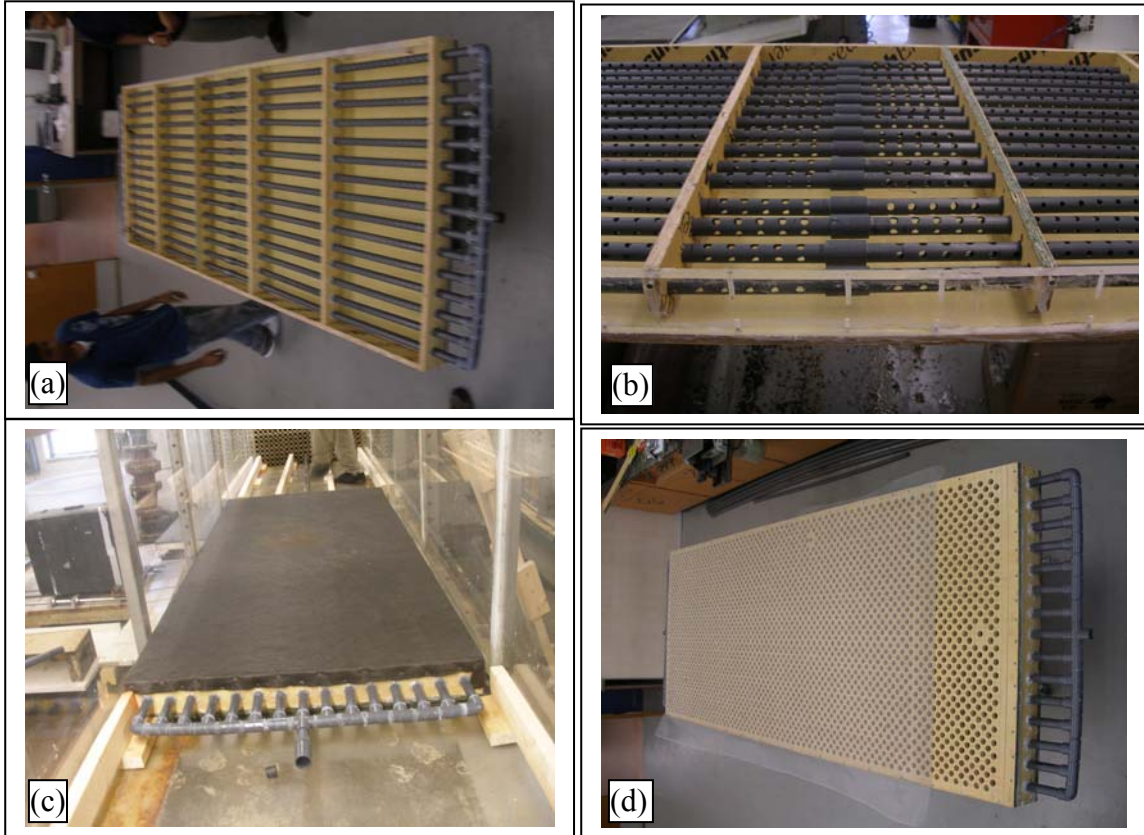


Figure 3.5: Pictures of seepage console, a) Seepage console setup, b) Perforated pipes, c) Filter net, d) Perforated plate.

## CHAPTER 4

### ROUGHNESS EFFECTS ON TURBULENCE CHARACTERISTICS

The present study was carried out to understand the effect of roughness and Reynolds number in open channel flow (OCF). To this extent, four different types of bed surface conditions consisting of smooth, distributed roughness, continuous roughness, natural sand bed were used. Two different Reynolds number were adopted for each bed surface. The variables of interest include the mean velocity, turbulence intensity, Reynolds shear stress, shear stress correlation and higher-order moments.

#### 4.1 Mean Velocity Profiles

##### 4.1.1 Outer Coordinates

The distributions of the streamwise component of the mean velocity in outer coordinates are shown in Figure 4.1. Maximum velocity ( $U_e$ ) and maximum flow depth ( $d$ ) are used to non-dimensionalize the mean velocity ( $U$ ) and the wall normal distance ( $y$ ), respectively. In the outer region, each velocity profile shows a slight dip (see inset in Figure 4.1) where the local maximum value ( $U_e$ ) occurs below the free surface and  $dU/dy$  is negative in the vicinity of the free surface. Although the velocity dip is largest for the sand bed, the smooth surface shows a greater dip than both the continuous roughness and the distributed roughness. In the region close to the bed, as rightly pointed out by Tachie et al. (2000), the effect of roughness is to increase the surface drag resulting in the velocity profile of the rough surface being less “full” when compared to smooth surface profile. One can note from Figure 4.1a that the distributed roughness exhibits the highest deviation from the smooth wall profile while the profiles for the continuous roughness

and natural sand bed show a similar deviation. Figure 4.1b shows the streamwise component of the mean velocity in outer coordinates at the lower Reynolds number. The results are similar to the higher Reynolds number except that the natural sand bed shows a higher deviation than continuous roughness for the lower Reynolds number. This may be an effect of momentum/energy loss due to the interchange of fluid and momentum across the permeable boundary. The effect of infiltration on mean velocity reduces as the Reynolds number increases.

#### 4.1.2 Inner Coordinates

The distributions of the streamwise component of the mean velocity in inner coordinates are shown in Figure 4.2. Friction velocity for smooth and rough beds were calculated using the Clauser method by fitting the mean velocity profiles with the classical log law,  $U^+ = \kappa^{-1} \ln y^+ + B - \Delta U^+$ . Here,  $U^+ = U/U_\tau$ ,  $y^+ = yU_\tau/\nu$ ,  $\kappa = 0.41$  and  $B = 5$  are log-law constants and  $\Delta U^+$  is the roughness function representing the downward shift of the velocity profile.  $\Delta U^+$  is zero for flow over the smooth bed. The smooth bed test data agrees well with the standard log-law (solid line). The expected downward-right shift of the profile is clearly visible for the rough beds. As the downward shift of the profile is a measure of the effect of roughness, the distributed roughness shows a maximum effect, followed by continuous roughness and natural sand bed. Figure 4.2b shows the streamwise component of the mean velocity in inner coordinates for lower Reynolds number. The results are similar to the higher Reynolds number.

Friction coefficient is calculated as,  $C_f = 2(U_\tau/U_e)^2$ , and found to be a maximum for distributed roughness followed by continuous roughness and sand bed. It was also

found that friction coefficient reduces as the Reynolds number increases. One can also note that for the flow over the natural sand bed,  $C_f$  is smaller compared to the flow over the impermeable rough surfaces (continuous roughness). The probable explanation can be the development of finite slip velocity at the interface of permeable layer which will eventually reduce the surface friction. However, Zagni and Smith (1976) noted that the boundary resistance of the permeable boundaries is higher than that of nonpermeable boundaries having identical rugosity and thought that it might be due to the net effect of combined loss of energy (energy dissipation within the transition zone in the porous medium and additional energy loss due to fluid and momentum exchange across the interface translated back into the main flow).

## **4.2 Turbulence Intensity**

### **4.2.1 Streamwise Turbulence Intensity**

Figure 4.3 shows the streamwise turbulence intensity for flow over the smooth and the rough beds. Directly measured quantities like depth of flow and maximum velocity are used as the length and velocity scales, respectively, to reduce any additional uncertainties related to scaling parameters with computed quantities. One can note from Figure 4.3a that streamwise turbulence intensity attains a maximum value very close to the bed, for all surfaces. The smooth bed profile shows the highest turbulence intensity at locations very close to the bed. Among the rough beds, the flow over distributed roughness shows the highest peak at  $y/d \sim 0.08$  followed by continuous roughness and natural sand bed at  $y/d \sim 0.04$ . At larger values of  $y/d$ , the streamwise turbulence intensity reduces towards the free surface. With the initial significant drop of streamwise

turbulence intensity for smooth bed surface condition, the reduction of streamwise turbulence intensity is more or less linear for all surface conditions. Closer to the free surface, the results indicate that the streamwise turbulence attains a near constant value, except for the case of the bed with distributed roughness. The location of attainment of constant streamwise turbulence intensity is different for the different beds. The distance from the bed to the start of the constant streamwise turbulence intensity is  $0.5d$  for smooth bed surface condition followed by continuous roughness and sand bed ( $\sim 0.62d$ ). Although the distance from bed to attain a constant value of streamwise turbulence intensity is the same for the continuous roughness and sand bed, the value of streamwise turbulence intensity is found to be higher for the sand bed condition. With the exception of the region very close to the bed, roughness effect is prevalent throughout the flow depth with distributed roughness showing a maximum deviation from a smooth bed followed by sand bed and continuous roughness. Although the same sand grain is used to create the three different rough bed conditions, the difference in turbulence intensity is an indication that the specific geometry of the roughness has an influence on turbulence structure.

The variation of streamwise turbulence intensity for the lower Reynolds number flow (Figure 4.3b) shows a trend similar to the higher Reynolds number flow (Figure 4.3a). However, the flow over distributed roughness shows more deviation at the lower Reynolds number. In addition, differences between sand bed and continuous roughness bed are negligible for flow at the lower Reynolds number.



### 4.2.2 Vertical Turbulence Intensity

The variation of vertical turbulence intensity is shown in Figure 4.4 and shows a trend similar to that of the streamwise turbulence intensity profile with the exception of locations very close to the bed. The streamwise turbulence intensity reduces but the vertical turbulence intensity increases at locations very close to the bed due to the introduction of roughness.

### 4.3 Reynolds Shear Stress

Figure 4.5 shows the Reynolds shear stress distribution on smooth and rough beds in outer variables. One can note from Figure 4.5a that the Reynolds shear stress attains a maximum value at a location near the bed ( $y/d < 0.2$ ). As expected, the flow over the rough beds generates higher Reynolds shear stress. The sand bed condition shows the highest peak followed by distributed roughness and fixed roughness. However, in the outer region ( $y > 0.2d$ ) the distributed roughness provides for the higher Reynolds shear stress followed by continuous roughness and the sand bed. Near the free surface, the Reynolds shear stress reduces and becomes negative for all bed conditions above the location where the corresponding value of  $dU/dy$  is negative. Results indicate that the reduction of Reynolds shear stress from its maximum value to zero is more or less linear for all surface conditions. One can clearly note from Figure 4.5 that effect of bed condition on the Reynolds shear stress is distinctly visible from the near-bed to the depth of flow as high as  $y \approx 0.7d$ . Krogstad et al (2005), Tachie (2001), Agelinchaab and Tachie (2006) found the influence of bed condition on Reynolds shear stress penetrates up to  $y \approx 0.2d \sim 0.3d$ . Grass (1971) did not find any significant difference in their

calculation of Reynolds shear stress for flow over smooth and rough bed (2 mm sand and 9 mm pebbles). However, results (of Grass, 1971) may have influenced by the small sample size. The variation of Reynolds shear stress for the lower Reynolds number (Figure 4.5b) shows a trend similar to that at the higher Reynolds number. However, in this case the distributed bed roughness shows the highest peak followed by sand bed and continuous roughness. Throughout the depth, distributed roughness bed also shows much more production of Reynolds shear stress than other rough beds. The flow over the discrete elements generates a series of wakes, which contribute to the generation of significantly higher Reynolds shear stress.

#### 4.4 Shear Stress Correlation Coefficient

Figure 4.6 shows the distribution of shear stress correlation coefficient  $\left( R = \frac{-\overline{uv}}{u \times v} \right)$

for the different bed conditions. R is a normalized covariance by which the degree of linear correlation between streamline and vertical turbulence intensity can be expressed. R = 1 is also an indication of increasing linear relationship whereas R = -1 is an indication of a decreasing linear relationship. Presence or absence of flow structures at a particular location can be identified by the local statistics of R. One can note from Figure 4.6a that correlation coefficient is particularly dependent on roughness in the outer region of the flow ( $y > 0.3d$ ). Variation of R in the outer region with respect to the near-bed, is an indication of the change in the flow structures between the near-bed and the outer region, clearly opposing the observation of Nezu (2005), Nezu and Nakagawa (1993), Tachie (2001). Nezu (2005) noted an existence of equilibrium region for  $0.1 \leq y/d \leq 0.6$  with a value of  $R = 0.4 \sim 0.5$  in open-channels, pipes, and boundary layers, irrespective

of whether the wall bed is smooth or rough. Nezu and Nakagawa (1993) also indicated that the distribution of  $R$  is universal and independent of the properties of the mean flow and the wall roughness. Tachie (2001) noticed a lower value of  $R$  for a smooth surface in the inner region ( $y/d < 0.15$ ) but found  $R$  to be independent of bed conditions for  $y/d > 0.15$  with the peak values were in the range of  $0.35 \pm 0.02$ . One can also note from Figure 4.6a that for the outer region ( $y > 0.3d$ ), distributed bed roughness shows the highest value of  $R$  followed by continuous roughness and sand bed. The value of  $R$  becomes negative irrespective of bed conditions above the location where Reynolds shear stress is negative. This observation is similar to that noted by Tachie (2001). The range of  $R$  as  $-0.3 < R < 0.5$  is also an indication of small to medium correlation between streamwise and vertical turbulence intensity throughout the depth of flow. The variation of  $R$  for lower Reynolds number flow is shown in Figure 4.6b and one can note that the profiles tend to be flatter from the bed up to  $y/d = 0.3$ .

#### 4.5 Higher-Order Moments

The distribution of different normalized velocity triple products  $\overline{u^3}$ ,  $\overline{u^2v}$ ,  $\overline{v^3}$  and  $\overline{v^2u}$ , which provide valuable information about the flow structures, are shown in Figure 4.7a to 4.7d. Directly measured quantities like depth of flow and maximum velocity are used as the length and velocity scales, respectively, to reduce any additional uncertainties related to scaling parameters with computed quantities. One can define  $\overline{u^3}$  and  $\overline{v^2u}$  as streamwise flux and  $\overline{u^2v}$  and  $\overline{v^3}$  as vertical transport/diffusion of the turbulent kinetic energy  $u^2$  and  $v^2$  respectively.  $\overline{v^2u}$  is also defined as wall normal transport of the Reynolds shear stress. Velocity triple products provide information about the ejection-

sweep cycle, which is the main turbulent motion responsible for most of the turbulent transport. One can also get an insight about the change/modification of turbulent transport mechanisms due to the change in bed condition by studying the variation of the different velocity triple products.

One can note from Figures 4.7a and 4.7b that for flow over a smooth bed,  $\overline{u^3}$  is negative and  $\overline{u^2v}$  is positive at locations very close to the bed. This indicates a slower moving fluid parcel with an upward transport of u momentum representing an ejection type motion. One can also note from the figures that  $\overline{u^3}$  and  $\overline{u^2v}$  change sign and become positive and negative, respectively, near the rough bed. A large positive value of  $\overline{u^3}$  and a negative value of  $\overline{u^2v}$  indicates a strong sweeping action motion in the streamwise direction that is partly directed towards the bed. As one progresses from the bed towards the free surface, both parameters change sign. A similar observation was made by Schultz and Flack (2007) and relate this change with changes of ejection-sweep cycle and modification of the longitudinal vortices with accompanying low-speed streaks produced by the rough bed. As one moves further from the bed ( $y > 0.08 d$ ), the value of  $\overline{u^3}$  becomes more negative causing a substantial reduction in the magnitude of the sweep event with the value being negative throughout the depth. One can also note the significant difference of  $\overline{u^3}$  between smooth and rough bed throughout the flow depth. This is in direct contrast with Flack et al. (2005), Schultz and Flack (2007) who didn't observe much variation at distance  $y/d > 0.2$ . However, Antonia and Krogstad (2001) found large differences in the variation of  $\overline{u^3}$  for flows over transverse rod roughness upto the edge of boundary layer. Grass (1971) related this difference to the lack of long

streamwise vortices near the rough wall. Grass (1971) also noted that the mechanics of the entrainment of low momentum fluid at the wall differed for rough bed conditions in comparison with the smooth wall. The trend in the variation of  $\overline{v^3}$  (Figure 4.7c) is very similar to the variation of  $\overline{u^2v}$  (Figure 4.7b) with the exception that  $\overline{v^3}$  is positive throughout the depth and the magnitude is much smaller (~60%) than  $\overline{u^2v}$ . Comparing  $\overline{v^2u}$  (Figure 4.7d) with  $\overline{u^3}$  (Figure 4.7a), one can qualitatively note a similar trend with the magnitude of  $\overline{v^2u}$  being much lower (about 20%~25%) than  $\overline{u^3}$ . Tachie (2001) and Balachandar and Bhuiyan (2007) in their open channel flow experiments and Schultz and Flack (2007) and Flack et al. (2005) in their turbulent boundary layer experiments had also noted a similar reduction. The differences between  $\overline{v^3}$  and  $\overline{u^2v}$  and  $\overline{v^2u}$  and  $\overline{u^3}$  are mainly due to the lower turbulent intensity in vertical direction. Although there are similarities in the magnitudes of the different triple products between open channel flow and turbulent boundary layer, there are differences in the extent over the depth these values are affected by roughness, mainly in the outer layer. One can note from Figure 4.7 that the value of normalized velocity triple products attain their local maxima/minima at similar locations ( $\approx 0.26d$  for smooth bed and  $\approx 0.33$  for different rough beds). One can also note a 200% to 300% change in magnitude of the different velocity triple products between the smooth and the rough beds. Balachandar and Bhuiyan (2007) also noticed significant decrease/increase ( $\sim 300\%$ ) between smooth bed and flow over dunes. This indicates that roughness has significant effect on the transportation of turbulent kinetic energy. As one moves from the location of the local maximum/minimum level towards the free surface, the magnitudes of the different velocity triple products approach zero for

all surfaces with the exception of  $\overline{u^3}$  for the distributed roughness. Distributed roughness shows significant turbulent activity even near free surface ( $y > 0.85d$ ).

One can note from above discussion that the near-zero value of triple correlations near the free surface is an indication of insignificant turbulent activity near the free surface. One can also note that the location of local maximum/minimum in the profiles is independent of the type of roughness. Distributed roughness profile shows the greatest variation followed by a similar variation in the case of the continuous roughness and the sand bed. Near-bed ( $y < 0.1 d$ ) turbulent activity also shows dependency on bed surface condition, such that, ejection type activity was observed for flow over smooth bed, whereas sweeping type of activity was observed for flow over rough bed. If one were to extrapolate the above mentioned flow process to real field scenario, such strong sweeping or ejection motions of fluid parcels could influence resuspension and transport. With exception of sweeping event observed at near-bed location of rough beds, ejection event was more prominent over the depth of flow. The strength of the ejection event again depends on the bed surface condition, with distributed roughness showing more ejection events than the other roughness conditions. The variation of different velocity triple products for lower Reynolds number is shown in Figure 4.8. The trend is very much similar to that for higher Reynolds number (Figure 4.7). One can note a reduction in difference in magnitude between smooth and rough surfaces (particularly for continuous and natural sand bed roughness) at the lower Reynolds number. One can also note a near-zero value of  $\overline{u^3}$  near the free surface for flow over all bed conditions, meaning a diminishing turbulent activity near free surface.

#### 4.6 Vertical Flux of the Turbulent Kinetic Energy

Describing  $F_{kv}$  as vertical flux of the turbulent kinetic energy, Figure 4.9 shows the variation of  $F_{kv}$  on smooth and rough surfaces in outer variables. Vertical flux of the turbulent kinetic energy is normally measured as  $0.5(\overline{v^3} + \overline{vu^2})$  for a two-dimensional flow (Balachandar and Bhuiyan, 2007). Due to the unavailability of the third component of turbulent intensity, an approximate method is adopted here by replacing the coefficient 0.5 with 0.75 (Krogstad and Antonia, 1999). One can note from Figure 4.9 that there is a significant change in the profile due to roughness and this is an indication that roughness has a significant effect on the transport of the turbulent kinetic energy in the vertical direction. The profiles of  $F_{kv}$  for rough beds are displaced higher from the smooth bed through most of the depth. It should be noted that for large-bottomed roughness, Balachandar and Bhuiyan (2007) did not find any difference in profiles for  $F_{kv}$  over the depth between flow between rough and smooth beds.

Tachie (2001) noted that the location of the outer (larger) peak of  $F_{kv}$  is closer to the wall (albeit slightly) as the roughness effect increases. Balachandar and Bhuiyan (2007) also noted the occurrence of a maximum value near the bed for rib roughness. However, although there is an obvious effect of roughness on the peak value of  $F_{kv}$ , the location of peak value ( $y/d \sim 0.3$ ) is nearly the same for all roughness. The gradient of  $F_{kv}$  is the indication of loss or gain of turbulent kinetic energy due to turbulent diffusion. The differences in magnitude of  $F_{kv}$  between smooth and rough bed is an indication of the differences in the strength in transport of turbulent kinetic energy between smooth and rough bed. The vertical flux of turbulent kinetic energy gradually reduces after a peak value around  $y = 0.3d$  and eventually approaches zero near the free surface. The vertical

flux of turbulent kinetic energy reaches zero for smooth surface first followed by different roughness. One can also note that the variation of  $F_{kv}$  is more or less same for both Reynolds number flows.

#### 4.7 Quadrant Analysis

Quadrant decomposition is a convenient tool to extract the magnitude of the Reynolds shear stress of turbulent bursting events. Turbulent flow over a fixed bed causes a hydrodynamically unstable low-speed fluid particle lifting up from the surface and eventually swept away by high-speed fluid moving towards the wall from the outer layer. Based on their sign, streamwise and vertical fluctuating velocity components  $u$  and  $v$  are separated into four groups to sort turbulent events which eventually play an important role in the turbulent phenomenon close to the wall. Four different turbulent bursting events are related to the four quadrants. Bursting effect related to Quadrant 1 (Q1:  $u > 0$  and  $v > 0$ ), Quadrant 2 (Q2:  $u < 0$  and  $v > 0$ ), Quadrant 3 (Q3:  $u < 0$  and  $v < 0$ ) and Quadrant 4 (Q4:  $u > 0$  and  $v < 0$ ) are known as outward interaction, ejection, inward interaction and sweep, respectively.

The contributions from Q2 and Q4 events to the Reynolds shear stress are shown in Figure 4.10 ( $Re = 47,500$ ) for different threshold values. One can note from Figures 4.10a and 4.10b that the magnitude of Q2 and Q4 contributions is higher for the rough walls than that of smooth wall for  $H = 0$  (i.e., inclusive of all turbulent events). The effect of roughness is clearly visible well beyond the near-bed region and deep into the outer layer ( $y/d \approx 0.7$ ). As one progresses from the bed towards the free surface, Q2 and Q4 contributions reach a local peak for all rough beds at  $y/d = 0.1 \sim 0.2$ . Following this local



peak, the magnitudes of the events reduce towards the free surface and attains a near-zero constant value. The location of attainment of a near-zero constant value is different for the different surface conditions. This distance is  $0.5d$  for the smooth bed surface,  $0.6d$  for continuous roughness and sand bed and  $0.75d$  for the distributed roughness. One can also note that the variation is very similar for continuous roughness and sand bed, while distributed roughness shows the maximum deviation from smooth wall value in the outer layer ( $y > 0.2d$ ). Schultz and Flack (2005) found the magnitude of Q2 and Q4 events to be significantly higher in the near-bed region but found the distribution for both the smooth and rough walls to be very similar in the outer layer.

Quadrant analysis was also carried out at different threshold levels ( $H = 2$  to  $5$ ) to investigate the contribution of the extreme turbulent events. This approach was taken to filter out the small random turbulent fluctuations and consider the contribution of the more energetic eddies. Figures 4.10c and 4.10d show the contributions from the events whose amplitude exceeds the threshold value of  $H = 2$ . Although the number of Q2 and Q4 events reduce sharply for change of threshold value from  $0$  to  $2$ , the events with  $H = 2$  produced very large instantaneous Reynolds shear stress ( $> 5.5 \overline{uv}$ ), which can potentially influence the sediment transport, resuspension of pollutant from the bed, bed formation, transport of nutrients, entrainment and the exchange of energy and momentum. The data trend at  $H = 2$  is very similar to  $H = 0$ , however, the affected region of the flow depth for Q4 events reduces in comparison to  $H = 0$ . Figures 4.10e to 4.10l show the contributions for other threshold levels ( $H = 2.5$  to  $5$ ). One can note that the affected region over the flow depth for Q4 events reduces with the increase of threshold value of  $H$ , but the Q2 events are clearly affected deep into the outer layer ( $y/d \sim 0.7$ ) for

the value of  $H$  as high as 5. Irrespective of the affected region of the depth, the increase in both Q2 and Q4 contribution to the Reynolds shear stress due to the incorporation of roughness is clearly visible. Schultz and Flack (2005) and Krogstad et al. (1992) found stronger Q2 events on a smooth wall compared to a rough wall for near-bed locations and relate this phenomena to strongly favored Reynolds stress contributions from ejection (Q2 events) for the smooth wall. Differences between turbulent boundary layer flow and open channel flow confirms that the effect of roughness on turbulent bursting and eventual production of Reynolds shear stress due to ejection and sweep is different for open channel flow. Balachandar and Bhuiyan (2007) noted significant ejection and sweep components throughout the depth with ejection events being dominant. They also noted significant variations with different types of rib roughness. In the present study, one can notice the dependence of Q2 and Q4 on bed roughness accompanied by significant drop of both events near the free surface. This signifies the importance of type of bed roughness on Q2 and Q4 events. Generation of turbulent activity near bed varies with type of bed roughness. Slow moving low momentum fluid from the near-bed and the fluid between the interstices of the roughness is ejected and travels towards the outer layer/free surface. Whereas, high momentum fluid from outer layer travels towards bed and sweep away the ejected low momentum fluid parcels. Existence of intermittent sweep and ejection events is universal but the extent of affected flow depth is dependent on the bed and the flow condition. The contributions from Q2 and Q4 events to the Reynolds shear stress for lower Reynolds number ( $Re = 31,000$ ) flow are shown in Figure 4.11 and the trends are very similar to the higher Reynolds number flow for the different threshold values.

The ratio of  $Q_2/Q_4$  to the Reynolds shear stress is shown in Figure 4.12 for  $H = 0$  to 5. One can note from Figures 4.12 that at the near-bed location, the  $Q_2/Q_4$  ratio is near unity, indicating identical strength of sweep and ejection events. As one progress from the bed towards the free surface, the ratio increases from one to a maximum at  $y \sim 0.5d$ , indicating relatively stronger ejection events. The strength of the ejection events in comparison to sweep events increases with increasing  $H$ . One can note a 100 fold increase for the threshold value of  $H = 5$  compared to  $H = 0$ . The ratio of Reynolds shear stress in  $Q_2$  and  $Q_4$  shows little dependency on bed condition for  $H = 0$  but shows some effect of roughness for  $y > 0.5d$ .

The ratio of the number of events in  $Q_2$  and  $Q_4$  is shown in Figure 4.13 for  $H = 0$  to 3. Unlike the ratio of  $Q_2$  and  $Q_4$  (Figure 4.12), the ratio of number of events contributing to  $Q_2$  and  $Q_4$  shows different trends for  $H = 0$  (Figures 4.13a and 4.13b) and  $H = 2$  to 3 (Figures 4.13c to 4.13h). One can note from Figures 4.13a and 4.13b that at the near-bed location, the occurrence of ejection and sweep events are almost equal but as one progress from the bed towards the free surface, the value of  $N_{Q_2}/N_{Q_4}$  reaches a minimum around  $y \sim 0.5d$ , indicating a reduction in ejection events. Moving farther from bed and towards the free surface, the value of  $N_{Q_2}/N_{Q_4}$  increases and reaches unity, indicating occurrence of identical number of sweep and ejection events. Figures 4.13c to 4.13h show a trend different from Figures 4.13a and 4.13b. As one progress from the bed towards the free surface, the value of  $N_{Q_2}/N_{Q_4}$  increases from near unity to thirty folds at around  $y \sim 0.5d$ , indicating increase in ejection events. The ratio of number of events in  $Q_2$  and  $Q_4$  shows little dependency on bed condition for  $H = 0$  but shows some effect of roughness for flow depth of  $y > 0.3d$ .

## 4.8 Conclusions

The present study was carried out to understand the extent of effect of roughness and Reynolds number on mean velocity, turbulence, Reynolds shear stress, velocity triple products in an open channel flow. To this end, four different types of bed surface conditions and two different Reynolds number were adopted in the study. Quadrant decomposition was also used to extract the magnitude of the Reynolds shear stress from the turbulent events. The present experimental results disputed the ‘wall similarity hypothesis’ initially proposed by Townsend (1976) and generalized by Raupach et al. (1991), where it was suggested that outside the roughness layer, the turbulent mixing properties in smooth and rough walls should be essentially the same. The main findings are summarized as follows:

1. Surface roughness increases the surface drag causing the mean velocity profile to be less full compared to the smooth bed. The effect of the roughness on the mean velocity profile is very much evident throughout the flow depth with the distributed roughness exhibiting the largest deviation from the smooth profile while the continuous roughness and natural sand bed show similar deviation for the higher flow Reynolds number. Natural sand bed shows a larger deviation than continuous roughness for the lower Reynolds number.
2. Based on the magnitude of friction velocity, in general, the results show that distributed roughness shows the greatest roughness effect followed by sand bed and continuous roughness. As expected, it was also found that friction coefficient reduces as the Reynolds number increases. Flow over a natural bed results in a reduction of friction coefficient compared to the flow over an impermeable rough surface.

3. With the exception of the region very close to the bed, roughness effect on turbulence intensity is present throughout the flow depth with distributed roughness profile showing a maximum deviation from a smooth bed, followed by sand bed and continuous roughness. Streamwise turbulence intensity reduces but wall-normal turbulence intensity increases at locations very close to the bed due to the introduction of roughness. Although the same sand grain is used to create the three different rough bed conditions, the difference in turbulence intensity is an indication that specific geometry of the roughness has an influence on turbulence structure.
4. The flow over the rough beds generates higher near-wall Reynolds shear stress than the smooth bed. The effect of bed condition on Reynolds shear stress is distinctly visible from near-bed to the depth of flow as high as  $y \approx 0.7d$ .
5. Variation of the correlation coefficient,  $R$  in the outer layer compared to the near-wall is an indication of change of flow structures between the two regions, clearly opposing the observation of Nezu and Nakagawa (1993) that the distribution of  $R$  is universal and independent of the properties of the mean flow and the wall roughness.
6. The result shows a 200% to 300% decrease/increase in magnitude of the different velocity triple products between smooth and rough beds. This indicates that roughness has a significant effect on the transportation of turbulent kinetic energy and Reynolds shear stress.
7. Near-bed turbulent activity also shows dependency on bed surface conditions, such that, ejection type activity dominates for flow over smooth bed, whereas sweeping dominates for flow over the rough bed. If one were to extrapolate the above

- mentioned flow process to real field scenario, such strong sweeping or ejection motions of fluid parcels could influence resuspension and sediment transport.
8. With exception of sweeping events observed at near-bed location for rough beds, ejection events were more prominent over the depth of flow. The strength of ejection event again depends on the bed surface condition, with distributed roughness showing more ejection events than other roughness conditions.
  9. Results from the analysis of turbulent bursting events (through quadrant decomposition) show clearly visible effect of roughness well beyond the near-bed region and deep into the outer layer ( $y/d \approx 0.7$ ). Results show that the magnitude of Q2 (ejection) and Q4 (sweep) contributions is very much higher for the rough walls than that of smooth wall for  $H = 0$ .
  10. By investigating the contribution of the extreme turbulent events ( $H = 2$  to  $5$ ), results show active Q2 (ejection) events for most of the flow depth, whereas, the affected flow depth for active Q4 (sweep) events reduces with increasing  $H$  value. Although the number of Q2 and Q4 events reduce sharply with change in threshold value, the extreme events produced very large instantaneous Reynolds shear stress ( $> 5.5 \overline{uv}$  for  $H = 2$ ), which can potentially influence the sediment transport, resuspension of pollutant from bed, bed formation, entrainment and the exchange of energy and momentum.
  11. The near unit value of the ratio of Reynolds shear stress for Q2 and Q4 events is an indication of identical strength of ejection and sweep for the lower and the upper third of the flow depth. Middle third of the flow depth shows relatively stronger ejection

events with the strength of ejection events increases sharply with the increasing  $H$  value.

12. Similar to the identical strength of ejection and sweep, the number of events for ejection and sweep is also identical for lower and upper third of the flow depth. However, the middle third of the flow depth shows relatively less ejection events for  $H = 0$  but shows much higher ejection events for  $H = 2$  or more.

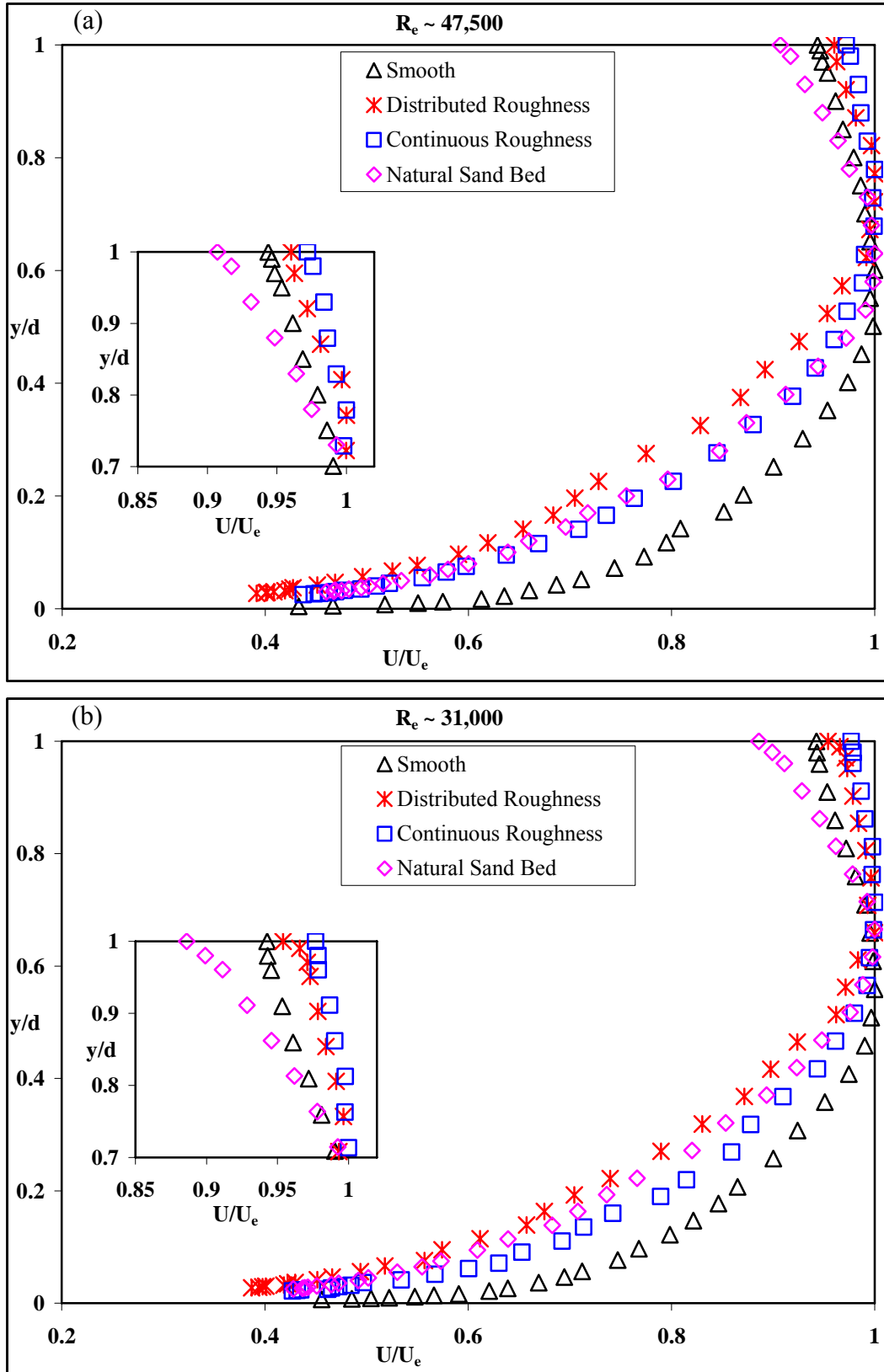


Figure 4.1: Streamwise mean velocity profile for flow over different bed condition.



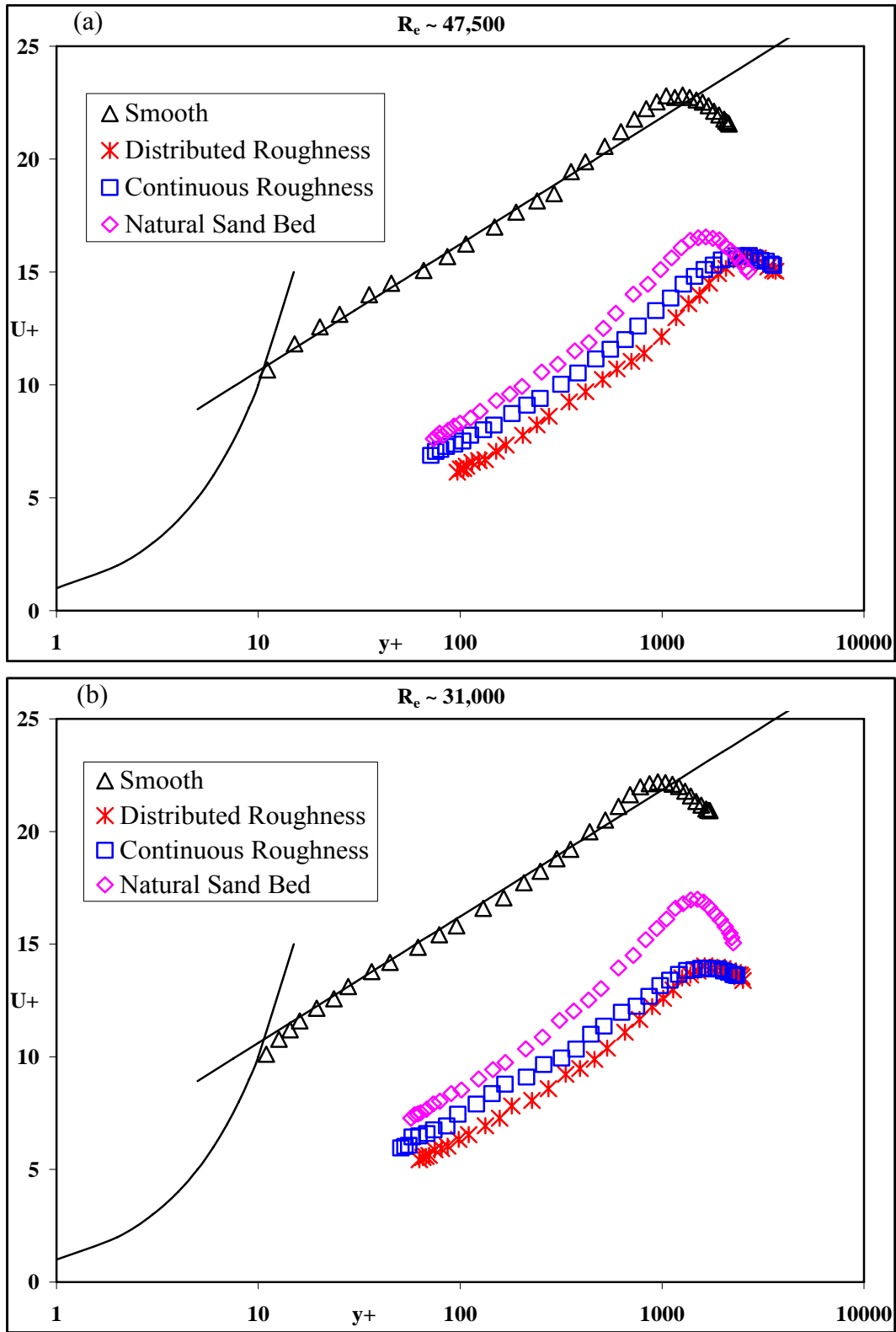


Figure 4.2: Mean velocity profile in inner coordinates for flow over different bed condition.

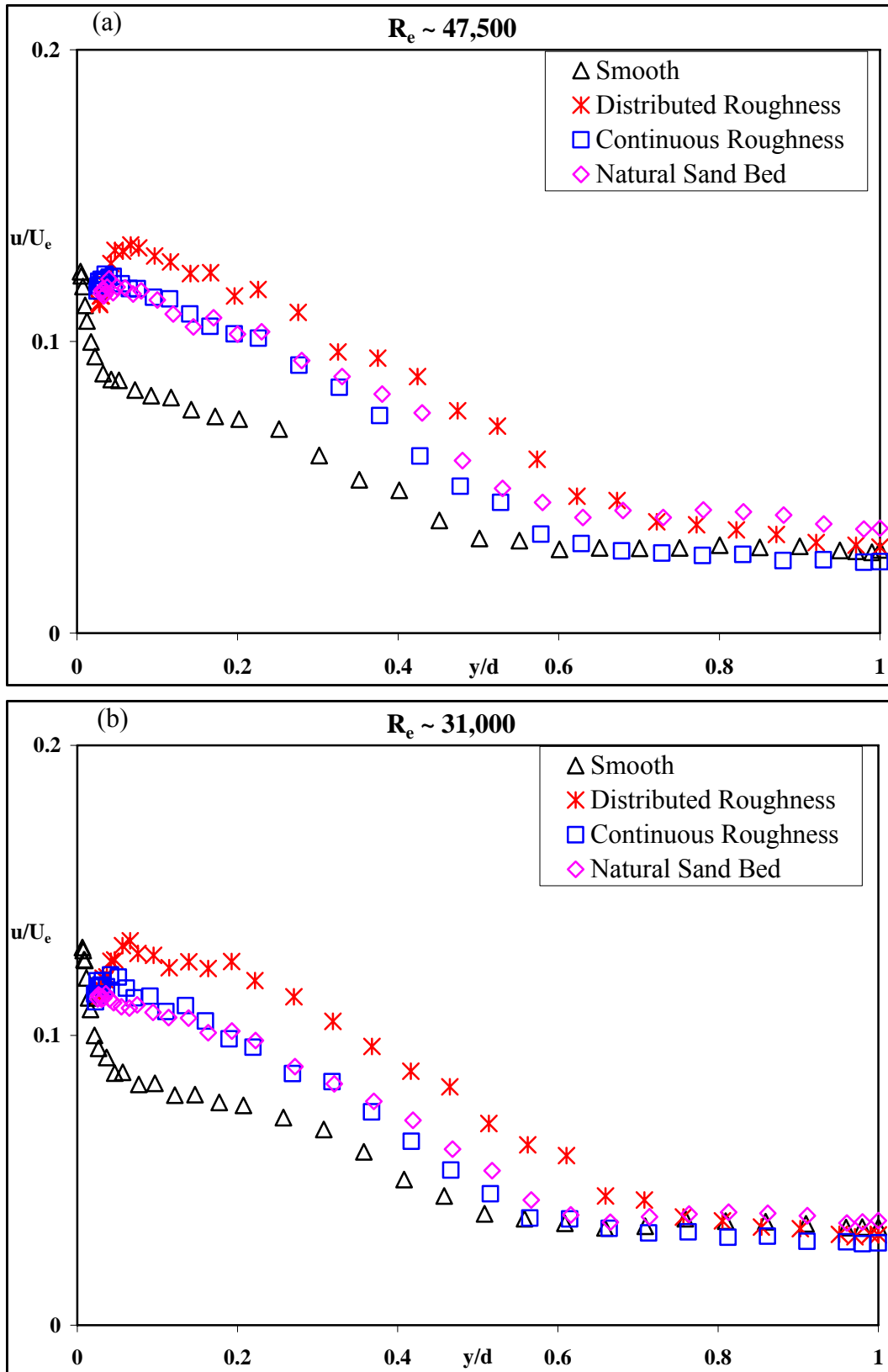


Figure 4.3: Streamwise turbulence intensity for flow over different bed condition.

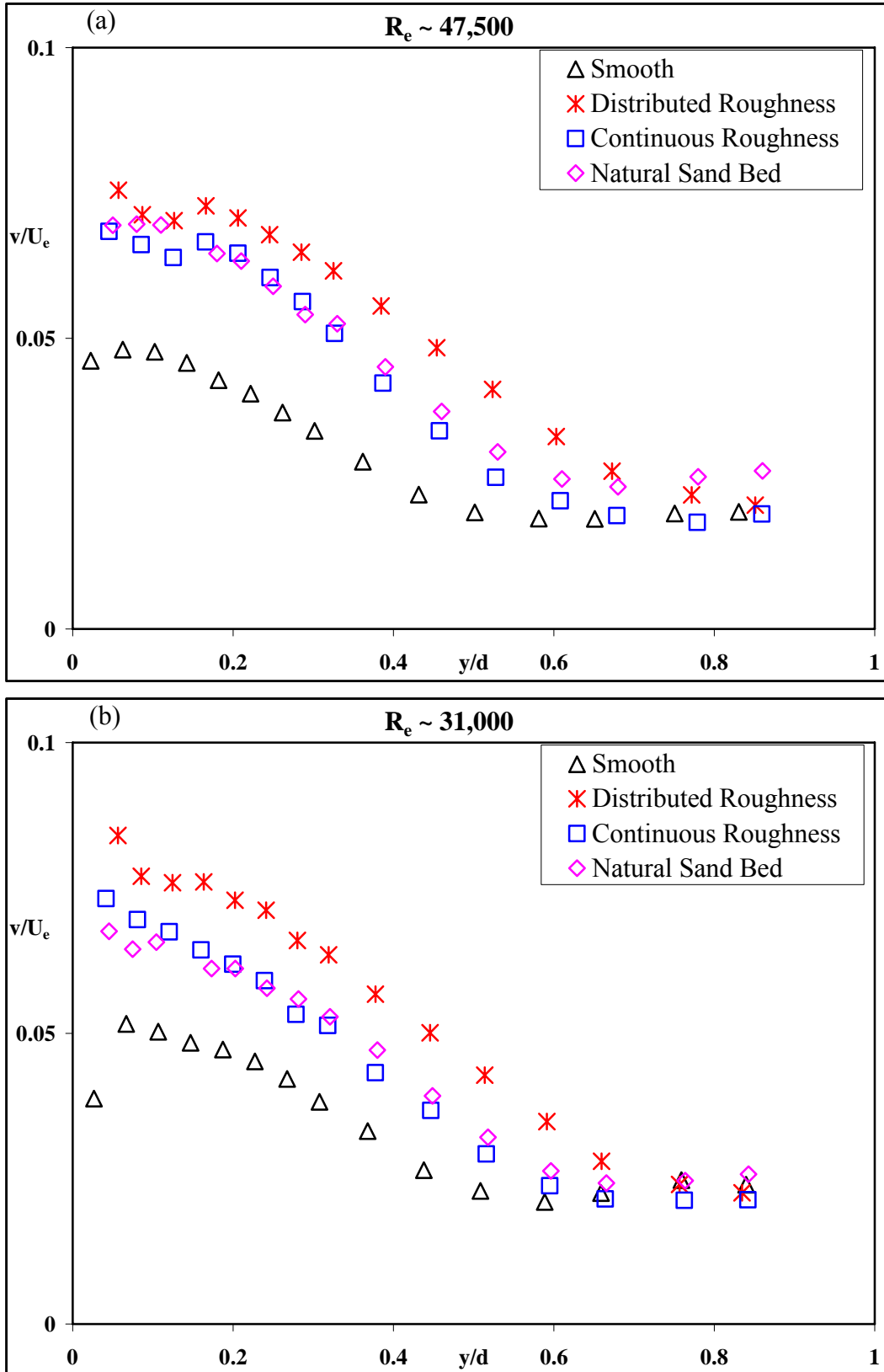


Figure 4.4: Vertical turbulence intensity for flow over different bed condition.

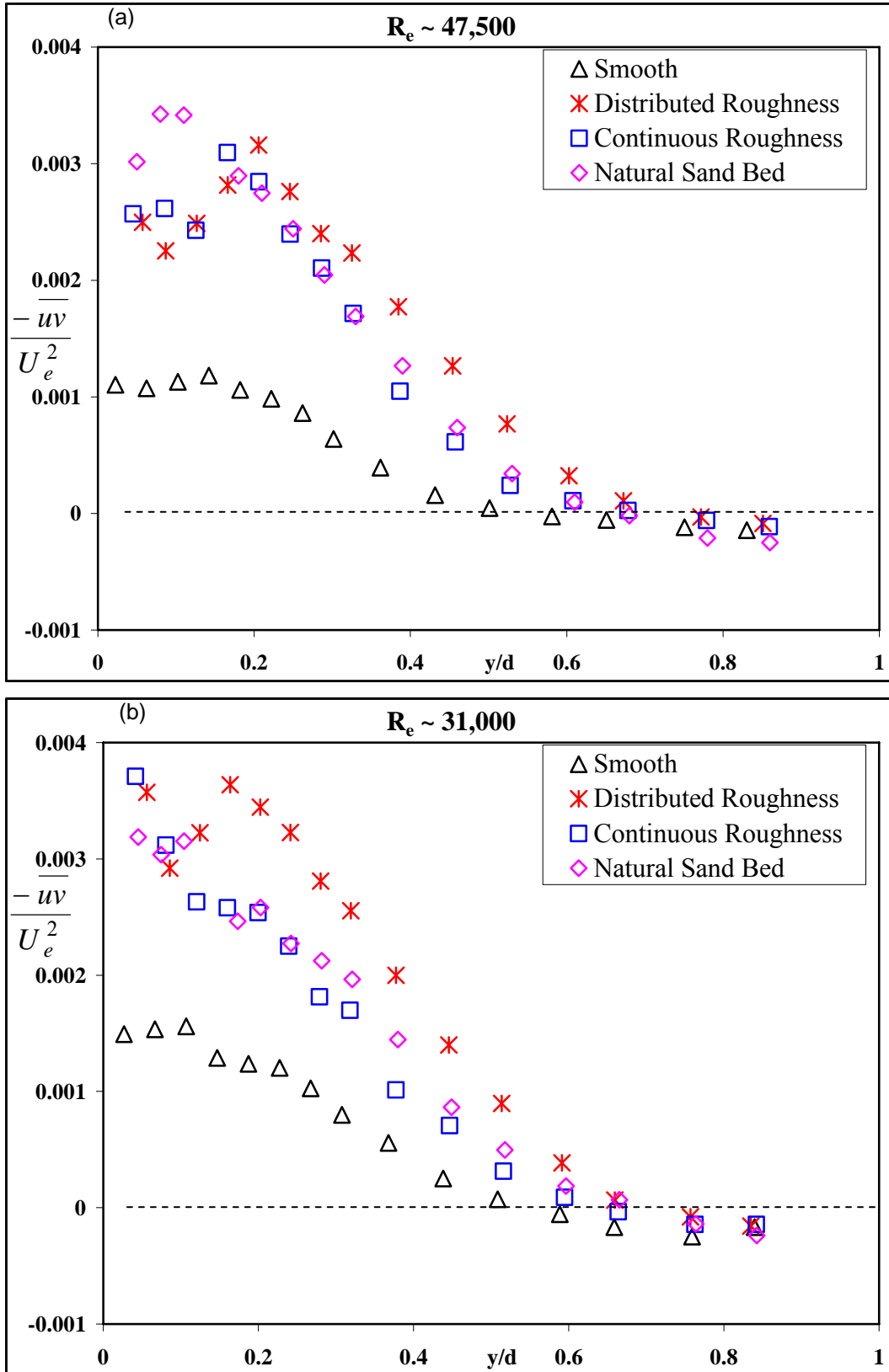


Figure 4.5: Reynolds shear stress distribution for flow over different bed condition.

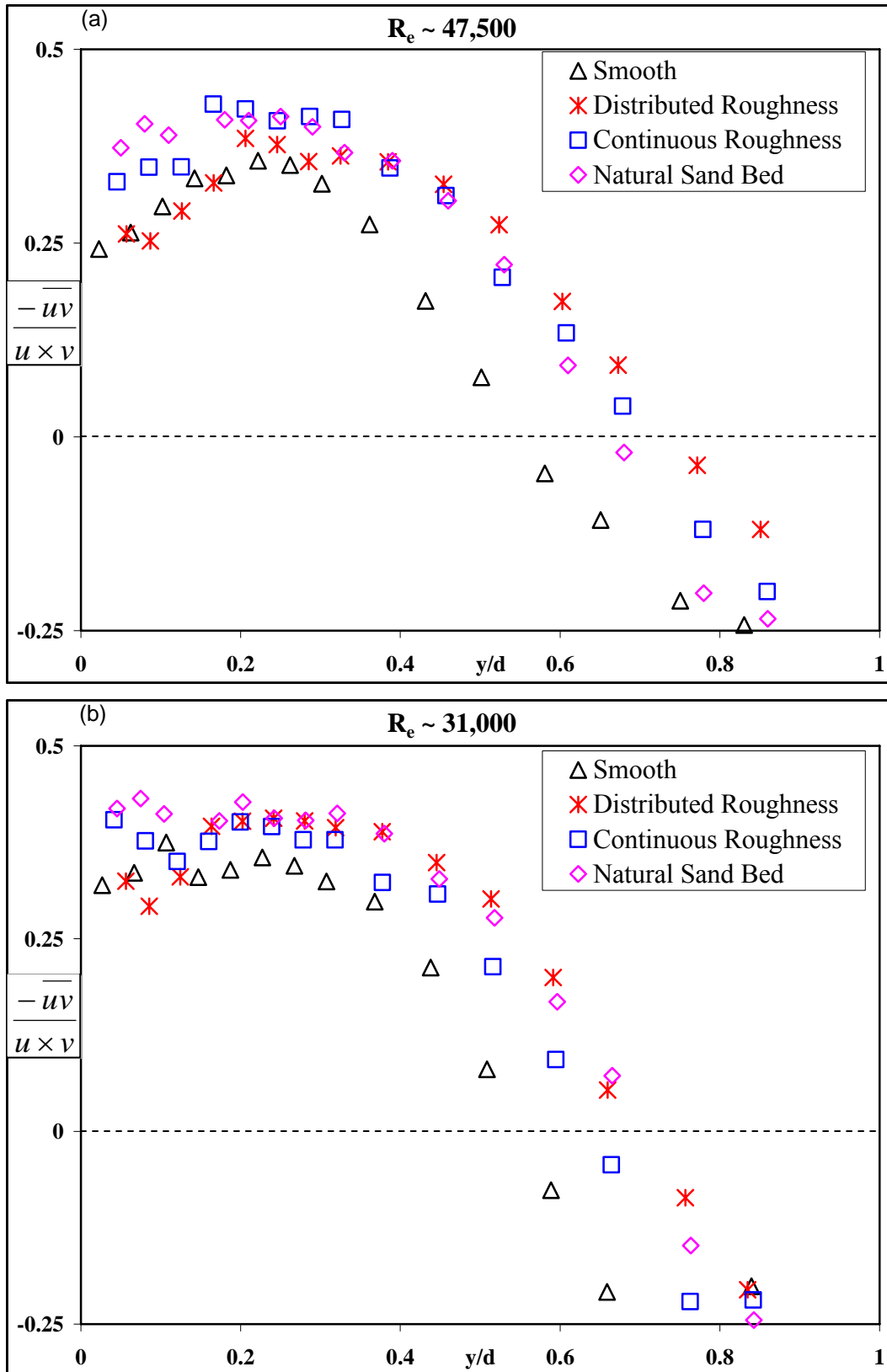


Figure 4.6: Distribution of correlation coefficient for flow over different bed condition.

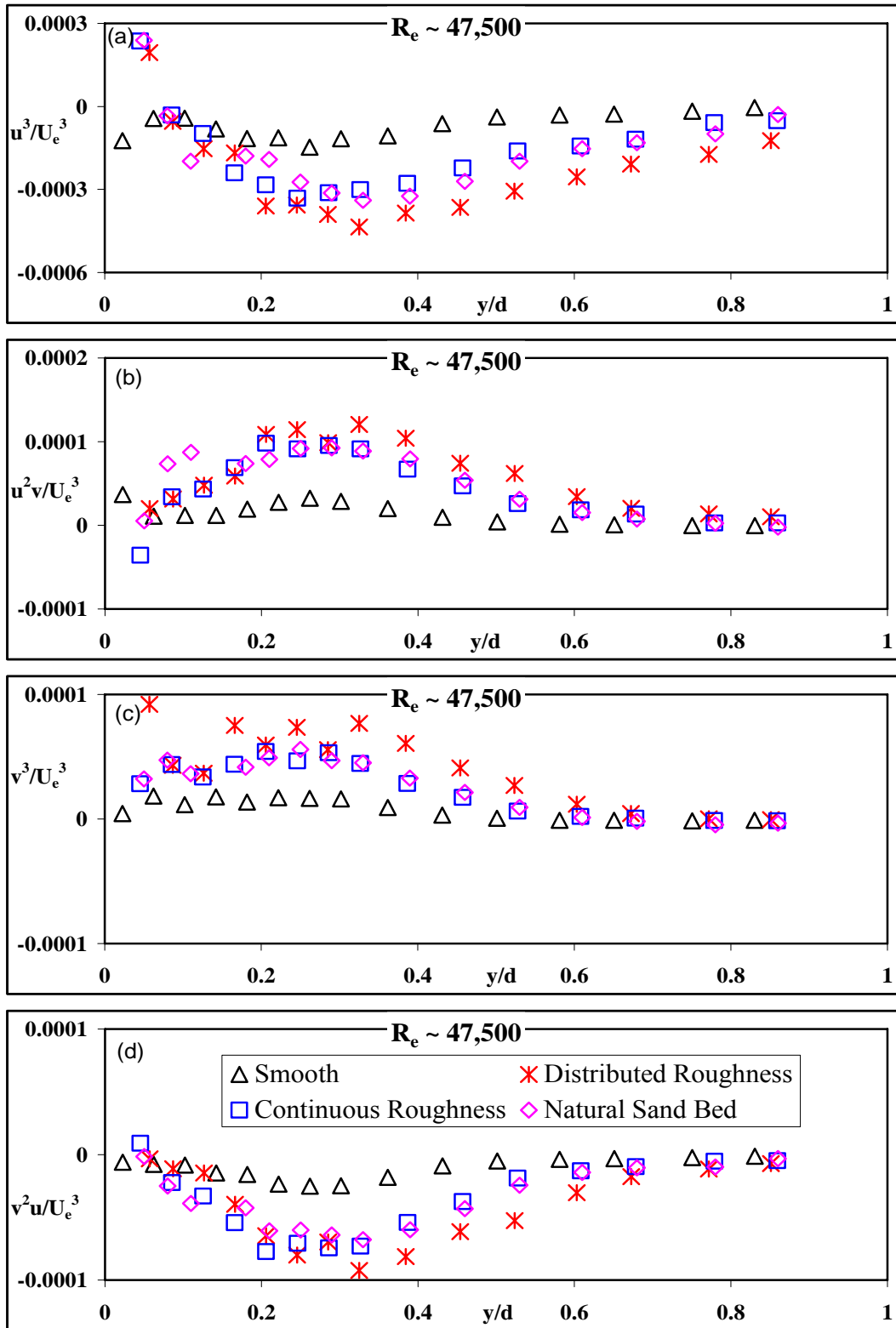


Figure 4.7: Distribution of different velocity triple products for flow over different bed condition at  $Re \sim 47,500$

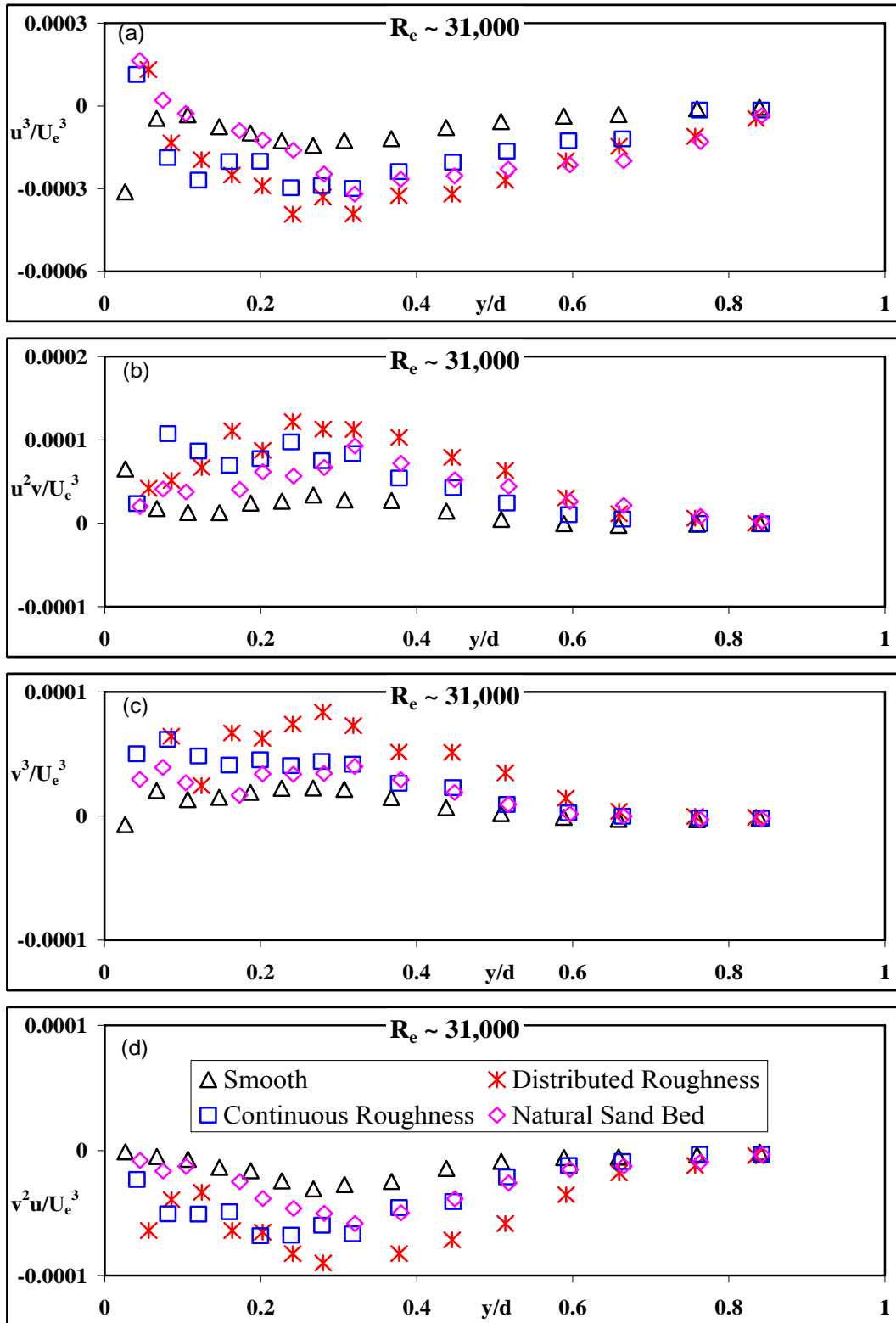


Figure 4.8: Distribution of different velocity triple products for flow over different bed condition at  $Re \sim 31,000$

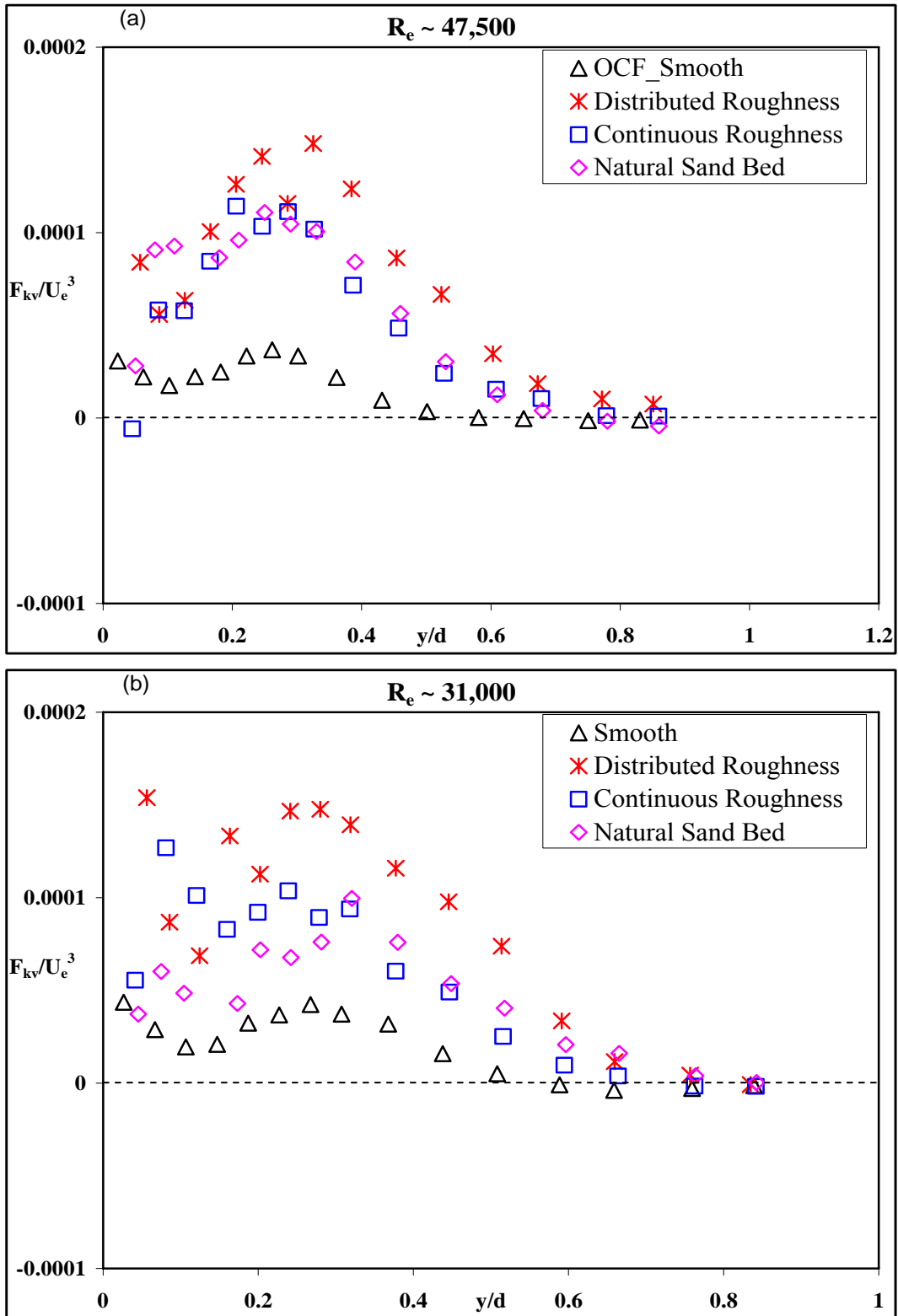


Figure 4.9: Distribution of vertical flux of the turbulent kinetic energy for flow over different bed condition



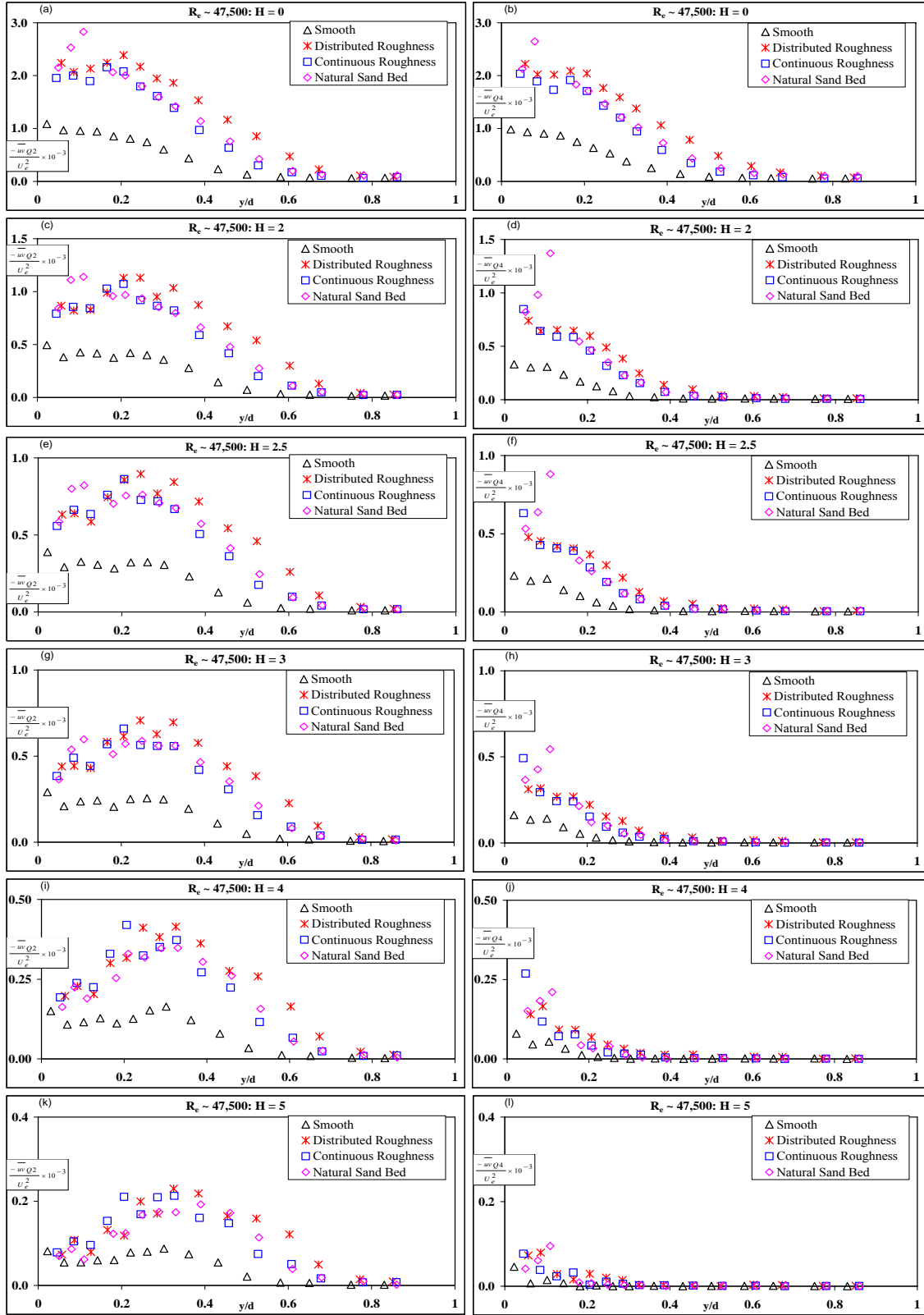


Figure 4.10: Contribution of different quadrant events to the Reynolds shear stress for flow over different bed condition with higher Reynolds number.

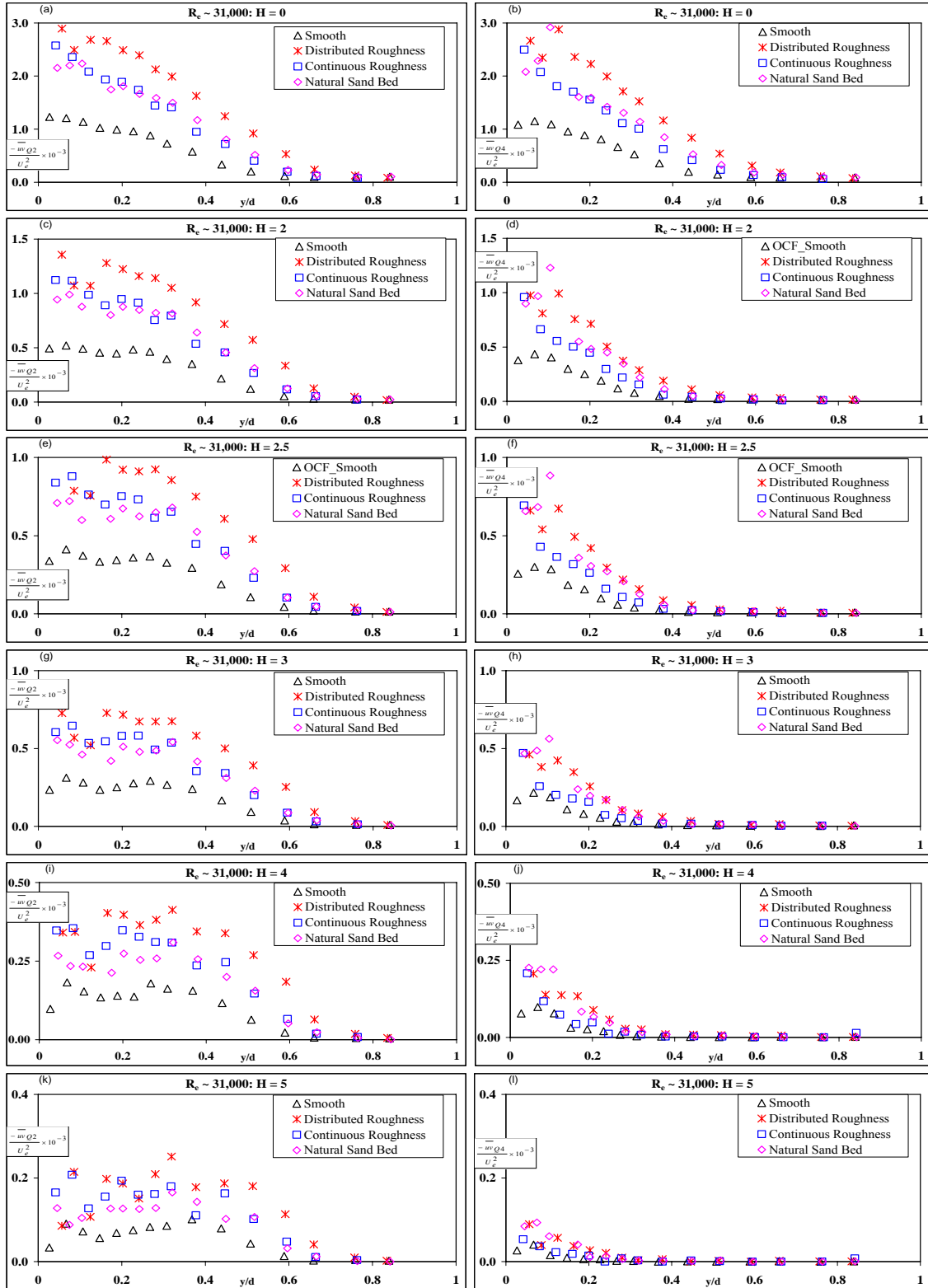


Figure 4.11: Contribution of different quadrant events to the Reynolds shear stress for flow over different bed condition with lower Reynolds number.

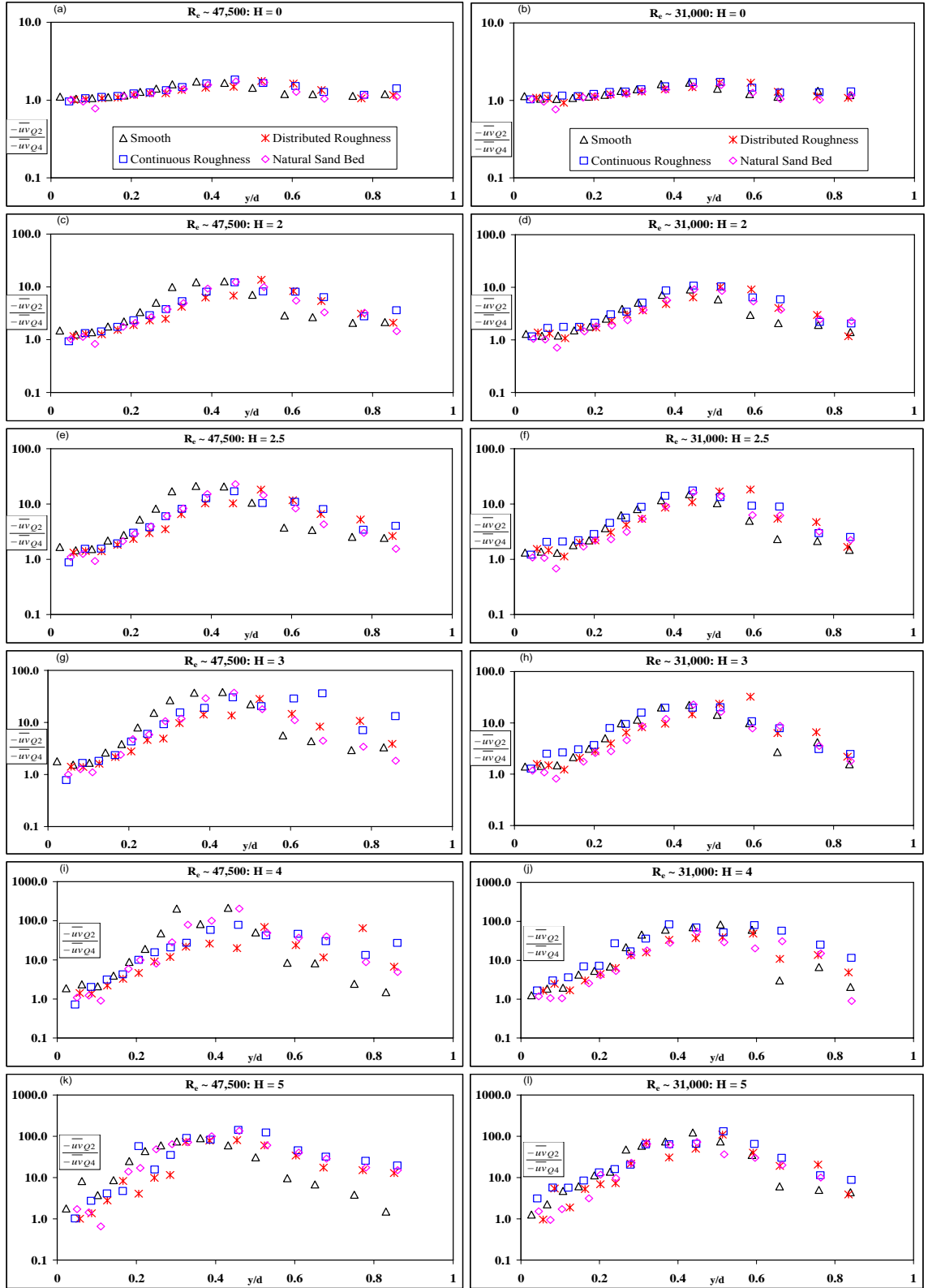


Figure 4.12: Ratio of different quadrant events to the Reynolds shear stress for flow over different bed condition.

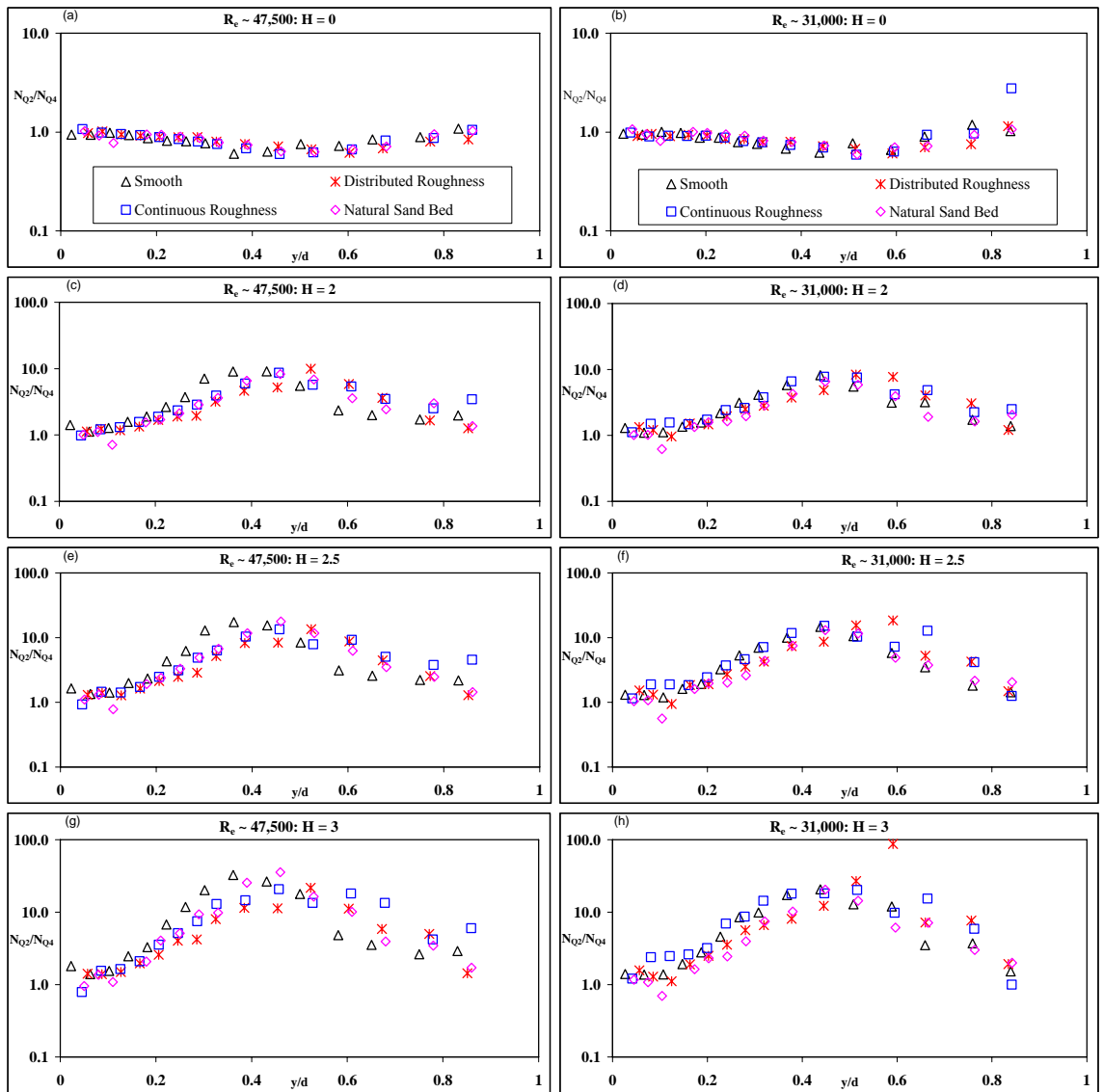


Figure 4.13: Ratio of number of different quadrant events for flow over different bed condition.

## CHAPTER 5

### SEEPAGE EFFECTS IN OPEN CHANNEL FLOW

This chapter focuses on the effect of the introduction of seepage on different turbulent characteristics in an open channel flow. Test results with both suction and injection are presented and discussed to understand the extent of influence of seepage in the depth-wise direction at two different flow rates. Particular attention is paid to mean velocity, turbulence intensity, Reynolds shear stress, shear stress correlation, higher-order moments and quadrant analysis.

#### 5.1 Mean Velocity Profiles

##### 5.1.1 Outer Coordinates

The distributions of the streamwise component of the mean velocity in outer coordinates are shown in Figure 5.1. Maximum velocity ( $U_e$ ) and flow depth ( $d$ ) are used to non-dimensionalize the streamwise mean velocity ( $U$ ) and the wall normal distance ( $y$ ), respectively. In each of the graphs accompanying this chapter, the legend notation is standardized to indicate the type of seepage (injection (INJ) or suction (SUC)) and the magnitude of the seepage (expressed as a % of the total flow rate). As presented in Figure 5.1a, for injection, one can note a decrease in velocity near the bed and an increase in velocity near the free surface in comparison to the no seepage condition. This is more clearly demonstrated in the insets of Figure 5.1a. A similar observation of decrease in the near bed velocity was also made by Watters and Rao (1971) and related it to a lower drag force on the bed material. One can also note from Figure 5.1a that the reduction of the near bed velocity and the increment in the near free surface velocity, increases with the

increase of injection rate. A similar streamwise mean velocity distribution was also observed (Figure 5.1b) for the higher flow rate, but the extent of respective reduction or increase in the velocity near the bed or near the free surface, is less than the variation observed with the lower flow rate (Figure 5.1a).

The distributions of the streamwise component of the mean velocity for suction conditions are shown in Figures 5.1c and 5.1d for the lower and higher flow rates, respectively. One can note from Figures 5.1c and 5.1d that the velocity profiles become more uniform in comparison to the no-seepage condition due to an increase in velocity near the bed. The increased velocity in the near-bed location causes the reduction in velocity near the free surface (see insets in Figures 5.1c and 5.1d) to satisfy continuity considerations. A similar observation was also made by Chen and Chiew (2004). Watters and Rao (1971) related the increase in the near-bed velocity to cause a higher drag force on the bed material. One can also note from Figure 5.1c that the increase of the near-bed velocity and the decrease in the free surface velocity, increases with the increase of suction rate. The effects of suction on streamwise mean velocity is very similar for both lower and higher flow rates.

In the outer region, each velocity profile shows a slight dip (insets in Figure 5.1) where the local maximum value ( $U_e$ ) occurs below the free surface and  $dU/dy$  is negative in the vicinity of the free surface. The magnitude of velocity dip varied with the variation of injection or suction rates. Results also show an increase in the maximum mean streamwise velocity due to the introduction of injection and show an opposite trend for suction. Richardson et al. (1985) also noted an increment in mean channel velocity with injection.

### 5.1.2 Inner Coordinates

The distributions of the streamwise component of the mean velocity in inner coordinates are shown in Figure 5.2. The friction velocity was calculated using the Clauser method by fitting mean velocity profiles into the classical log law with  $U^+ = \kappa^{-1} \ln y^+ + B - \Delta U^+$ . Here,  $U^+ = U/U_\tau$ ,  $y^+ = yU_\tau/\nu$ ,  $\kappa = 0.41$  and  $B = 5$  are log-law constants and  $\Delta U^+$  is the roughness function representing the downward shift of the velocity profile. One can note from Figure 5.2a that there is clearly a visible downward shift of the profile compared to the no seepage condition. The downward shift of the profile can also be related to an increasing roughness which corresponds to an increase in the friction velocity. Figure 5.2b shows the streamwise component of the mean velocity in inner coordinates for the higher Reynolds number. The results are similar to that of the lower Reynolds number.

The distributions of the streamwise component of the mean velocity for suction in inner conditions are shown in Figures 5.2c and 5.2d for the two flow rates, respectively. One can note from the figures that there is clearly a visible upward shift of the profiles with respect to the no-seepage condition. The upward shift indicates a decrease in friction with increasing suction.

## 5.2 Bed Stability

Channel bed particles are subjected to a number of forces in open channel flow. Some of the forces act as resistance to the movement of particles (weight, friction of bed particles, vertical downward drag for suction etc.) while some forces (streamwise drag force, lift, vertical upward drag for injection etc.) are favorable to the movement. As the

value of static friction coefficient is much higher than kinetic friction coefficient, the bed particles become more susceptible to erosion when the bed is transporting or eroding initially. Due to the very low magnitude of vertical velocity (due to introduction of seepage), the contribution of the vertical downward drag for suction or the vertical upward drag for injection can be assumed to be negligible for bed motion. The stability of the bed particles is expected to depend largely on the net increase or decrease of the streamwise drag force due to seepage.

From Figures 5.1 and 5.2, one can see a change in the near-bed velocity, which is responsible for the form drag (of the individual particle) and a change in friction velocity, which is responsible for surface drag (bed) due to incorporation of seepage (injection/suction). The near-bed velocity reduces with increasing injection but increases with increasing suction. The friction velocity increases with increasing injection but decreases with increasing suction. The percentage variation of near bed velocity and friction velocity in comparison with no seepage condition is shown in Table 5.1. As the stability of the bed particles depend on the net increase or decrease of the total drag force, one can note from injection perspective that a reduction in the near bed velocity is much more than the relative increment of friction velocity. This results in an increase in bed stability (Table 5.1). Similarly, one can note from the suction perspective that the increment of near bed velocity is much more than the relative reduction of friction velocity, thus resulting in reduced bed stability (Table 5.1). These observations are consistent with previous observations of increased bed stability with injection and reduced bed stability with suction by Rao and Sitaram (1999) and Watters and Rao (1971).



## 5.3 Turbulence Intensity

### 5.3.1 Streamwise Turbulence Intensity

Figure 5.3 shows the streamwise turbulence intensity in outer variables. Once again, directly measured quantities like depth of flow and maximum velocity are used as the length and velocity scales, respectively, to reduce any additional uncertainties related to scaling parameters with computed quantities. One can note from Figure 5.3a that streamwise turbulence intensity attains a maximum value very close to the wall ( $y/d \sim 0.02$ ) for all flow conditions. There is no significant effect of injection that can be observed from the bed up to the location of this peak. With the exception of the region very close to the bed, effect of injection is prevalent through most of the flow depth ( $0.05d \sim 0.8d$ ). For this region, streamwise turbulence intensity increases with injection rate. For  $y/d > 0.8$ , the streamwise turbulence intensity reduces towards the free surface and attains a nearly constant value for all flow conditions. Similar streamwise turbulence intensity distribution can also be observed (Figure 5.3b) for the higher flow rate, but the increase in magnitude with increasing injection is much lower than those for the lower flow rate. It can also be observed that the portion of constant streamwise turbulence near the free surface tends to increase with increasing flow rates.

The variation of streamwise turbulence intensity for suction are shown in Figures 5.3c and 5.3d for the lower and higher flow rates, respectively. Suction causes a reduction of streamwise turbulence intensity for most of the flow depth ( $0.05d \sim 0.75d$ ). However, beyond  $y = 0.75$ , an increase in the streamwise turbulence intensity can be seen up to the free surface, albeit small. Unlike injection, the effects of suction on streamwise turbulence intensity are very similar for both lower and higher flow rates.

### 5.3.2 Vertical Turbulence Intensity

Figure 5.4 shows the vertical turbulence intensity in outer variables. One can note from Figures 5.4a and 5.4b that vertical turbulence intensity increases with the introduction of injection in comparison to no seepage condition for most of the depth but the difference is less for higher flow rates. On the other hand, Figures 5.4c and 5.4d show a reduction of vertical turbulence intensity with suction in comparison to the no seepage condition and the difference is very similar for both lower and higher flow rates. Although the intensity of vertical turbulence is around 50% of the streamwise turbulence, this value can be a major contributing factor to mixing.

### 5.4 Reynolds Shear Stress

Figure 5.5 shows the Reynolds shear stress distribution in outer variables. For injection (Figure 5.5a), one can note an increase in Reynolds shear stress in comparison to the no seepage condition for most of the depth. A similar distribution was also observed for the higher flow rate (Figure 5.5b), but the amount of increment and the affected region of flow depth is less than the variation observed with the lower flow rate. One can see a reduction in Reynolds shear stress in comparison to the no seepage condition with the introduction of suction (Figures 5.5c and 5.5d) and the difference is distinctly visible for  $y < 0.7d$ . Unlike injection, the effects of suction on Reynolds shear stress are very similar for both lower and higher flow rates. One can also note from Figure 5.5 that near the free surface, the Reynolds shear stress reduces and becomes negative for all flow conditions above the location where  $dU/dy$  is negative.

## 5.5 Shear Stress Correlation Coefficient

Figure 5.6 shows the distribution of the shear stress correlation coefficient  $\left( R = \frac{-\overline{uv}}{u \times v} \right)$  for the different seepage conditions and the two flow rates. R is a normalized covariance by which the degree of linear correlation between streamline and wall normal turbulence intensity can be expressed. One can note from Figure 5.6a that the value of correlation coefficient is higher for injection in comparison to no seepage condition in the outer region of the flow ( $y > 0.5d$ ). A similar distribution was also observed (Figure 5.6b) for the higher flow rate, but the amount of increment is much less than the variation observed with the lower flow rate. The value of correlation coefficient reduces in comparison with the no seepage condition with the introduction of suction (Figures 5.6c and 5.6d) for the outer region of the flow ( $y > 0.5d$ ). The value of R becomes negative irrespective of the flow conditions above the location where Reynolds shear stress is also negative.

## 5.6 Higher-Order Moments

The distribution of velocity triple products  $\overline{u^3}$  and  $\overline{v^3}$ , normalized by maximum mean velocity, which provide valuable information about turbulence flow structures, are shown in Figure 5.7. One can define  $\overline{u^3}$  and  $\overline{v^3}$  as the streamwise and vertical turbulent transport of kinetic energy  $\overline{u^2}$  and  $\overline{v^2}$  respectively. Due to physical obstruction of second component of the laser beam by the sand bed, only variation of  $\overline{u^3}$  can be seen for the locations close to the bed ( $y < 0.15d$ ). As one can note from Figure 5.7a that  $\overline{u^3}$  is positive close to the bed for all flow conditions. Moving farther from bed, a rapid decrease in the

value of  $\overline{u^3}$  was observed, and  $\overline{u^3}$  becomes negative around  $y = 0.04d$  for the no seepage condition and stays negative for the remainder of the depth. Grass (1971) also observed  $\overline{u^3}$  to be negative through most of the depth and indicated that the sweep event is significant only near the bed, whereas the ejection events are prevalent through most of the boundary layer. With the introduction of injection, the value of  $\overline{u^3}$  becomes negative at locations farther away from the wall ( $y \approx 0.1d \sim 0.2d$ ) in comparison to the no seepage condition. The variation of  $\overline{u^3}$  in the negative territory is very mild, reaching a local maximum negative value at  $y \sim 0.3d$  for no seepage condition followed by  $y \sim 0.4d$  with injection. The value of  $\overline{u^3}$  increases beyond this and reaches a near-zero value at  $y \sim 0.85d$  for no seepage. With injection, the magnitude of  $\overline{u^3}$  tends to remain non-zero even close to the free surface. In the region of negative  $\overline{u^3}$ , one can note that for  $y < 0.4d$ , injection reduces the absolute value of  $\overline{u^3}$  and increases the absolute value of  $\overline{u^3}$  beyond this ( $y > 0.4d$ ). Injection also nominally increases the maximum positive value of  $\overline{u^3}$  at locations very close to the bed. The variation of  $\overline{v^3}$  is found to be positive throughout the depth for all flow conditions (Figure 5.7b). Similar observation of positive  $\overline{u^3}$  near the bed and positive  $\overline{v^3}$  throughout the depth was also made by Balachandar and Bhuiyan (2007). A change in the sign of  $\overline{u^3}$  is an indication of change in turbulent events. Much higher positive value of  $\overline{u^3}$  near the bed is a sign of strong sweep events and injection has a very nominal effect on the near-bed turbulent activity. Negative value of  $\overline{u^3}$  and the positive value of  $\overline{v^3}$  indicate a slower moving fluid parcel with an upward transport of  $u$  momentum representing an ejection type motion and can be seen throughout the depth

with the exception of the near-bed location. The near-zero value of  $\overline{u^3}$  at  $y < 0.2d$  is a cancellation effect of sweep and ejection type events. Farther from the wall, the strength of ejection event increases with increasing negative value of  $\overline{u^3}$  and increasing positive value of  $\overline{v^3}$ . Rapidly diminishing values of both  $\overline{u^3}$  and  $\overline{v^3}$  in the outer layer is an indication of reducing turbulent bursts and approach to a non-turbulent zone close to the free surface. Figures 5.7c and 5.7d show the variation of  $\overline{u^3}$  and  $\overline{v^3}$  for higher flow rates. Trends are more or less similar to the lower flow rate except the increased magnitude of  $\overline{u^3}$  and reduced magnitude of  $\overline{v^3}$  with effect of injection is less than that noted for the lower flow rate.

The variation of normalized velocity triple products  $\overline{u^3}$  and  $\overline{v^3}$  for low and high flow rates with the introduction of suction is shown in Figure 5.8. The overall variation of both triple products is very similar to injection. However, the location where  $\overline{u^3}$  changes sign moves closer to the bed with the introduction of suction narrowing the zone of strong sweep events.

Turbulence diffusion in the longitudinal direction  $D_u (\overline{v^2u})$  and in the vertical direction  $D_v (\overline{u^2v})$ , normalized by maximum mean velocity is shown in Figure 5.9. As seen in Figure 5.9, the values of  $D_u$  and  $D_v$  are always negative and positive, respectively, for the present range of measurements. One can note from Figure 5.9a that the value of  $D_v$  increases with increasing distance from the bed and attain a maximum value around  $y = 0.4d$ . This is an indication of high diffusion of streamwise turbulence in the upward direction. A similar trend was observed by Balachandar and Bhuiyan (2007) but the location of the peak was much closer to the wall ( $y \sim 0.2d$ ) for the flow over dunes. The

value of  $D_v$  reduced beyond  $y = 0.4d$  and becomes negligible near the free surface. Although no distinct effect of injection in the variation of  $D_v$  can be noted up to  $y = 0.45d$ , one can note a higher value of  $D_v$  with the introduction of injection from  $y = 0.45d$  to the free surface. As shown in Figure 5.9b, the value of  $D_u$  tends to be more negative with increasing distance from the bed and indicates a reduction in streamwise diffusion of vertical turbulence. The value of  $D_u$  attains a minimum at around the same location ( $y \sim 0.4d$ ) as the location of maximum  $D_v$ . The value of  $D_u$  increases beyond  $y > 0.4d$  and attains a near-zero value near the free surface. Effect of injection on  $D_u$  is found to be very similar to the effect of injection on  $D_v$ . The distribution of  $D_v$  and  $D_u$  is found to be very similar for the higher flow rate as seen in Figures 5.9c and 5.9d, respectively.

Figure 5.10 shows the variation of  $D_u$  and  $D_v$  with the introduction of suction for two different flow rates. The effect of suction is clearly opposite to that noticed by injection for  $y > 0.4d$ . As mentioned by Balachandar and Bhuiyan (2007) that the trend of the variation of  $D_u$  and  $D_v$  for  $y < 0.2d$  seen in Figures 5.9 and 5.10 could be a reflection of the change in dominance of the type of turbulent bursting event (sweep vs. ejection).

## 5.7 Quadrant analysis

The contribution from Q2 and Q4 events to the Reynolds shear stress are shown in Figure 5.11 for different threshold values. One can note from Figures 5.11a and 5.11b that the magnitude of Q2 and Q4 contributions increase with the introduction of injection for  $H = 0$  in comparison to no seepage condition. The effect of injection is clearly visible well beyond the near-bed region and deep into the outer layer ( $y/d \approx 0.7$ ). The magnitude of the events reduce towards the free surface, more or less linearly, and attain a near-zero

constant value. The effect of injection is quite distinct near the bed and reduced as one move farther towards free surface.

Quadrant analysis was also carried out at different threshold levels ( $H = 2$  to  $5$ ) to investigate the contribution of the extreme turbulent events. This approach was taken to filter out the small random turbulent fluctuations and consider the contribution of the more energetic eddies. Figures 5.11c and 5.11d only show the contributions from the events whose amplitude exceeds the threshold value of  $H = 2$ . Although the number of Q2 and Q4 events reduce sharply for change of threshold value from 0 to 2, the events with  $H = 2$  produced very large instantaneous Reynolds shear stress ( $> 5.5 \overline{uv}$ ), which can potentially influence the sediment transport, resuspension of pollutant from bed, bed formation, entrainment and the exchange of energy and momentum. The data trend at  $H = 2$  is very similar to  $H = 0$ , however, the affected flow depth for Q4 events reduces with increasing  $H$  value. Balachandar and Bhuiyan (2007) noted significant ejection and sweep components throughout the depth with ejection events being dominant. Effect of injection on extreme turbulent events is also visible for  $H = 2$ .

Figures 5.11e to 5.11l show the contribution from Q2 and Q4 events to the Reynolds shear stress for other threshold levels ( $H = 2.5$  to  $5$ ). One can note that the affected regions over the flow depth for Q4 events reduces with the increase of threshold value of  $H$ , but Q2 events are clearly affected deep into the outer layer ( $y/d \approx 0.7$ ) for the value of  $H$  as high as 5. Irrespective of the affected depth, the increase of both Q2 and Q4 contribution to the Reynolds shear stress due to injection is still visible. Result of quadrant analysis for higher flow rate is shown in Figure 5.12. The results are very similar to the lower flow rate (Figure 5.11) but the effect of injection is less significant.

Figures 5.13 and 5.14 show the contribution from Q2 and Q4 events to the Reynolds shear stress for different threshold levels ( $H = 0$  to 5) with the introduction of suction for lower and higher flow rate, respectively. Suction reduces the magnitude of Q2 and Q4 contributions for different threshold levels which is clearly opposite to that noticed by injection.

The ratio of Q2/Q4 to the Reynolds shear stress is shown in Figure 5.15 for  $H = 0$  to 3. One can note from Figures 5.15a ( $H = 0$ ) that at near-bed locations, the Q2/Q4 ratio is near unity, indicating identical strength of sweep and ejection. As one progress from the bed towards the free surface, the ratio of Reynolds shear stress for Q2 and Q4 increases from a near unit value to a maximum at around  $y \sim 0.6d$ , indicating relatively stronger ejection events. Moving farther from the bed and towards the free surface, the ratio of Reynolds shear stress between Q2 and Q4 reduces. The effect of injection on Q2/Q4 ratio is only visible for  $y > 0.6d$  with the increased ratio of Q2/Q4 in comparison to no seepage condition. Figure 5.15b shows a trend different from Figure 5.15a. As one progress from the bed towards the free surface, the value of Q2/Q4 increases from a near unit value to ten folds at around  $y \sim 0.6d$ , indicating much stronger ejection events. Moving farther from bed and towards the free surface the ratio of Reynolds shear stress between Q2 and Q4 reduces. The effect of injection on Q2/Q4 ratio is again visible for  $y > 0.6d$  with the increased ratio of Q2/Q4 in comparison to no seepage condition. One can see stronger ejection events with increased threshold value (Figures 5.15c and 5.15d) with effect of injection being more visible for  $y > 0.6d$ . The Q2/Q4 ratio for the higher flow rate is shown in Figures 5.15e to 5.15h. The results are very similar to lower flow rate (Figures 5.15a to 5.15d). Figures 5.16 shows the ratio of Q2/Q4 events to the



Reynolds shear stress for different threshold levels with the introduction of suction for lower and higher flow rate. The effect of suction on  $Q2/Q4$  ratio is visible for most of the depth with the increased ratio of  $Q2/Q4$  in comparison to no seepage condition.

## 5.8 Conclusions

The present study was carried out to understand the effects of seepage on mean velocity, turbulence, Reynolds shear stress and, velocity triple products in open channel flow (OCF) for two different flow rates. Quadrant decomposition technique was also used to extract the magnitude of the Reynolds shear stress of the turbulent bursting events. The main findings are summarized as follows:

1. Injection decreases the near-bed velocity causing the mean velocity profile to be less full compared to the no seepage condition. However, suction increases the near-bed velocity causing the mean velocity profile to become more uniform compared to the no seepage condition.
2. Injection increases the bed shear stress as noted by an increase in  $u_\tau$ , whereas, suction decreases the bed shear stress due to decrease in  $u_\tau$ .
3. For the range of test conditions used in the present study, injection results in an increase in bed stability, while suction reduces the bed stability.
4. Injection causes an increment of both streamwise and vertical turbulence intensity whereas suction reduces the values.
5. Reynolds shear stress increases with the introduction of injection for most of the depth, whereas suction reduces the Reynolds shear stress.

6. Effect of injection on mean velocity, turbulence intensity, Reynolds shear stress is found to be less significant for the higher flow rate.
7. Results from the analysis of turbulent bursting events (through quadrant decomposition) show clearly visible effect of seepage well beyond the near-bed region and deep into the outer layer ( $y/d \approx 0.7$ ). Results show that the magnitude of Q2 (ejection) and Q4 (sweep) contributions is very much higher with the introduction of injection and much lower for suction than that for no seepage condition for a threshold hole size,  $H = 0$ .
8. By investigating the contribution of the extreme turbulent events ( $H = 2$  to  $5$ ), results show active Q2 (ejection) events for most of the flow depth, whereas, affected flow depth for active Q4 (sweep) events reduces with increasing  $H$  value. Injection increases the magnitude of Reynolds stress by extreme turbulent events whereas suction reduces it. Although the number of extreme events reduce sharply for higher threshold value, the extreme events would produce very large instantaneous Reynolds shear stress ( $> 5.5 \overline{uv}$  for  $H = 2$ ), which can potentially influence the sediment transport, resuspension of pollutant from bed, bed formation, entrainment and the exchange of energy and momentum.

Table 5.1: Comparison of percentage change of near bed velocity and friction velocity

Tests	Rate of Suction & Injection	% change in friction velocity	% change in near bed velocity
Seepage (Injection) (450 GPM)	5%	0.62	-17.21
	7%	5.56	-25.45
	9%	9.88	-36.59
	12%	17.28	-44.05
	14%	23.46	-51.12
Seepage (Injection) (720 GPM)	3%	1.89	-5.26
	5%	5.66	-11.41
	7%	8.30	-15.51
	9%	13.21	-23.66
Seepage (Suction) (450 GPM)	5%	-1.23	10.71
	7%	-7.41	25.53
	9%	-11.11	37.99
	12%	-14.81	48.55
	14%	-16.67	48.13
Seepage (Suction) (720 GPM)	3%	-6.42	7.79
	5%	-9.43	17.31
	7%	-13.21	34.37
	9%	-16.98	39.92
<b>Note: +ve represents increase and -ve represents decrease in comparison to no seepage condition.</b>			

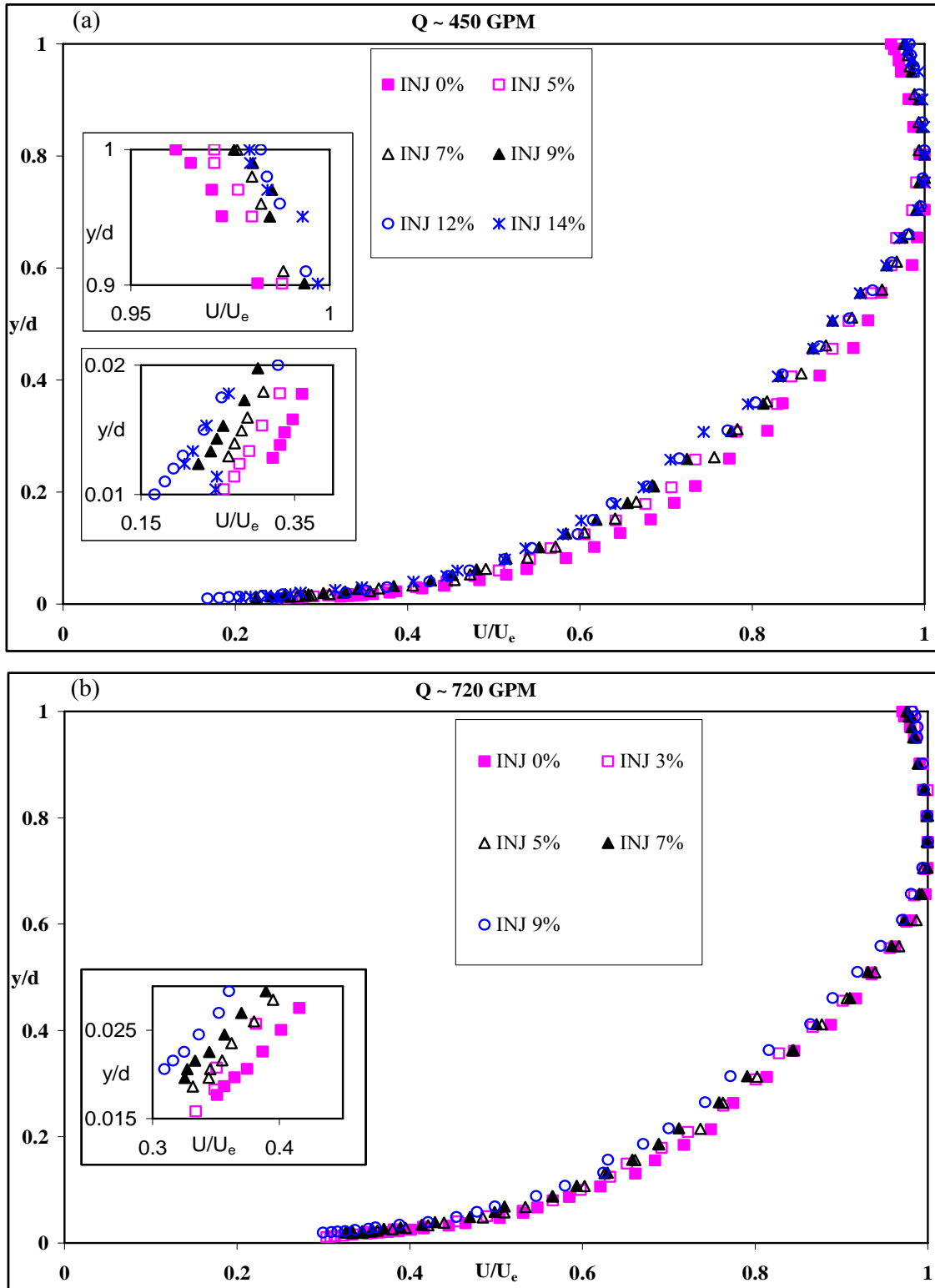


Figure 5.1: Mean velocity profile in outer coordinates for, a) Injection\_450 GPM, b) Injection\_720 GPM

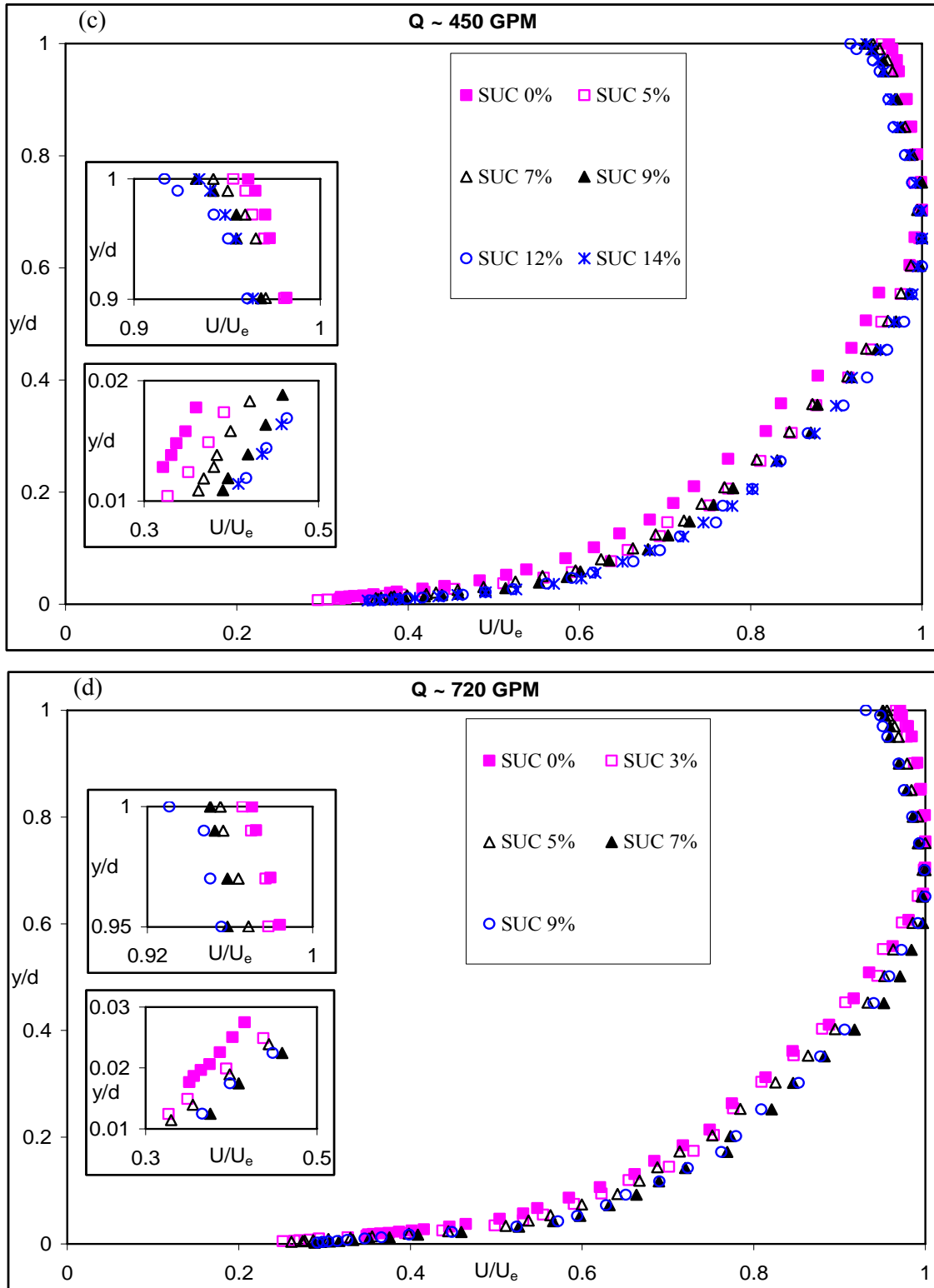


Figure 5.1: Mean velocity profile in outer coordinates for, c) Suction\_450 GPM, d) Suction\_720 GPM.

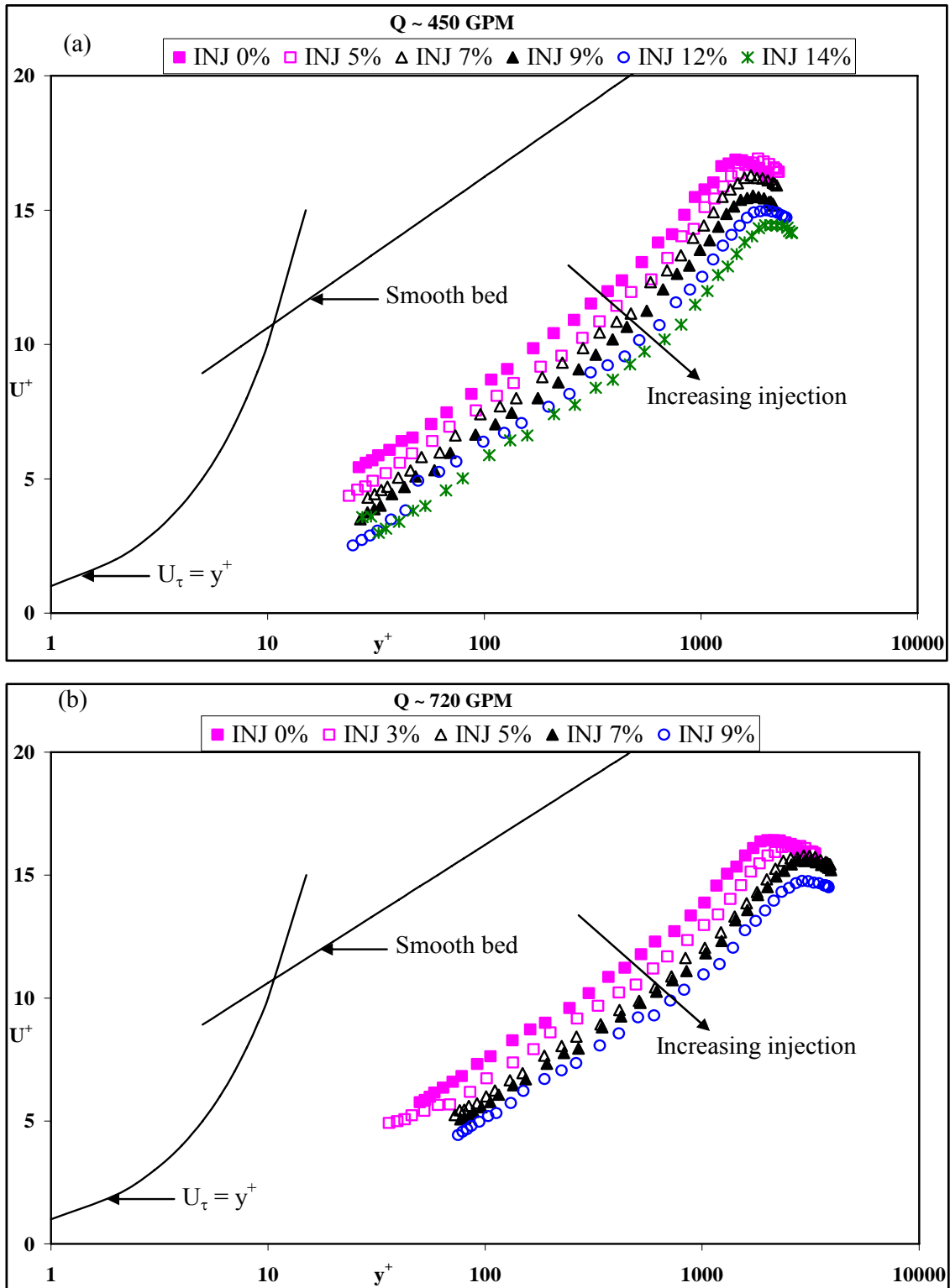


Figure 5.2: Mean velocity profile in inner coordinates for, a) Injection\_450 GPM, b) Injection\_720 GPM

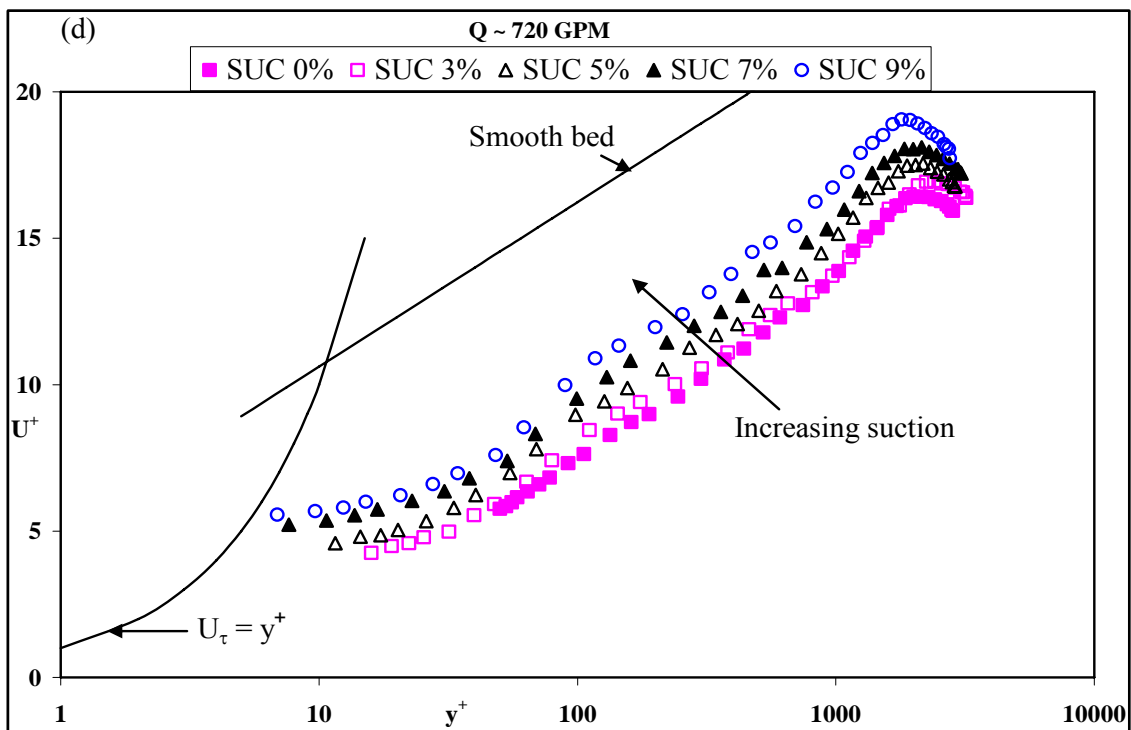
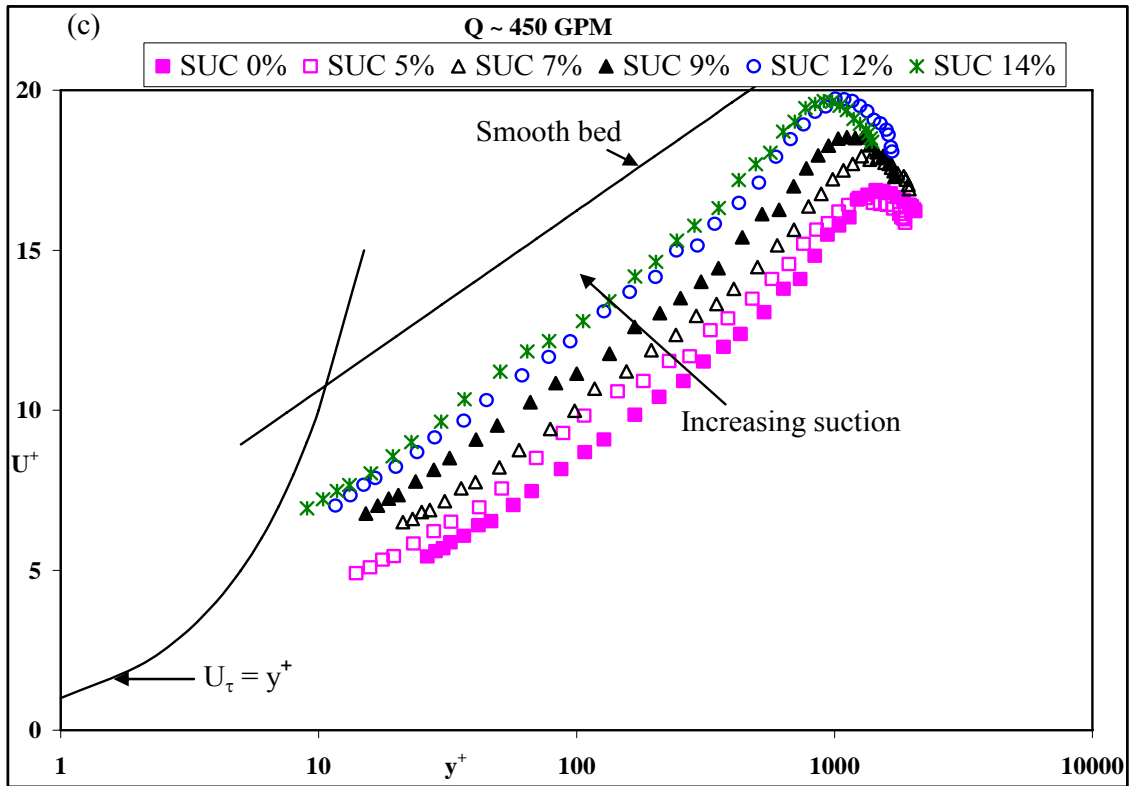


Figure 5.2: Mean velocity profile in inner coordinates for, c) Suction\_450 GPM, d) Suction\_720 GPM.

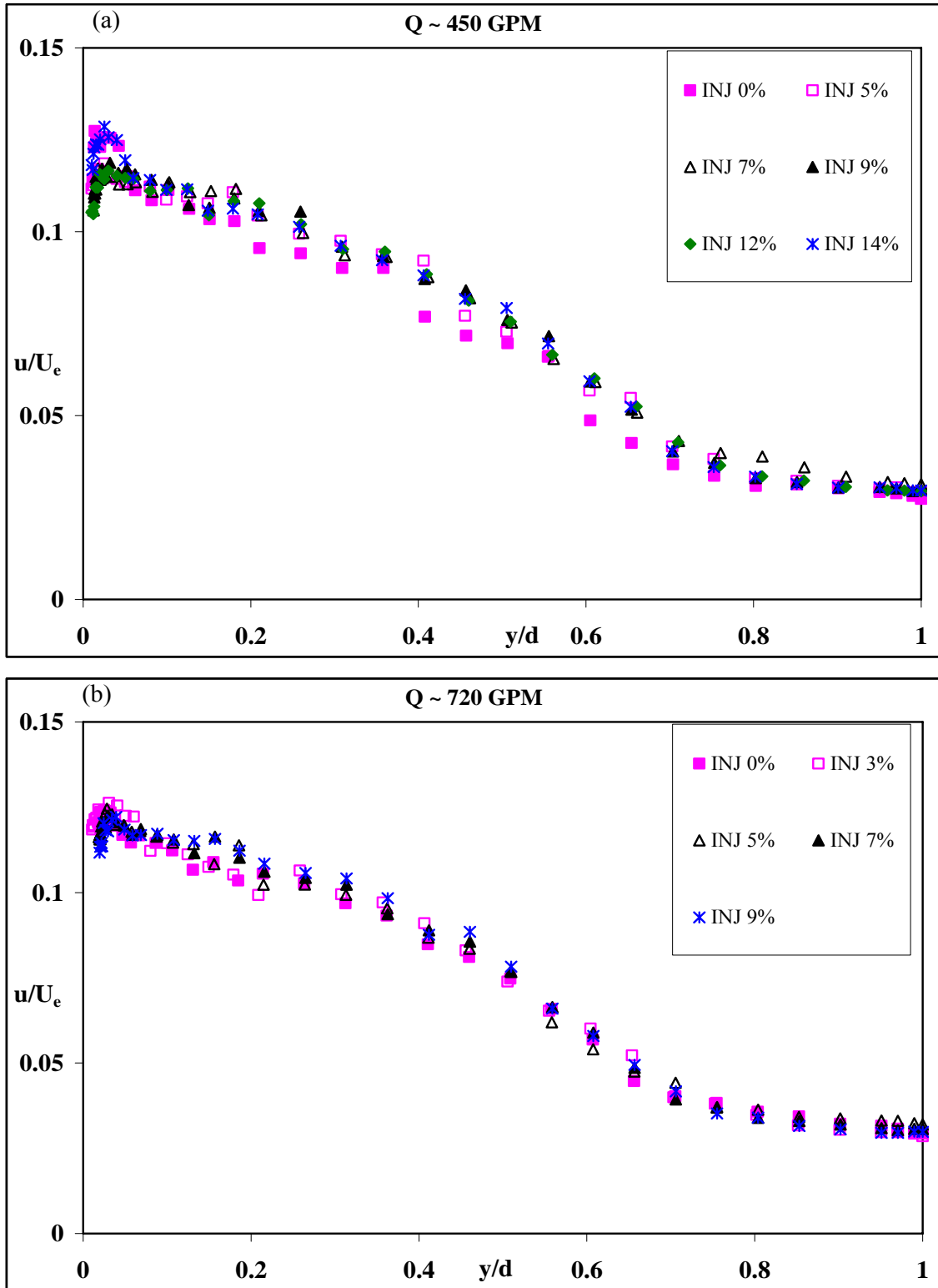


Figure 5.3: Streamwise turbulence intensity for, a) Injection\_450 GPM, b) Injection\_720 GPM



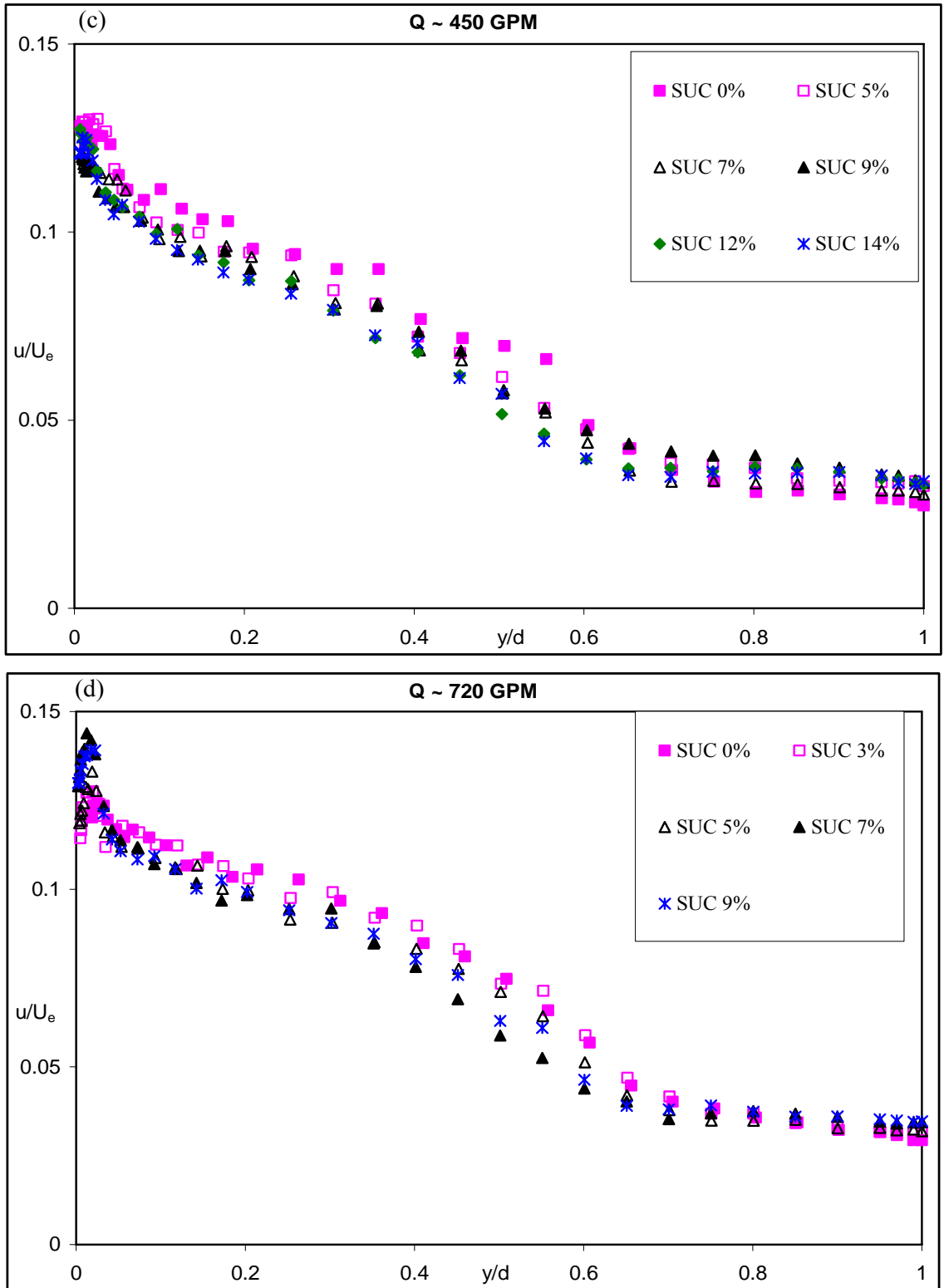


Figure 5.3: Streamwise turbulence intensity for, c) Suction\_450 GPM, d) Suction\_720 GPM.

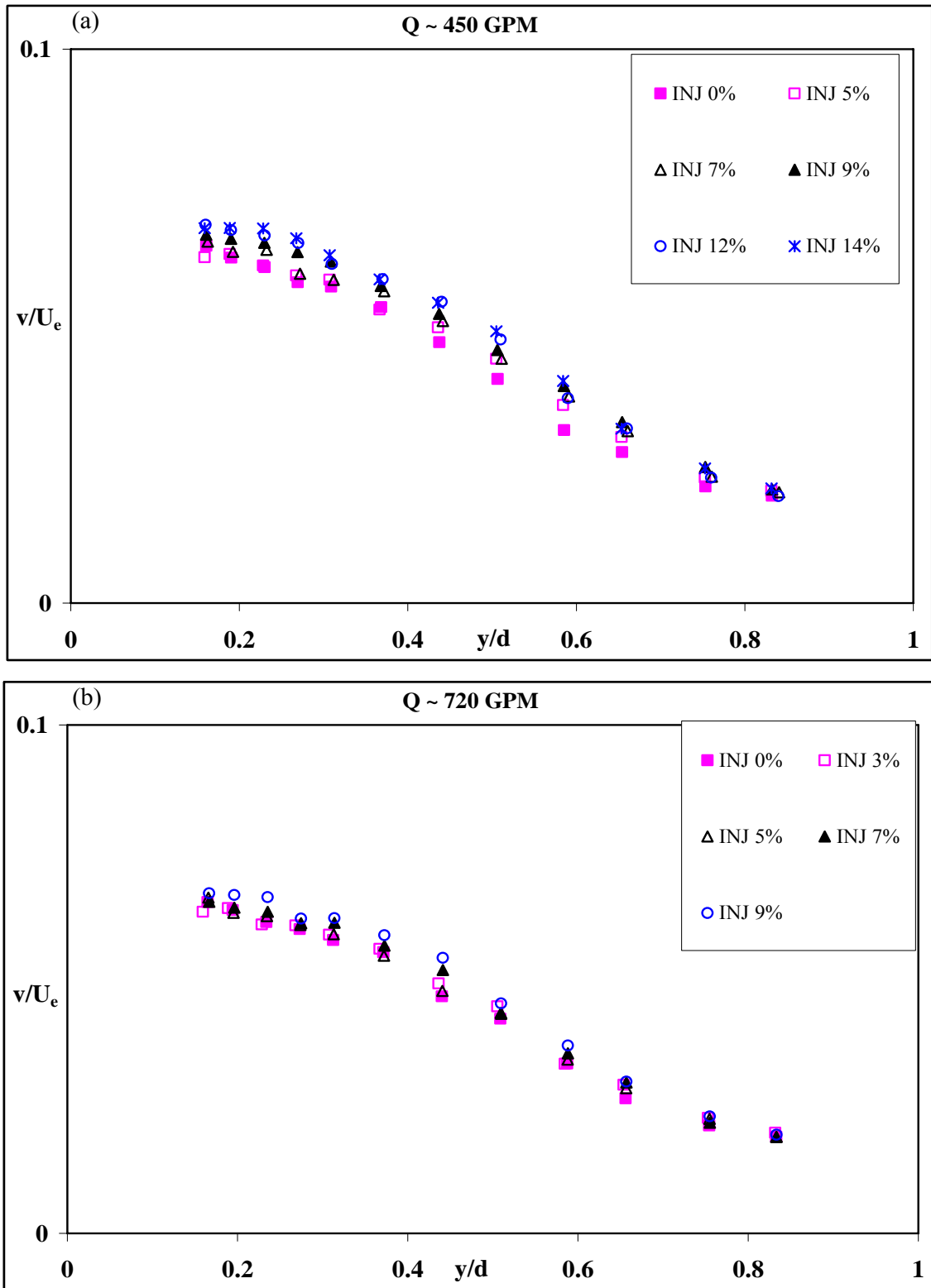


Figure 5.4: Vertical turbulence intensity for, a) Injection\_450 GPM, b) Injection\_720 GPM

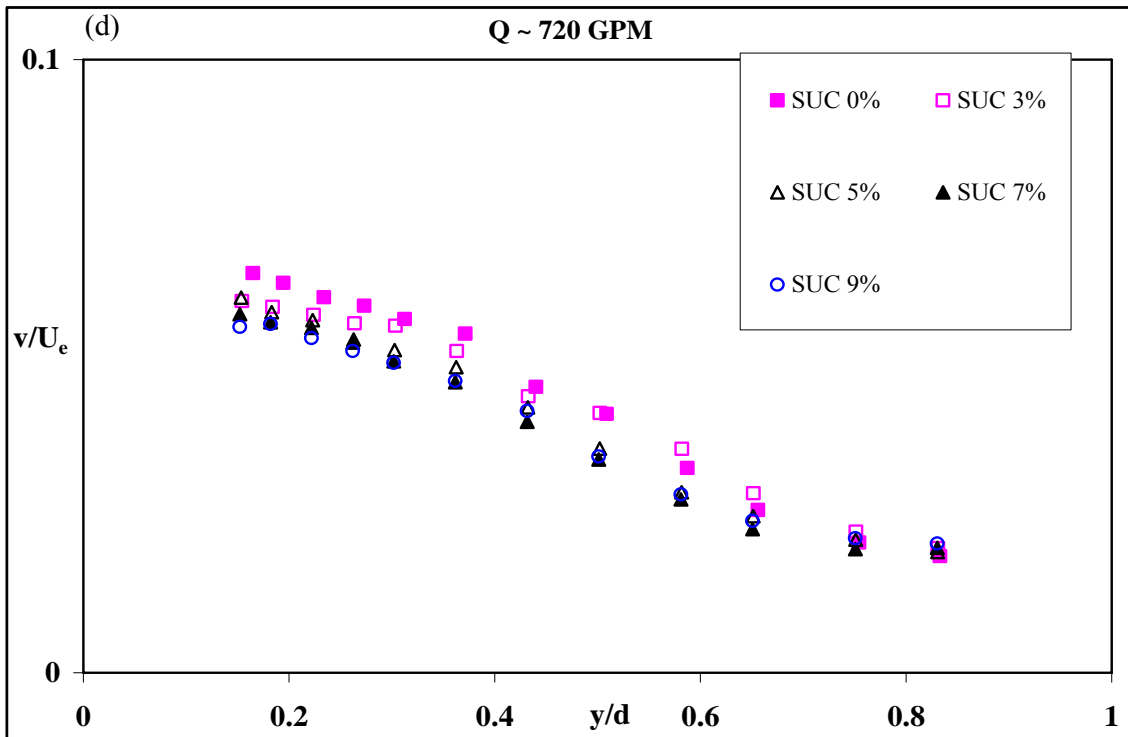
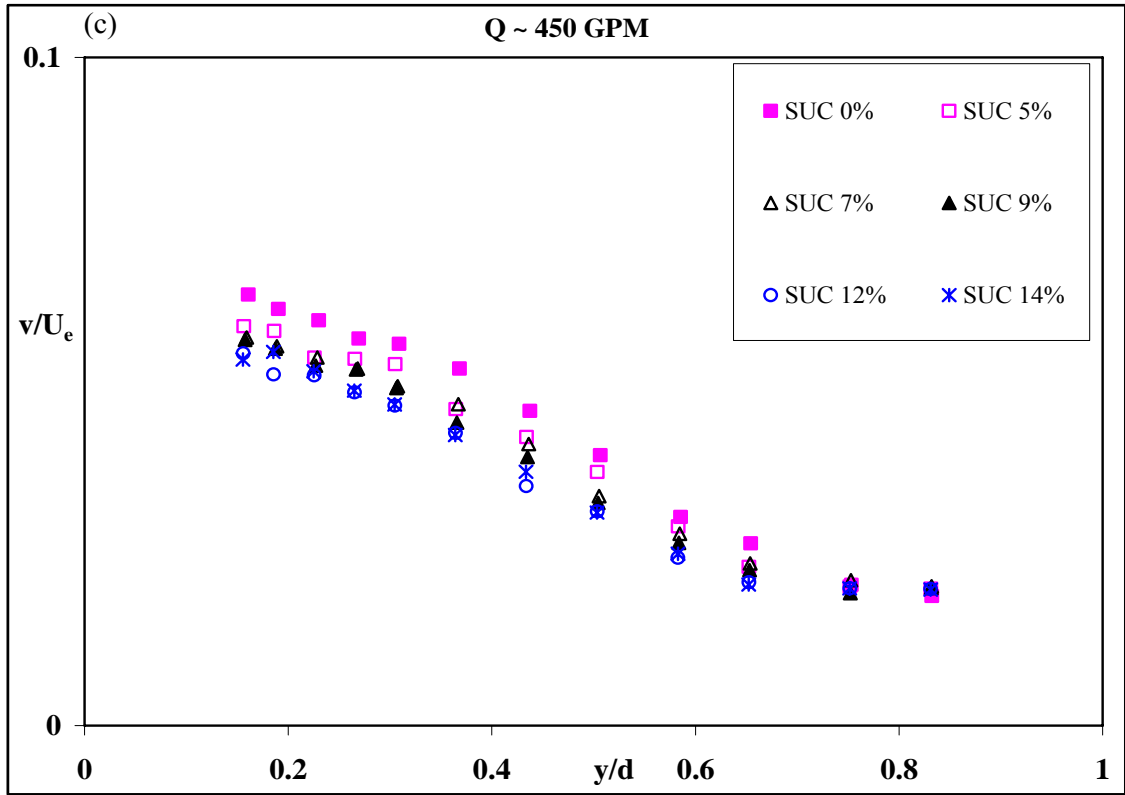


Figure 5.4: Vertical turbulence intensity for, c) Suction\_450 GPM, d) Suction\_720 GPM.

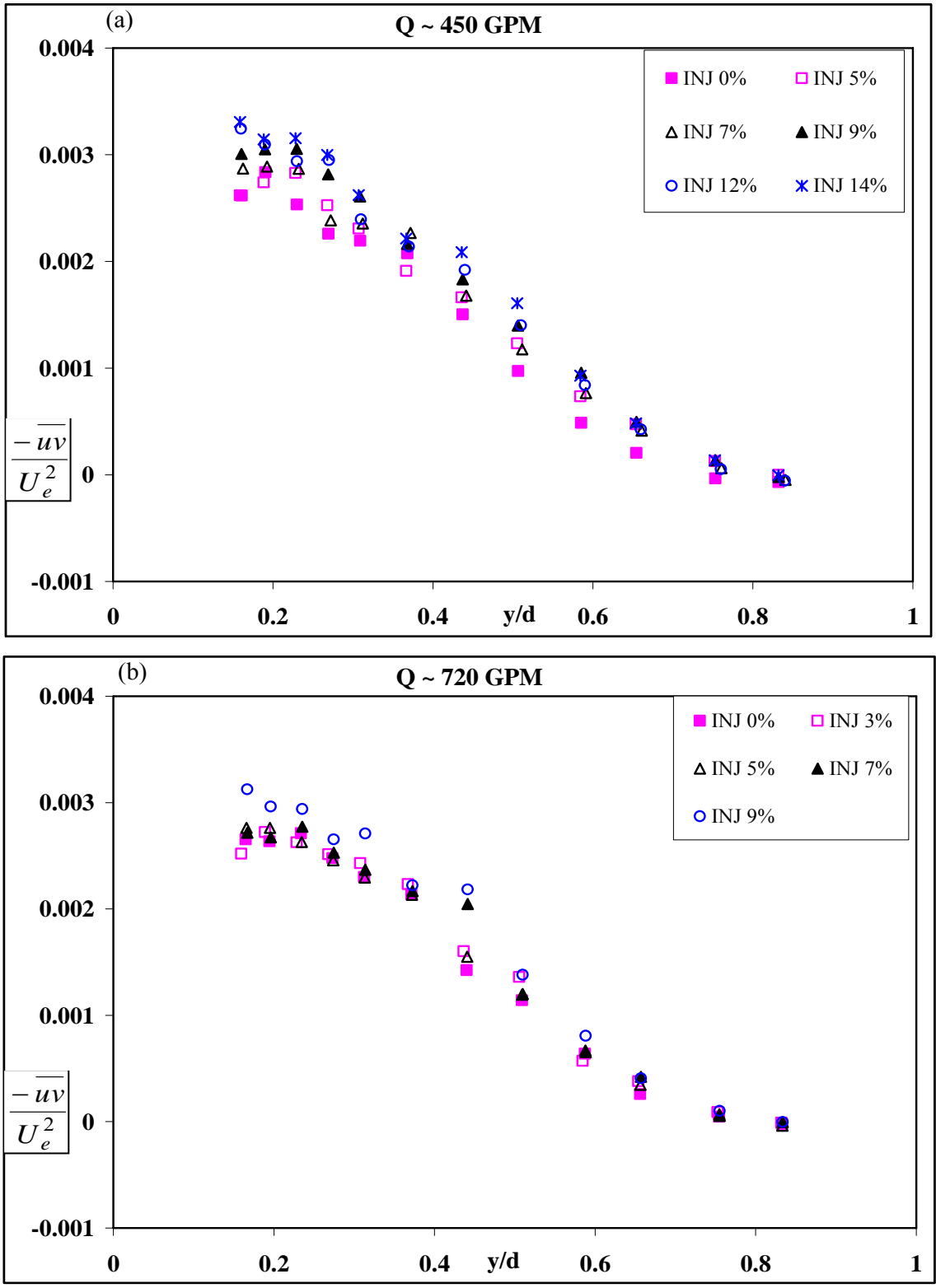


Figure 5.5: Reynolds shear stress for, a) Injection\_450 GPM, b) Injection\_720 GPM

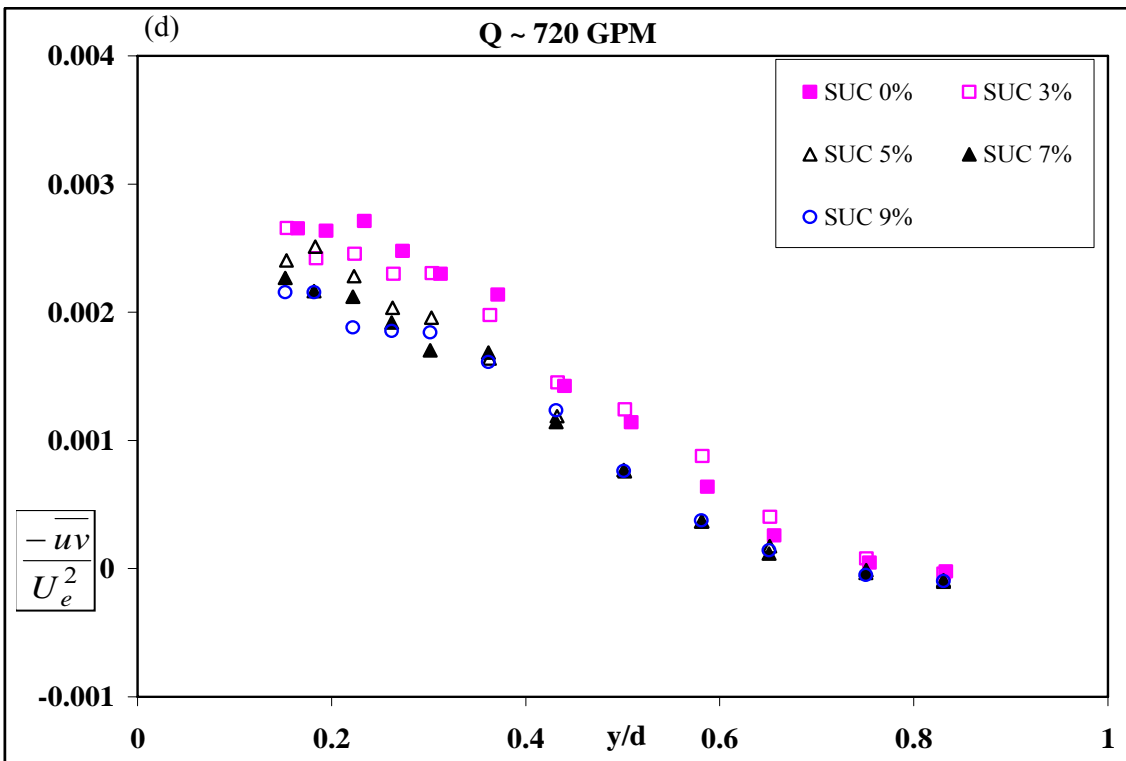
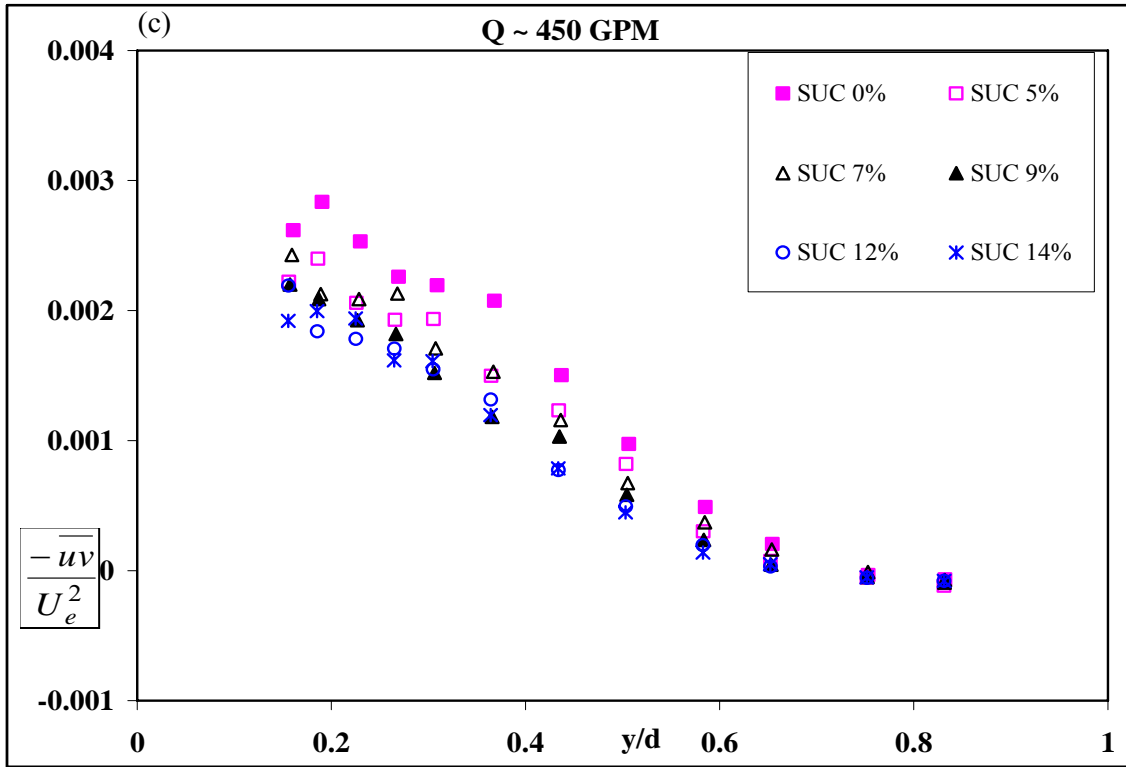


Figure 5.5: Reynolds shear stress for, c) Suction\_450 GPM, d) Suction\_720 GPM.

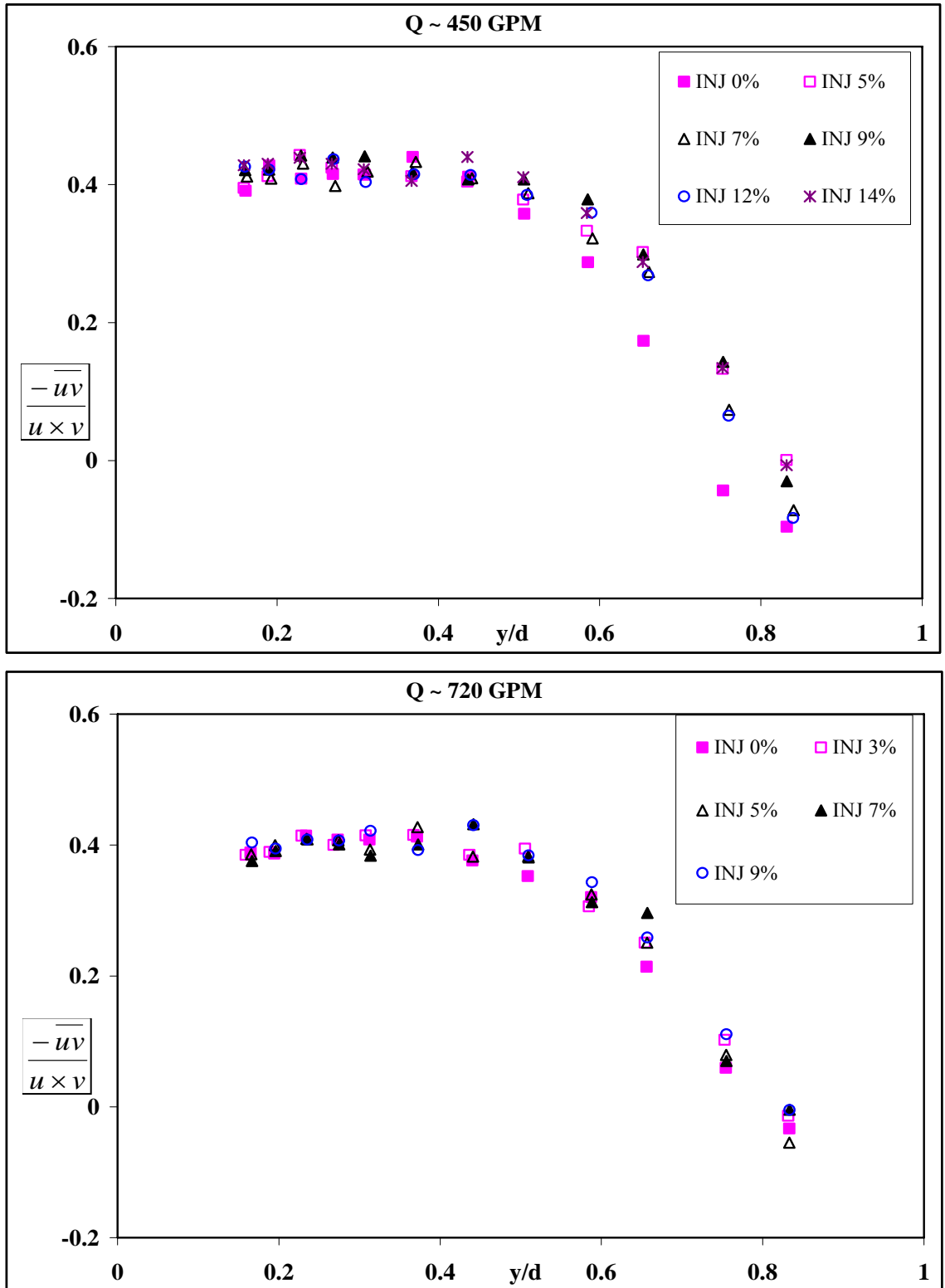


Figure 5.6: Distribution of correlation coefficient for, a) Injection\_450 GPM, b) Injection\_720 GPM

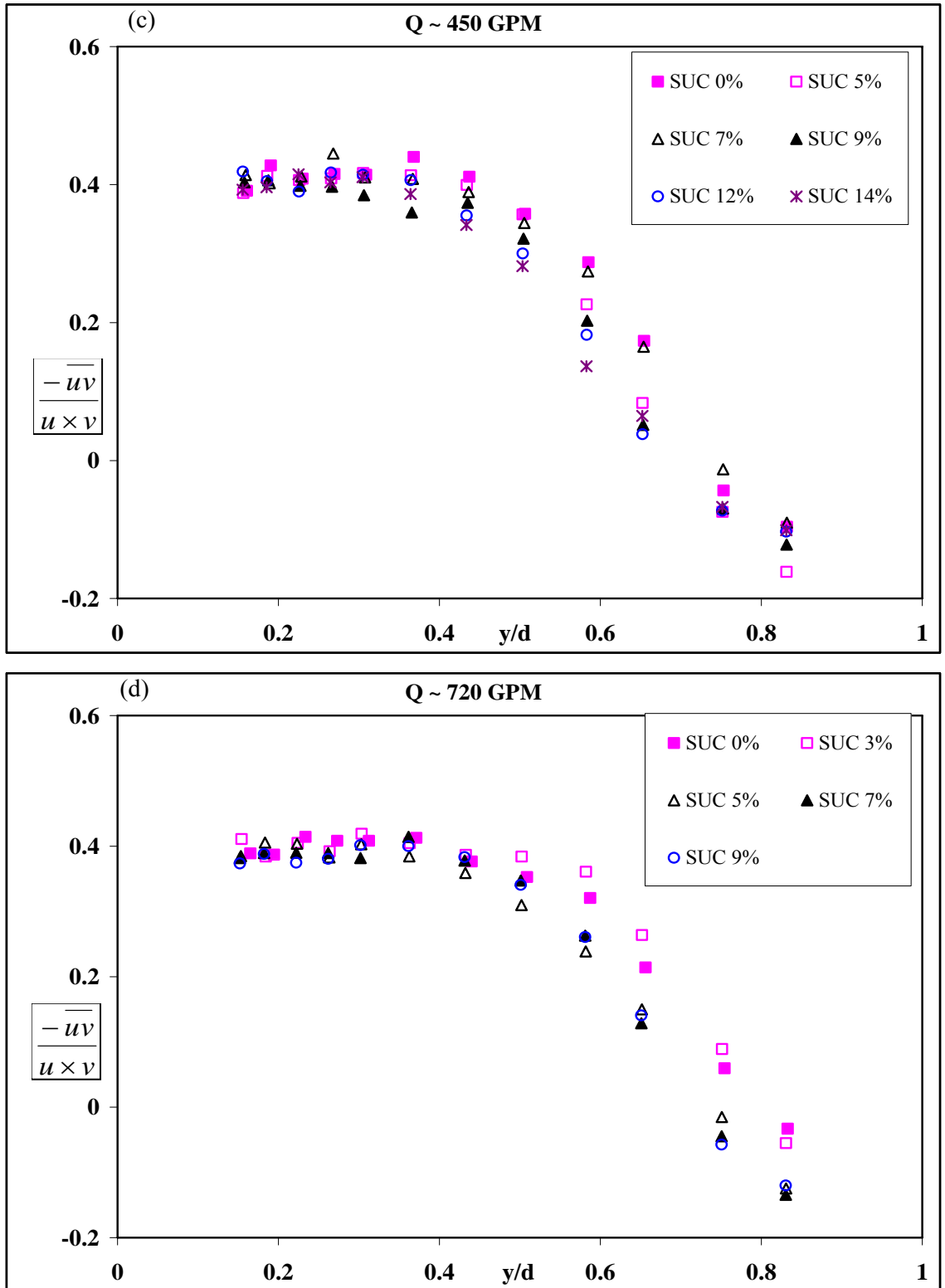


Figure 5.6: Distribution of correlation coefficient for, c) Suction\_450 GPM, d) Suction\_720 GPM.

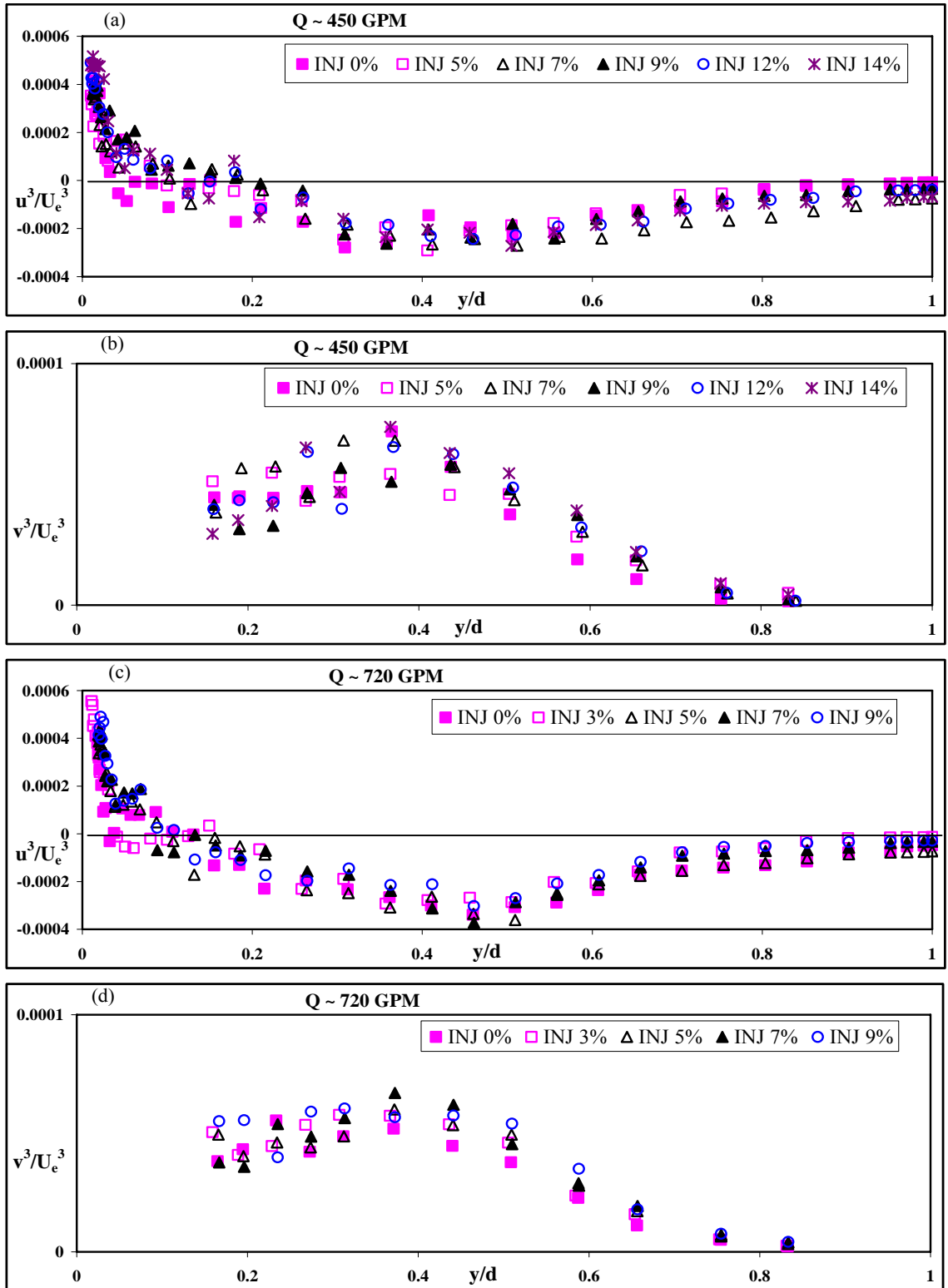


Figure 5.7: Distribution of different velocity triple product, a)  $u^3$ : Injection\_450 GPM, b)  $v^3$ : Injection\_450 GPM, c)  $u^3$ : Injection\_720 GPM, d)  $v^3$ : Injection\_720 GPM.



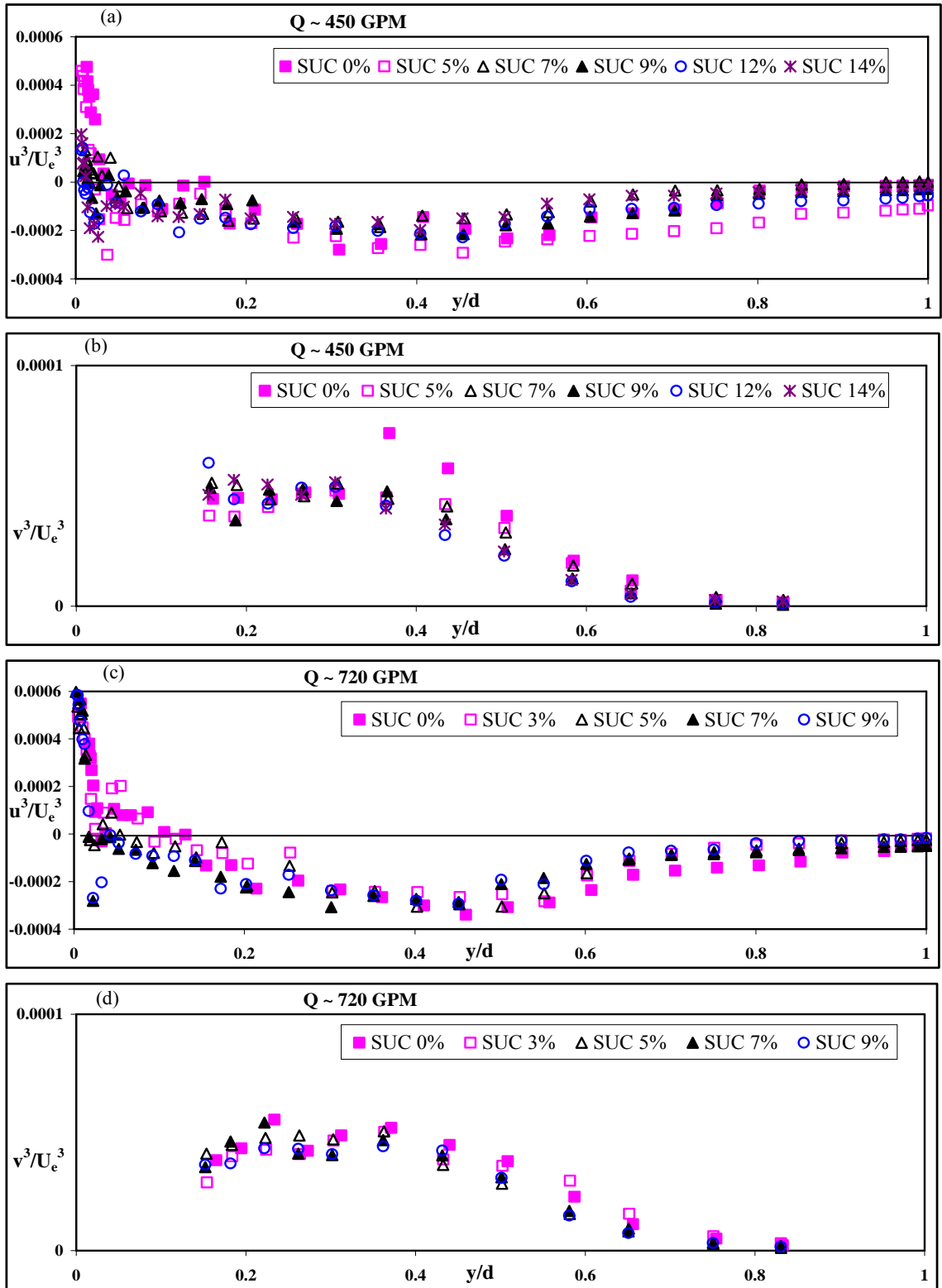


Figure 5.8: Distribution of different velocity triple product, a)  $u^3$ : Suction\_450 GPM, b)  $v^3$ : Suction\_450 GPM, c)  $u^3$ : Suction\_720 GPM, d)  $v^3$ : Suction\_720 GPM.

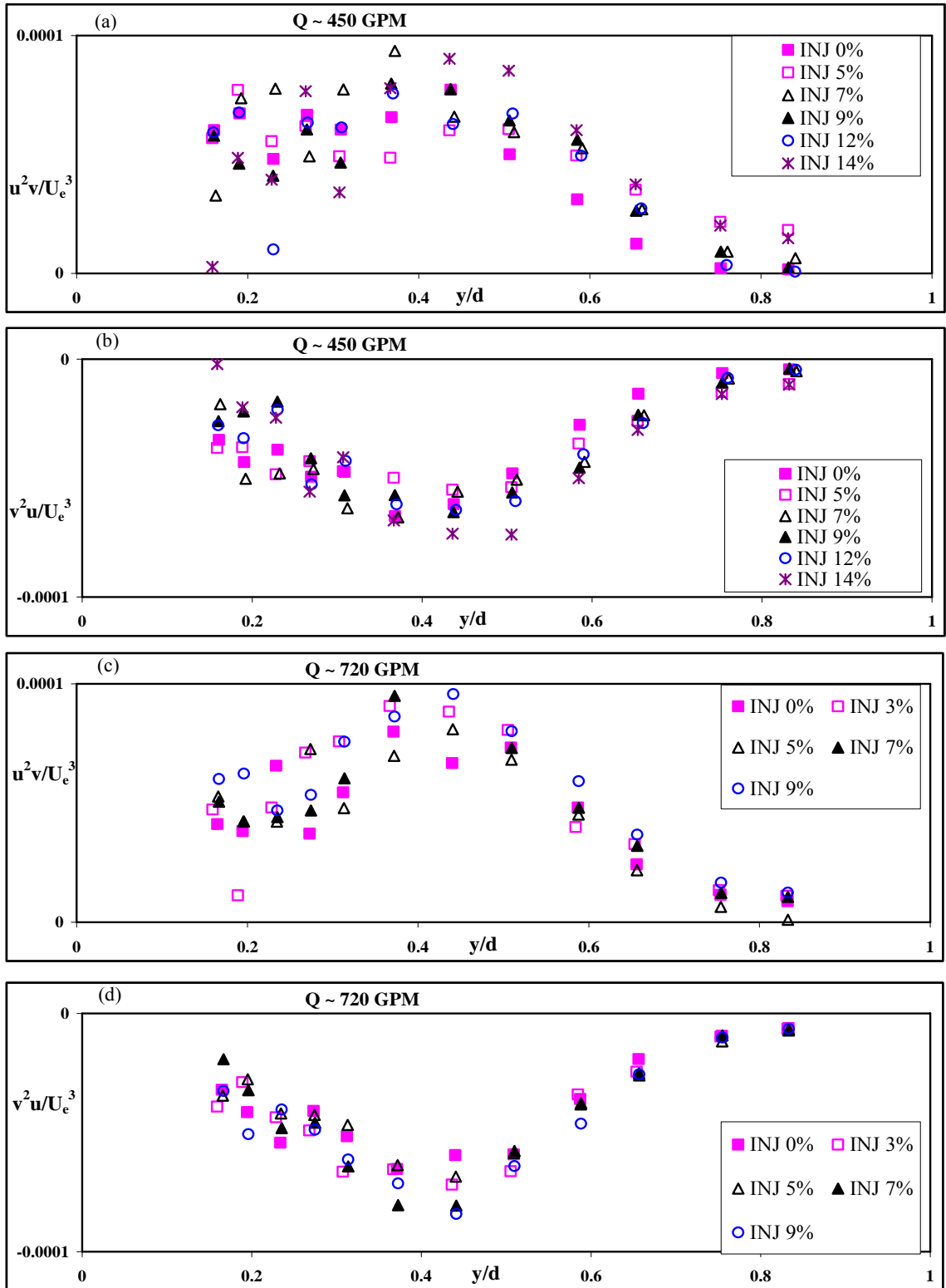


Figure 5.9: Distribution of different velocity triple product, a)  $D_v$ : Injection\_450 GPM, b)  $D_u$ : Injection\_450 GPM, c)  $D_v$ : Injection\_n\_720 GPM, d)  $D_u$ : Injection\_720 GPM.

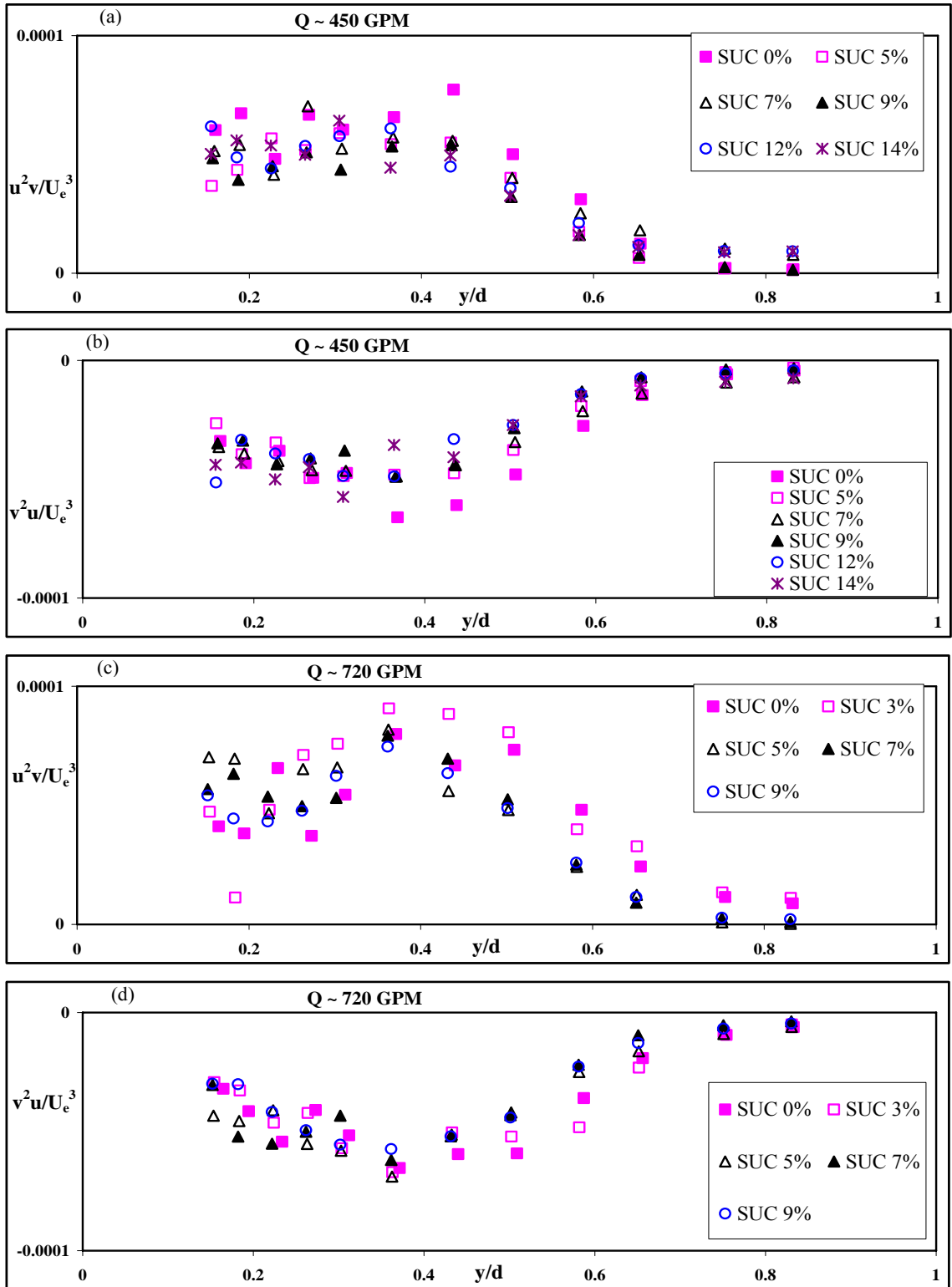


Figure 5.10: Distribution of different velocity triple product, a)  $D_v$ : Suction\_450 GPM, b)  $D_u$ : Suction\_450 GPM, c)  $D_v$ : Suction\_720 GPM, d)  $D_u$ : Suction\_720 GPM.

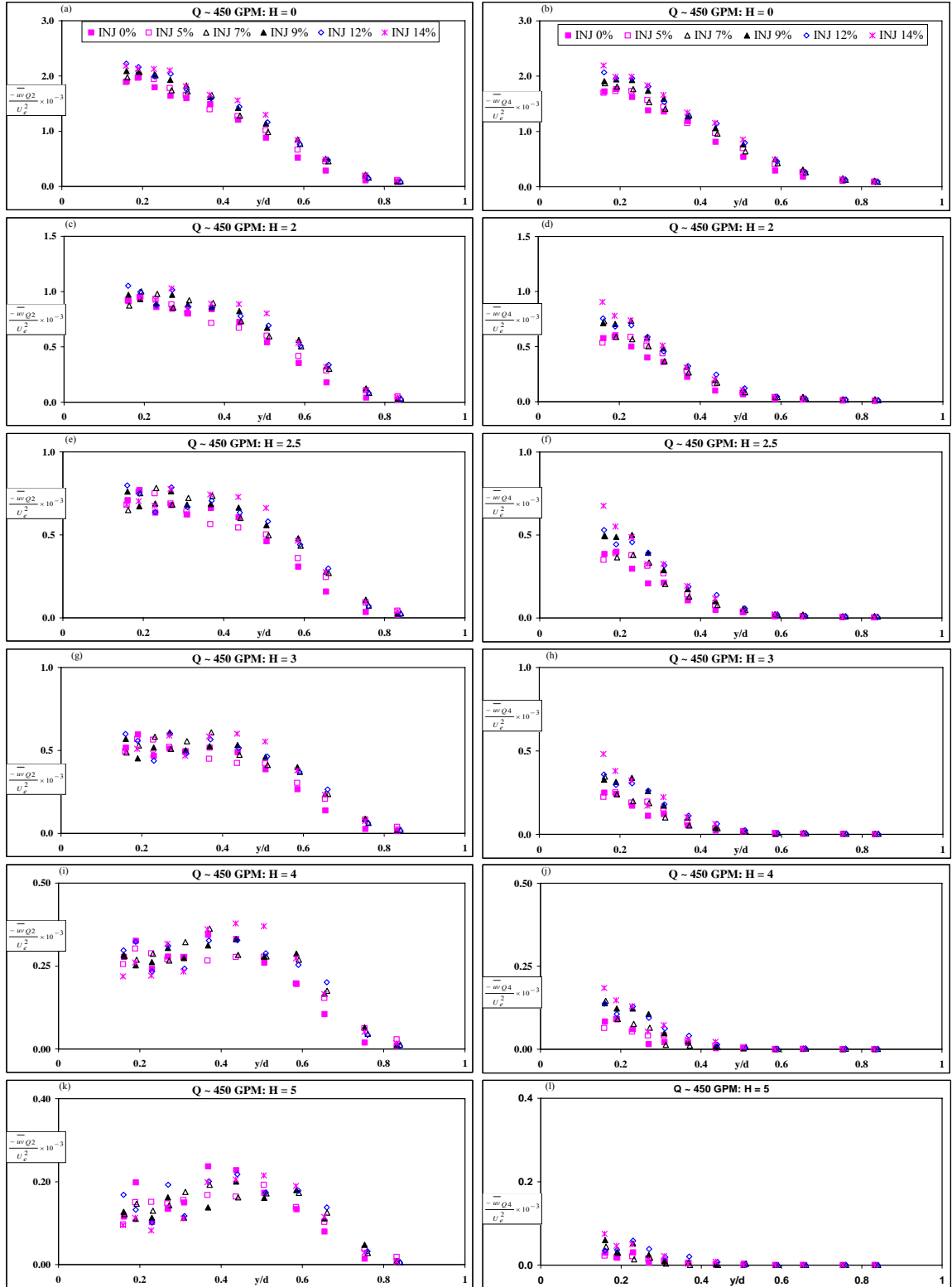


Figure 5.11: Contribution of different quadrant events to the Reynolds stress for lower flow rates and with introduction of injection.

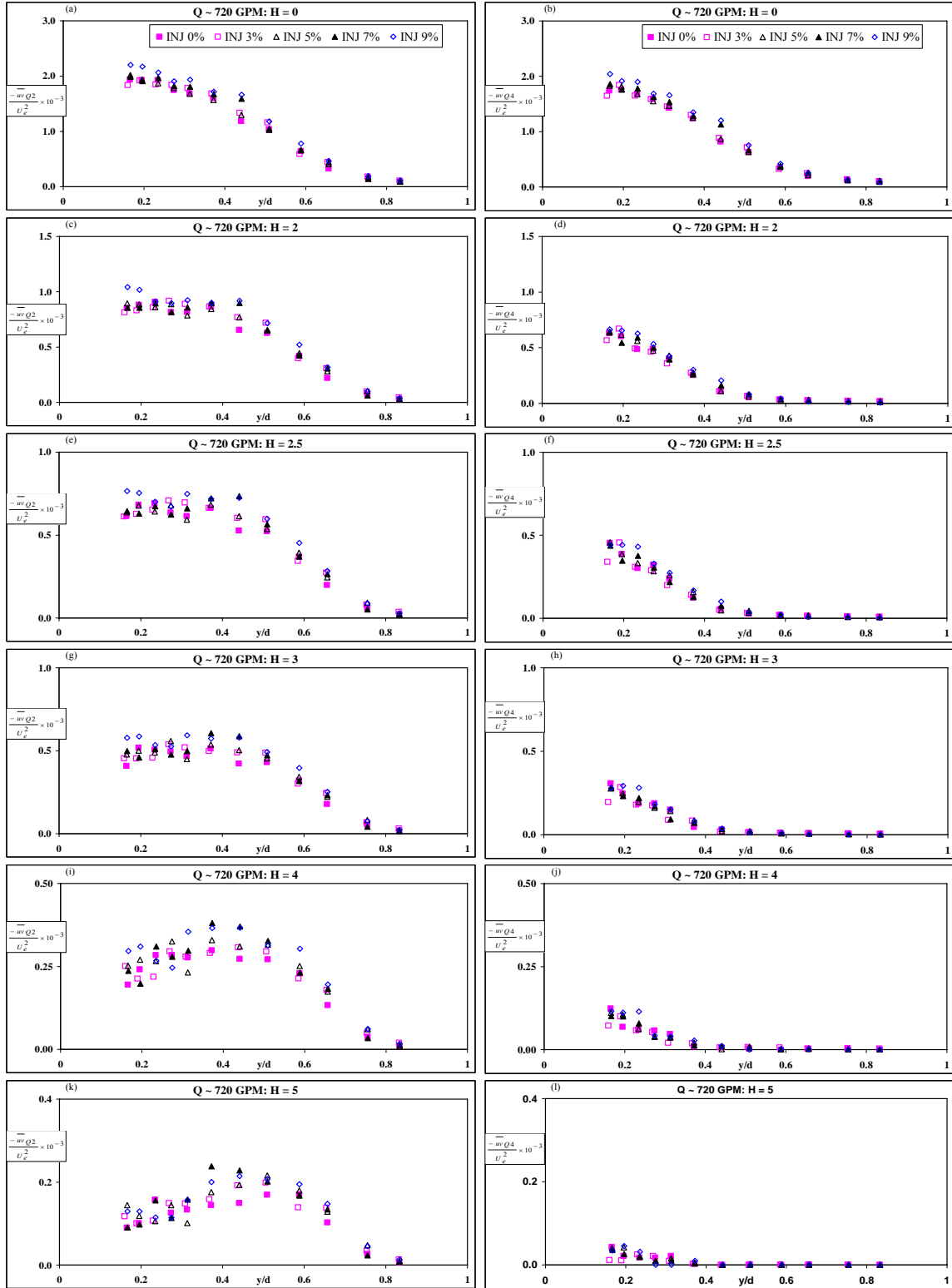


Figure 5.12: Contribution of different quadrant events to the Reynolds stress for higher flow rates and with introduction of injection.

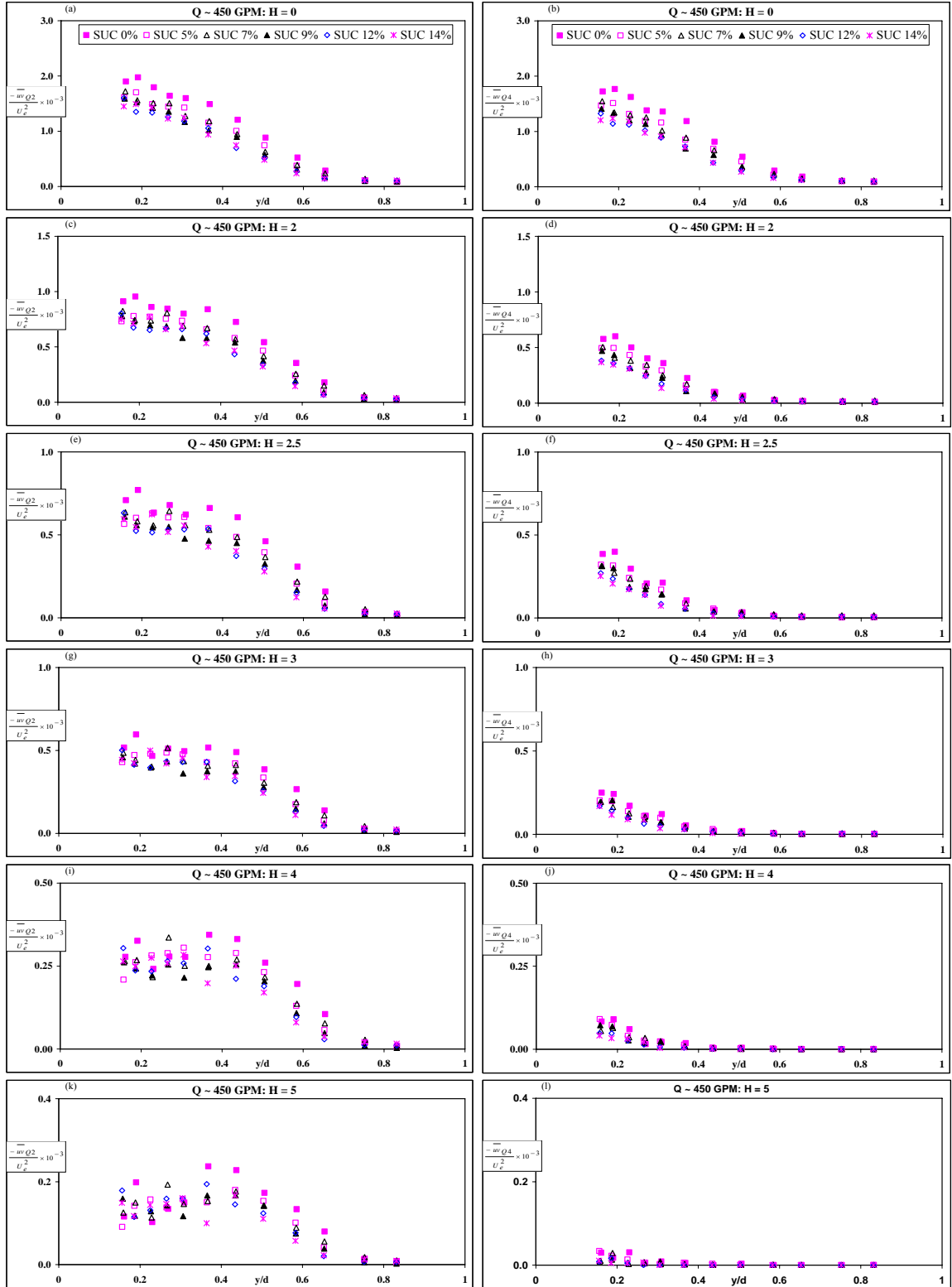


Figure 5.13: Contribution of different quadrant events to the Reynolds stress for lower flow rates and with introduction of suction.

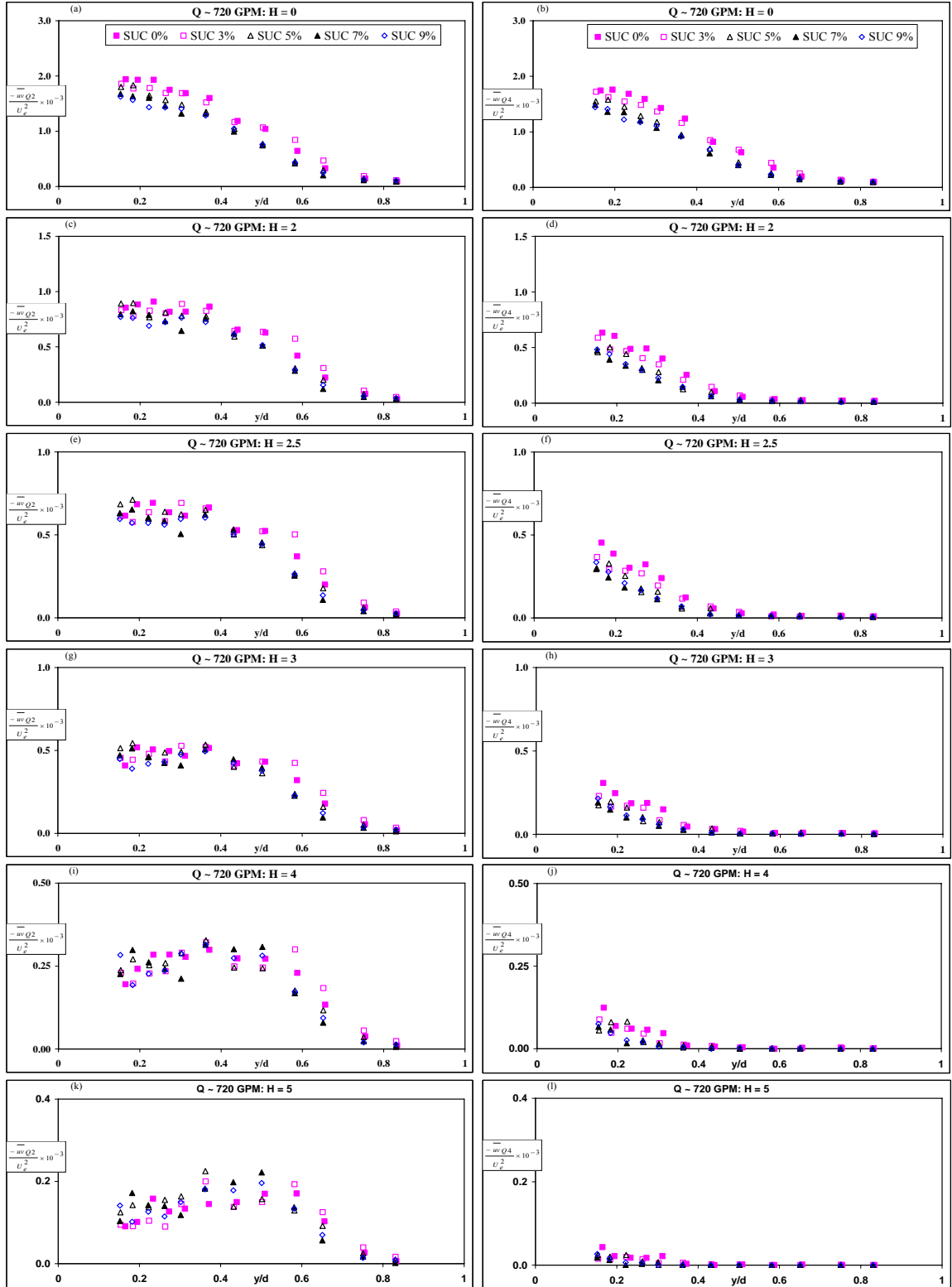


Figure 5.14: Contribution of different quadrant events to the Reynolds stress for higher flow rates and with introduction of suction.

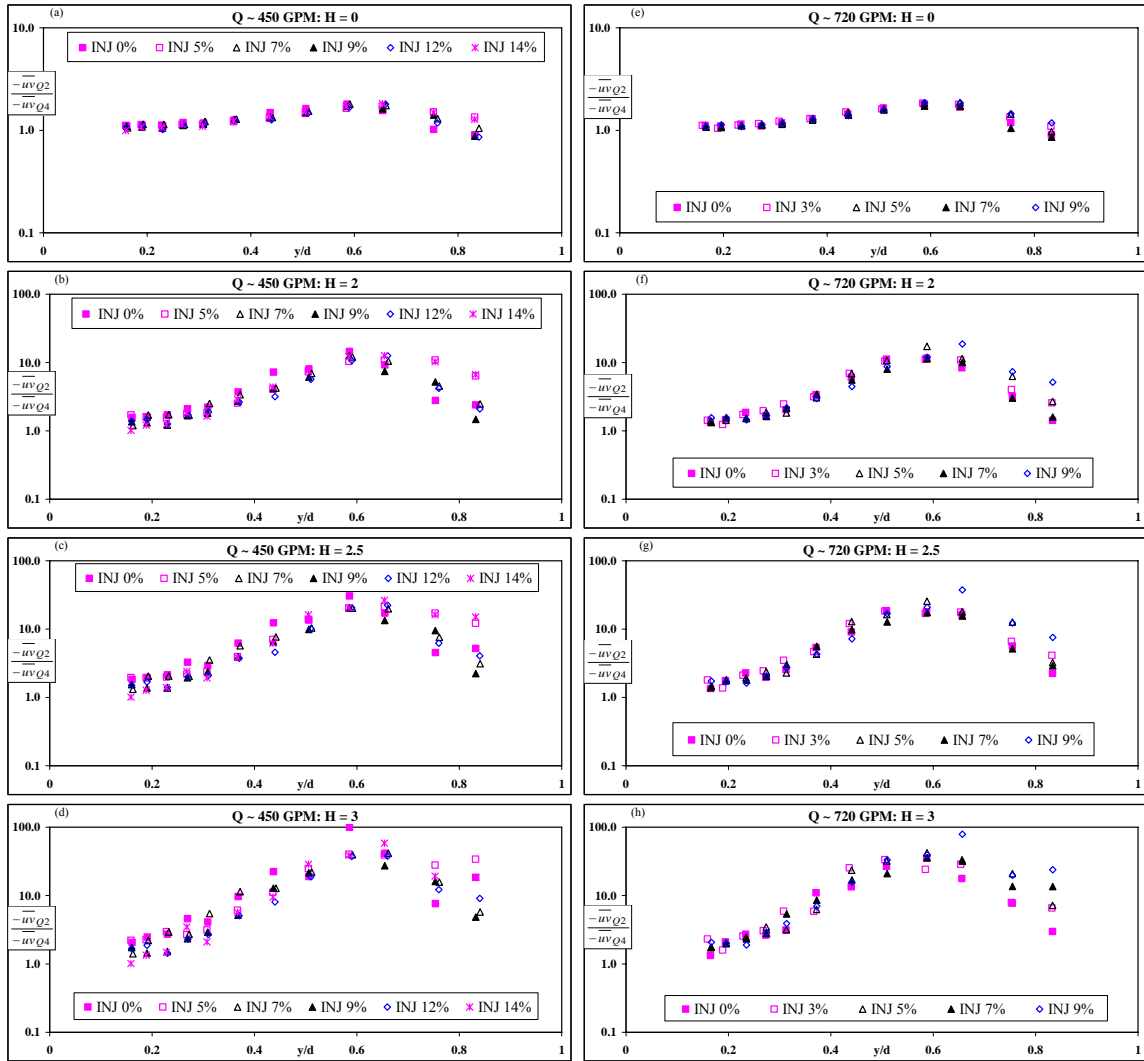


Figure 5.15: Ratio of different quadrant events to the Reynolds stress for different flow rates and with introduction of injection.



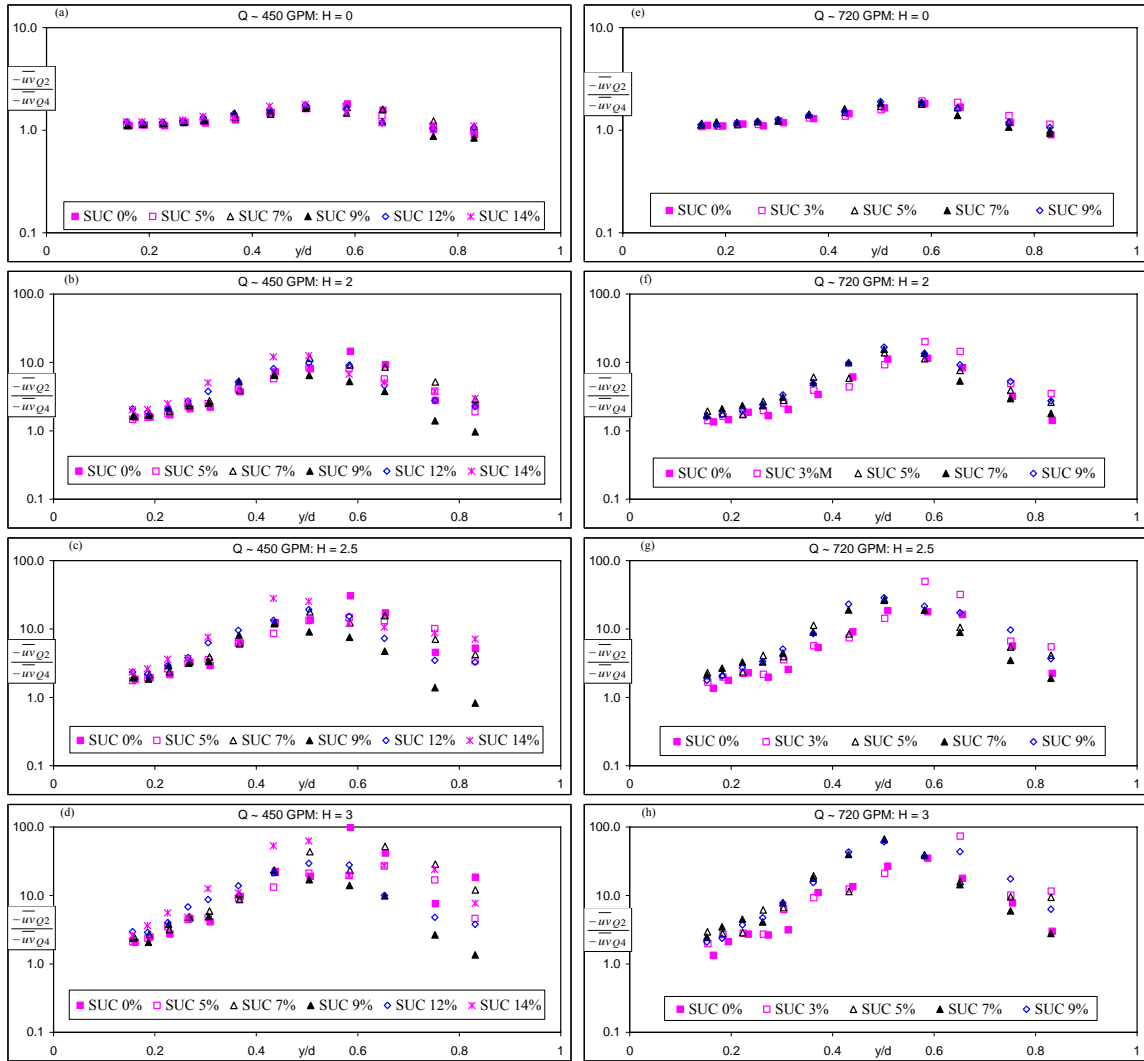


Figure 5.16: Ratio of different quadrant events to the Reynolds stress for different flow rates and with introduction of suction.

## CHAPTER 6

### ICE COVERED OPEN CHANNEL FLOW

This chapter discusses the effects of ice cover on flow in open channels. Two types of ice cover, denoted as Cover 1 and Cover 2 are used. The same four bed conditions used in the previous tests (Chapter 4: Roughness effects on turbulence characteristics) are used here. The same two Reynolds numbers ( $Re \sim 47,500$  and  $31,000$ ) are continued to be used in this series of tests.

#### 6.1 Mean Velocity Profiles

##### 6.1.1 Outer Coordinates

The distributions of the streamwise component of the mean velocity in outer coordinates are shown in Figures 6.1 to 6.6. Average velocity ( $U_{avg}$ ) and flow depth ( $d$ ) are used to non-dimensionalize the streamwise mean velocity ( $U$ ) and the wall normal distance ( $y$ ), respectively. Figure 6.1 shows the mean velocity profiles for flow over a smooth bed with three different surface (cover) conditions. One can note an increase in velocity near the bed and a decrease in velocity near the surface with the introduction of cover. The introduction of the cover, introduces friction and shear stress, in an otherwise zero-stress free surface. The larger friction generated by the more rough Cover 2 causes a greater decrease in the velocity. The corresponding increase in the near bed velocity is more with Cover 2 (rougher cover) flow. This is more clearly demonstrated in the insets of Figure 6.1, which shows the velocity near the bed. One can also note from Figure 6.1 that the maximum mean streamwise velocity (in the flow) increases with the introduction of cover with the rougher Cover 2 showing higher increment than the relatively smoother

Cover 1. The vertical location of the maximum streamwise velocity is found to move closer to the bed for the rougher cover. A similar streamwise mean velocity distribution was also observed (Figure 6.1b) for the lower Reynolds number flow, but the difference in profile between the smoother cover and rougher cover seems to be more.

The distributions of the streamwise component of the mean velocity for the different rough bed conditions are shown in Figures 6.2 to 6.4. The effect of cover is very similar to the flow over the smooth bed with the exception that the maximum value of the mean velocity for flow over rough beds tends to be larger. Figures 6.5 and 6.6 show the velocity profile with different bed conditions with the Cover 1 and 2, respectively. One can note a decrease in velocity near the bed for the rough beds in comparison to the smooth bed. One can also note from Figures 6.5 and 6.6 that the distributed roughness exhibits the highest deviation from the smooth bed profile.

Two-point method of calculating the average velocity in an ice covered flow is a widely used method. Teal et al. (1994) and Lau (1982) found that the average of the velocities at 0.2 and 0.8 of the depth is nearly equal to the overall average velocity. One can note from Figure 6.1 that the average of the velocities at 0.2 and 0.8 of the depth matches quite well with the overall average velocity.

### **6.1.2 Inner Coordinates**

An attempt was made to analyze the streamwise component of the mean velocity in inner coordinates. To this end the data was plotted in two sets, one commencing from the bed (bottom) to the point of maximum velocity and the other is from the cover (top) to the point of maximum velocity. The respective  $U_{\tau}$  values were obtained from the

Clauser plot. Figures 6.7 and 6.8 show the velocity profile in inner coordinates for four different bed conditions with Cover 1 and Cover 2, respectively. The effects of cover and the bed are clearly distinguishable in the graphs of the two figures, with the effect of roughness being consistent with previous rough wall experiments in open channel. One can also note from Figures 6.7 and 6.8 that the total resistance of flow under the cover is higher than the flow without cover due to the additional resistance imposed on the flow. A similar observation under an ice cover has been made by Ashton (1986). However, Helmiö (2001) indicated that the total resistance coefficients of the channel were remarkably lower with ice cover. One can also note from Figures 6.7 and 6.8 that the frictional resistance of the cover could be higher than the resistance of the bed depending on both cover and bed conditions. The results with the lower flow Reynolds number (Figures 6.9 and 6.10) show a trend similar to those at the higher Reynolds number (Figures 6.7 and 6.8). The present results also show that the influence of the cover can be higher than that of the bed (see Figure 6.8d).

## **6.2 Turbulence Intensity**

### **6.2.1 Streamwise Turbulence Intensity**

Figure 6.11 shows the streamwise turbulence intensity in outer variables. Once again, directly measured quantities like depth of flow and maximum velocity are used as the length and velocity scales, respectively, to reduce any additional uncertainties related to scaling parameters with computed quantities. The results clearly show that up to  $y = 0.4d$  for the smooth bed) and  $y = 0.5d$  for rough beds, the distributions do not show any difference due to different surface conditions. However, for greater bed-normal distances,

there are clear differences in streamwise turbulence intensity with changing surface conditions. A similar variation was observed for the flow with lower Reynolds number (Figure 6.12). In each flow condition, the rougher cover (Cover 2) shows the highest deviation in the upper half of the flow.

The same data can be re-plotted to understand the effect of bed roughness. Figure 6.13 shows the data with Cover 1 and two different Reynolds numbers. The bed effects are clearly distinguishable in the bottom region of the flow. While, at the higher Reynolds number, the effect of cover is more prevalent in the upper half of the flow. Figure 6.14 shows the data with the rougher cover (Cover 2) for the two Reynolds numbers. One interesting feature is that the effect of cover is more demonstrated with lower Reynolds number for the upper half of the flow ( $y > 0.5d$ ).

## **6.2.2 Vertical Turbulence Intensity**

Figures 6.15 and 6.16 show the vertical turbulence intensity in outer variables. The variation is very similar to that for streamwise turbulence intensity (Figures 6.11 and 6.12) with the rougher cover (Cover 2) showing the highest deviation in the upper half of the flow. Figures 6.17 and 6.18 show the results for the different bed conditions with Cover 1 and Cover 2, respectively with the two Reynolds numbers. The effect of the bed is distinguishable up to  $y = 0.5d$ . The effect of cover takes precedence after this and is more visible at higher Reynolds number and with Cover 2.

### **6.3 Reynolds Shear Stress**

Figures 6.19 and 6.20 show the Reynolds shear stress distribution for two different Reynolds number in outer variables. The distributions do not show any difference between open-water and Cover 1 throughout the depth. However, there are clear differences in Reynolds shear stress for different bed conditions with the rougher cover (Cover 2) in the upper portion of the flow depth. Both Reynolds numbers show similar trends and the distributed bed roughness provides for the highest Reynolds shear stress in the upper portion of the flow depth followed by the continuous roughness and the natural sand bed.

The same data can be re-plotted to understand the influence of bed roughness. Figures 6.21 and 6.22 show the results with Cover 1 and Cover 2 with the two Reynolds numbers. The bed effects are clearly distinguishable in the bottom region of the flow for Cover 1 and the bed effects are prevalent throughout the depth with relatively rougher Cover 2.

### **6.4 Conclusions**

The present study was carried out to understand the effects of ice cover on the mean velocity, turbulence, Reynolds shear stress in open channel flow (OCF) for two different flow rates. The main findings are summarized as follows:

1. The near-bed velocity increases and the near-surface velocity decreases due to the introduction of ice cover.
2. With increasing cover roughness, the near-bed velocity increases.

3. The maximum streamwise velocity occurring in the flow increases with the introduction of cover and the rougher cover causes the maximum increment.
4. Vertical location of the maximum streamwise velocity is found to move closer to the bed with the introduction of cover and the location is closer to the bed for a rougher cover.
5. Ice cover causes relatively higher maximum mean velocity for flow over rough beds in comparison to smooth bed.
6. Although the individual magnitude of streamwise velocity at 0.2 and 0.8 of the depth may deviate significantly from the overall average velocity depending on the type of cover, the average of the velocities at 0.2 and 0.8 of the depth matches quite well with the overall average velocity. The accuracy of the widely used “two-point method” of calculating the average velocity in an ice covered flow is thus verified.
7. The total resistance under the cover is found to be higher than the flow without the cover due to the additional resistance imposed in the flow.
8. The friction resistance of the cover could be higher than the frictional resistance of the bed depending on both cover and bed conditions.
9. There is no significant effect of cover observed on both of the streamwise and vertical turbulence intensity for the bottom half of the flow depth but an increased intensity was observed for the upper half of the flow depth due to introduction of cover for all beds.
10. The distribution of the Reynolds shear stress does not show any difference between open-water and smooth cover. However, there are clear differences in

Reynolds shear stress in the upper portion of the flow depth for different bed conditions with the rougher cover.

11. The effect of bed roughness on Reynolds shear stress can be seen throughout the flow depth with the introduction of rougher cover and the affected region of the flow depth reduces with the reduction of surface roughness.



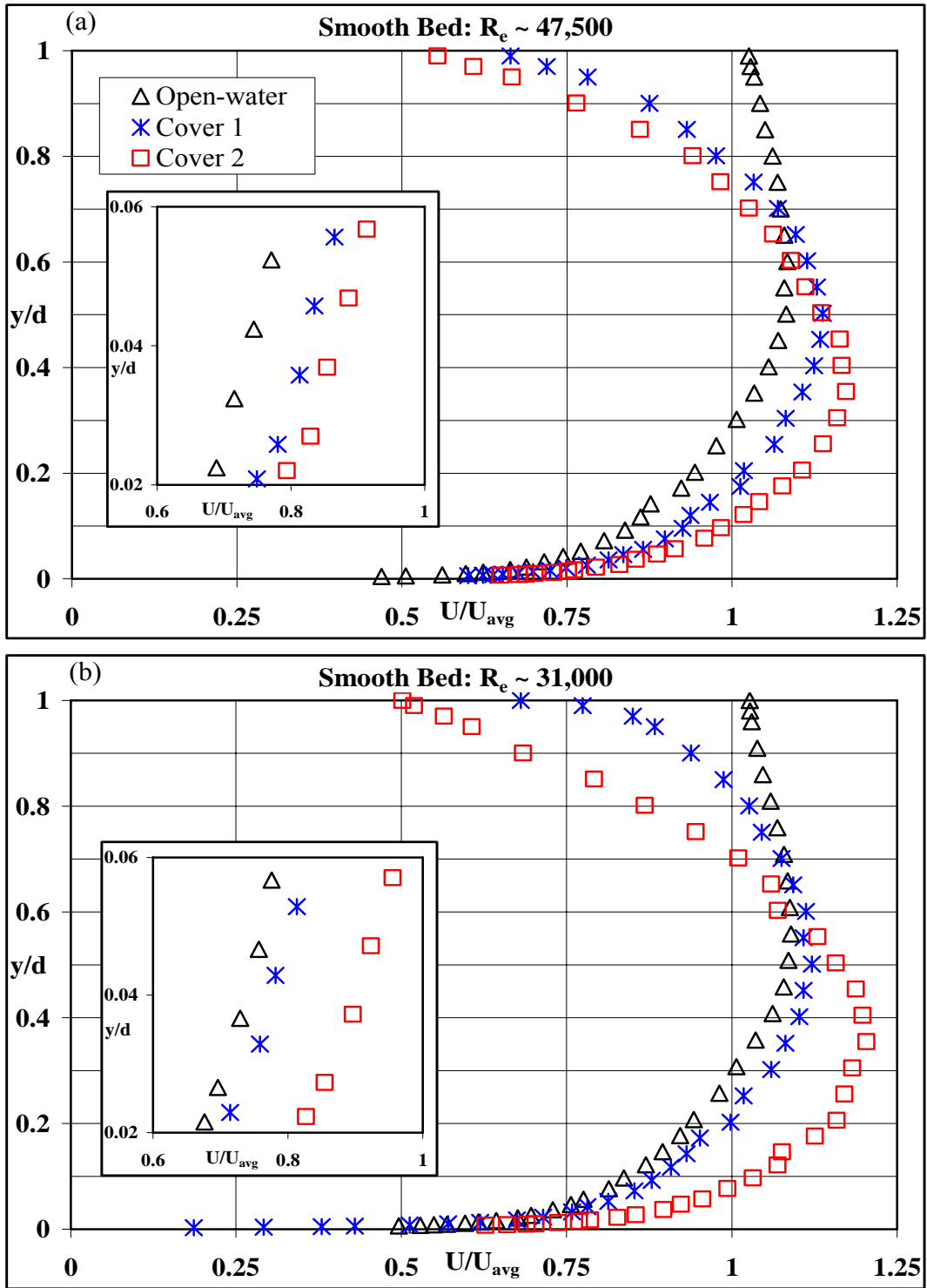


Figure 6.1: Mean velocity profile in outer coordinates for flow over, a) Smooth Bed:  $R_e \sim 47,500$ , b) Smooth Bed:  $R_e \sim 31,000$

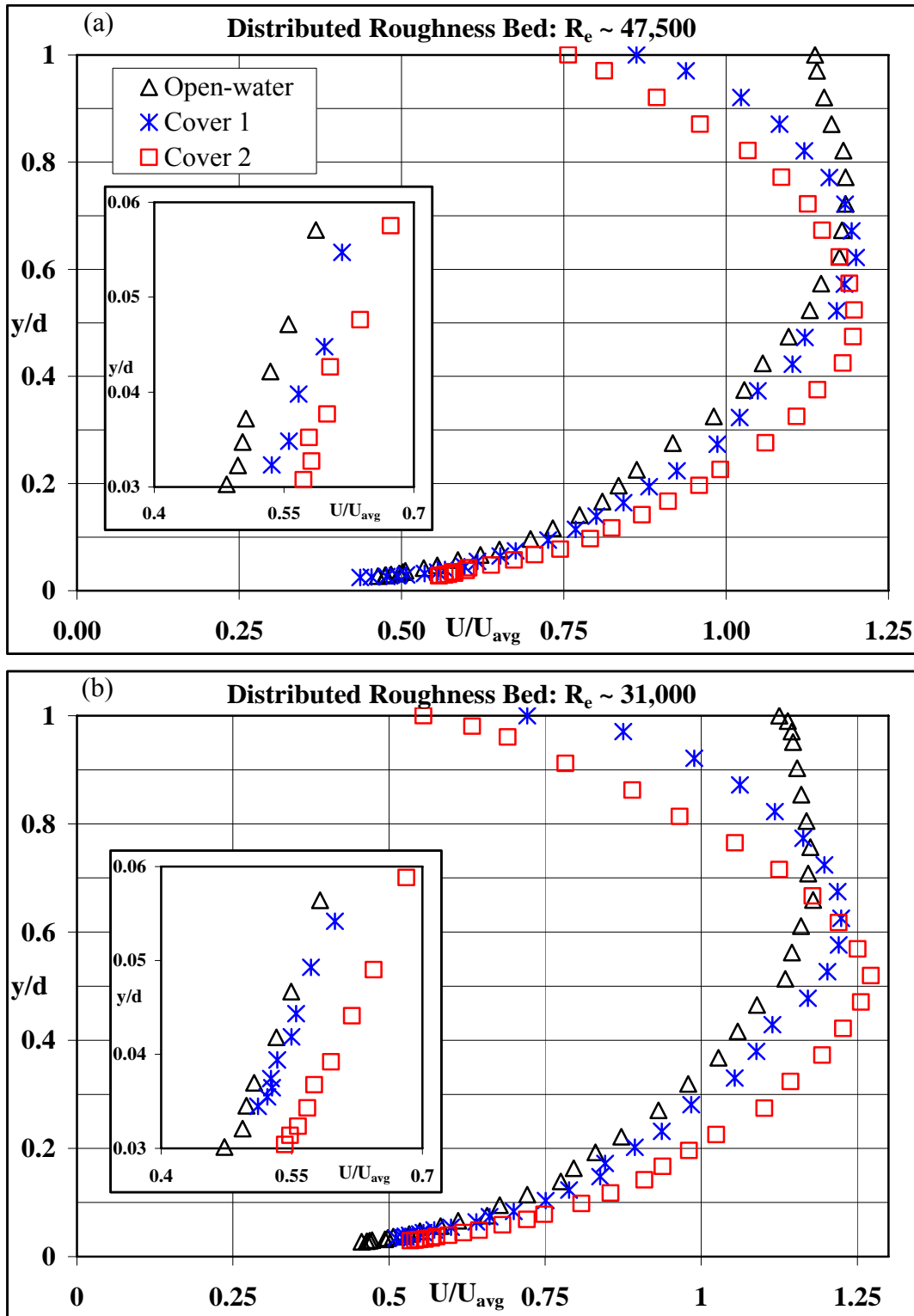


Figure 6.2: Mean velocity profile in outer coordinates for flow over, a) Distributed Roughness Bed:  $R_e \sim 47,500$ , b) Distributed Roughness Bed:  $R_e \sim 31,000$

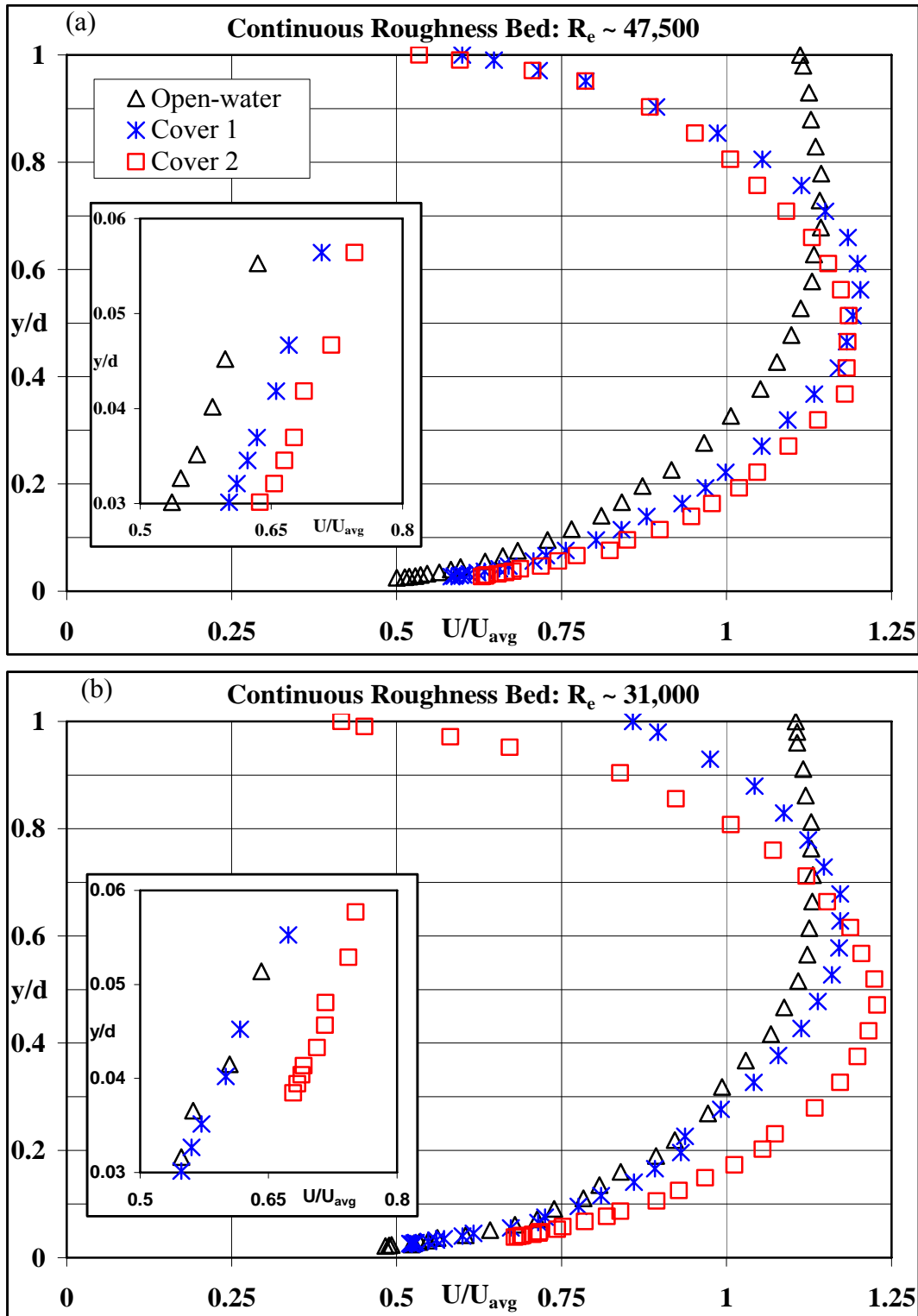


Figure 6.3: Mean velocity profile in outer coordinates for flow over, a) Continuous Roughness Bed:  $R_e \sim 47,500$ , b) Continuous Roughness Bed:  $R_e \sim 31,000$

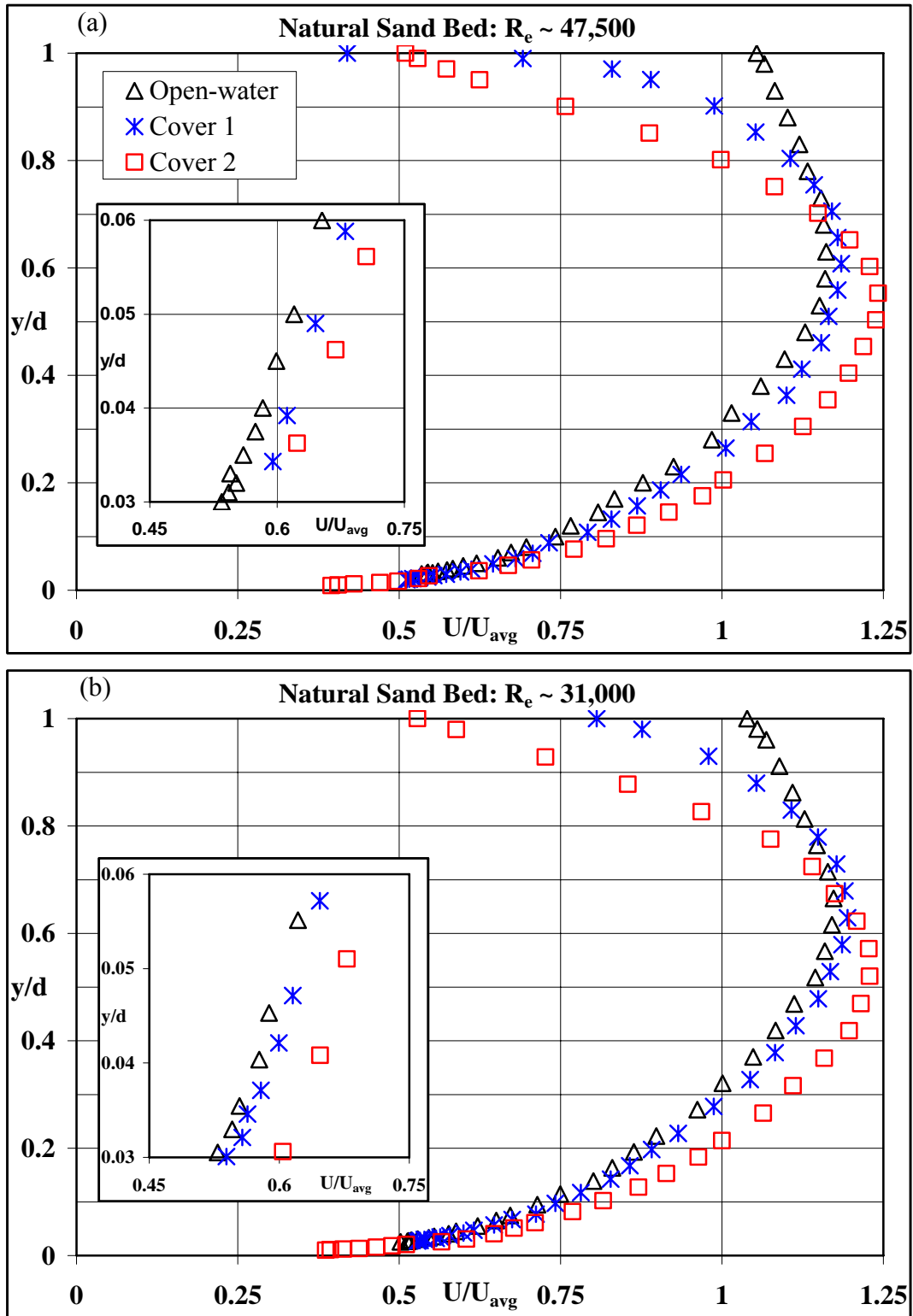


Figure 6.4: Mean velocity profile in outer coordinates for flow over, a) Natural Sand Bed:

$R_e \sim 47,500$ , b) Natural Sand Bed:  $R_e \sim 31,000$

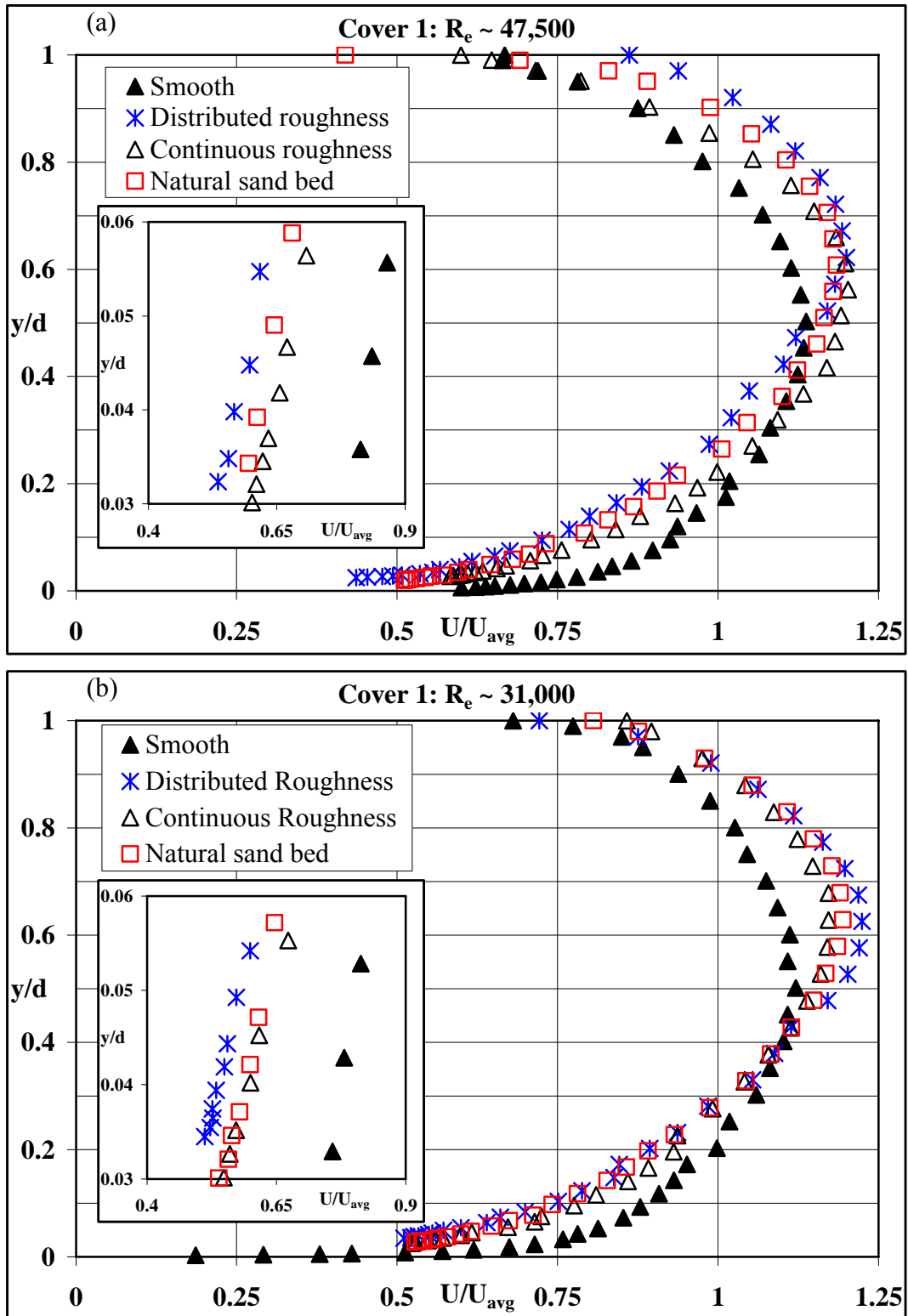


Figure 6.5: Mean velocity profile in outer coordinates for flow over different beds with, a) Cover 1:  $Re \sim 47,500$ , b) Cover 1:  $Re \sim 31,000$

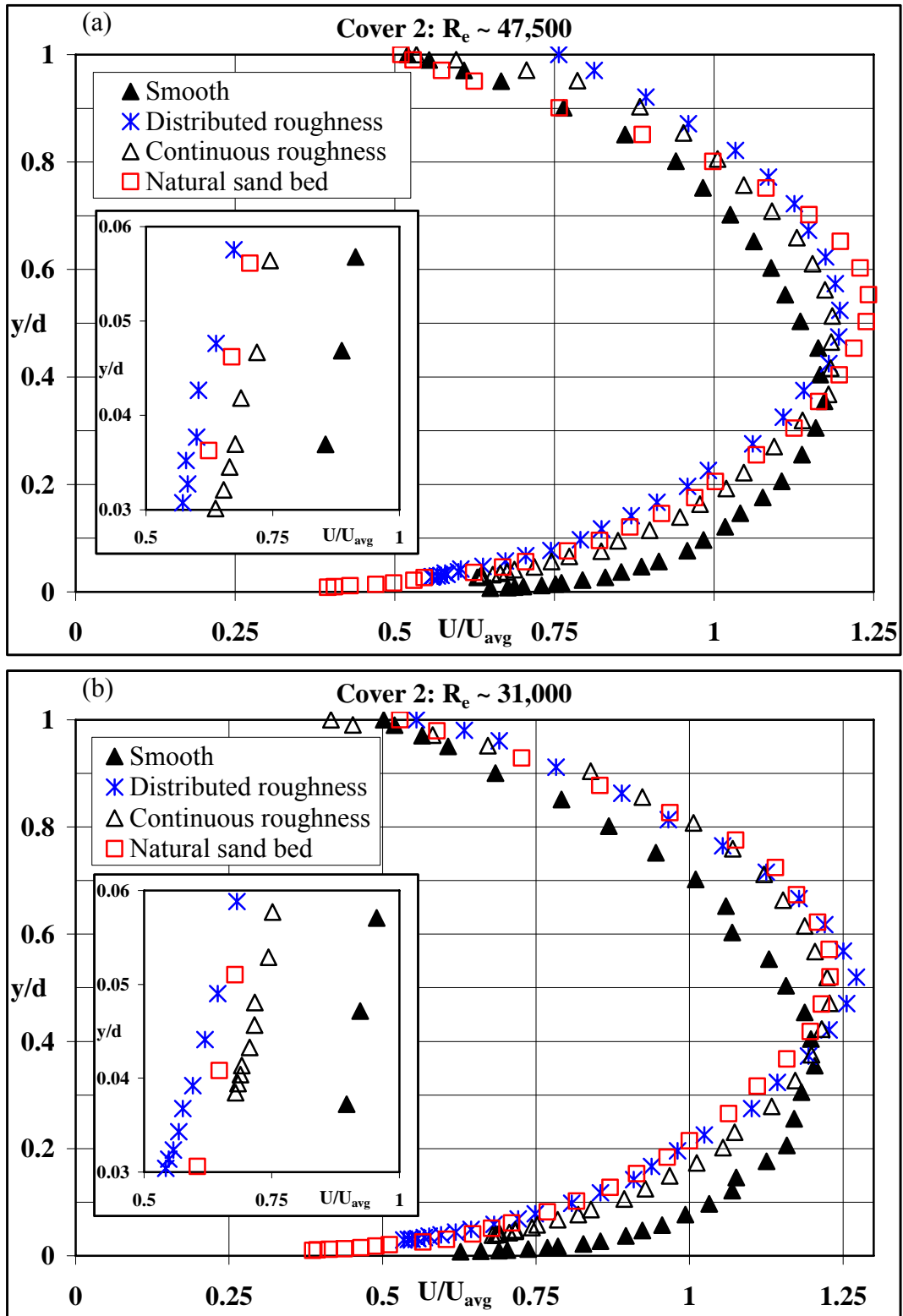


Figure 6.6: Mean velocity profile in outer coordinates for flow over different beds with,  
a) Cover 2:  $R_e \sim 47,500$ , b) Cover 2:  $R_e \sim 31,000$

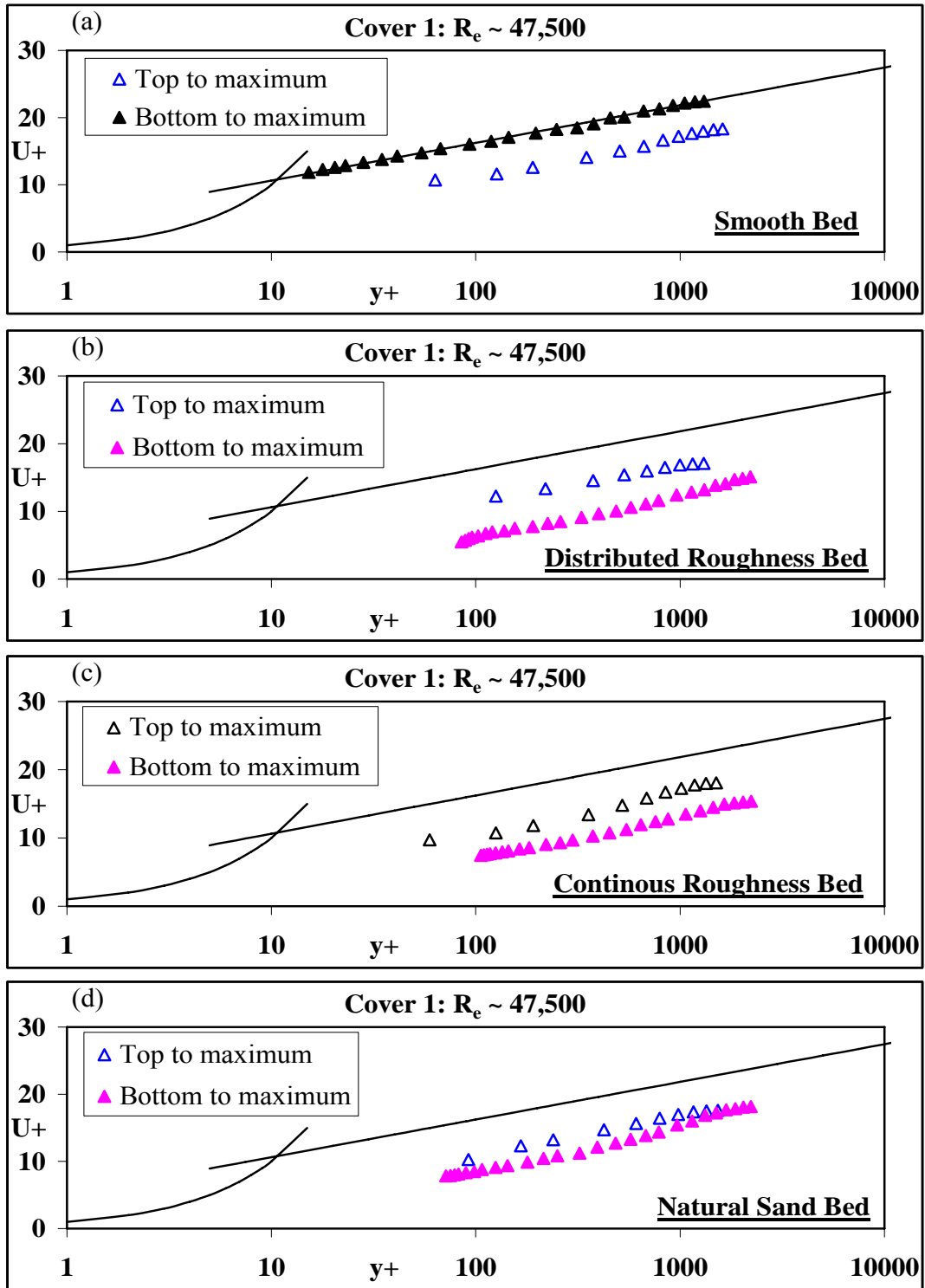


Figure 6.7: Mean velocity profile in inner coordinates with Cover 1 and  $Re \sim 47,500$  for flow over, a) Smooth Bed, b) Distributed Roughness Bed, c) Continuous Roughness Bed, d) Natural Sand Bed

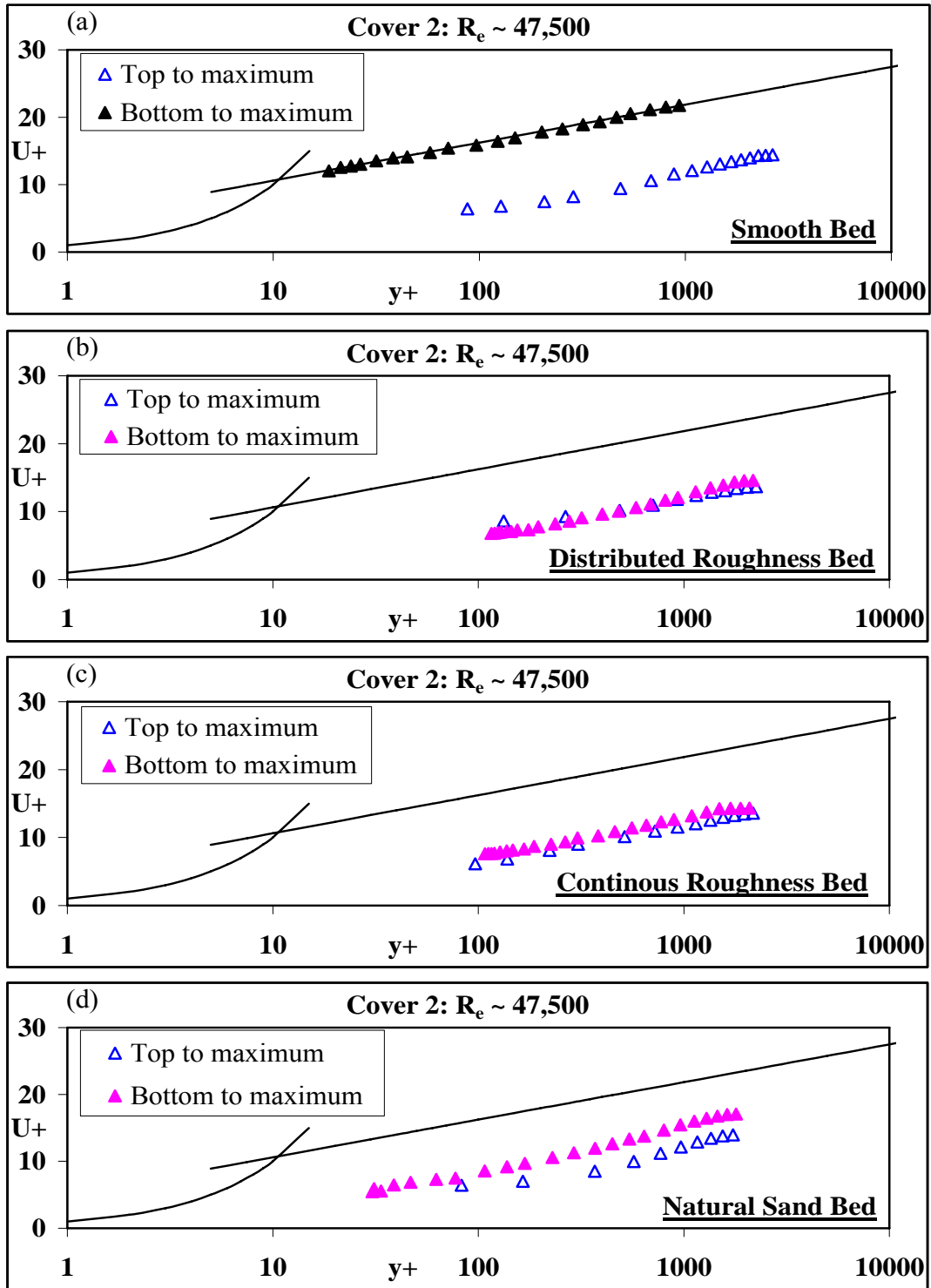


Figure 6.8: Mean velocity profile in inner coordinates with Cover 2 and  $R_e \sim 47,500$  for flow over, a) Smooth Bed, b) Distributed Roughness Bed, c) Continuous Roughness Bed, d) Natural Sand Bed



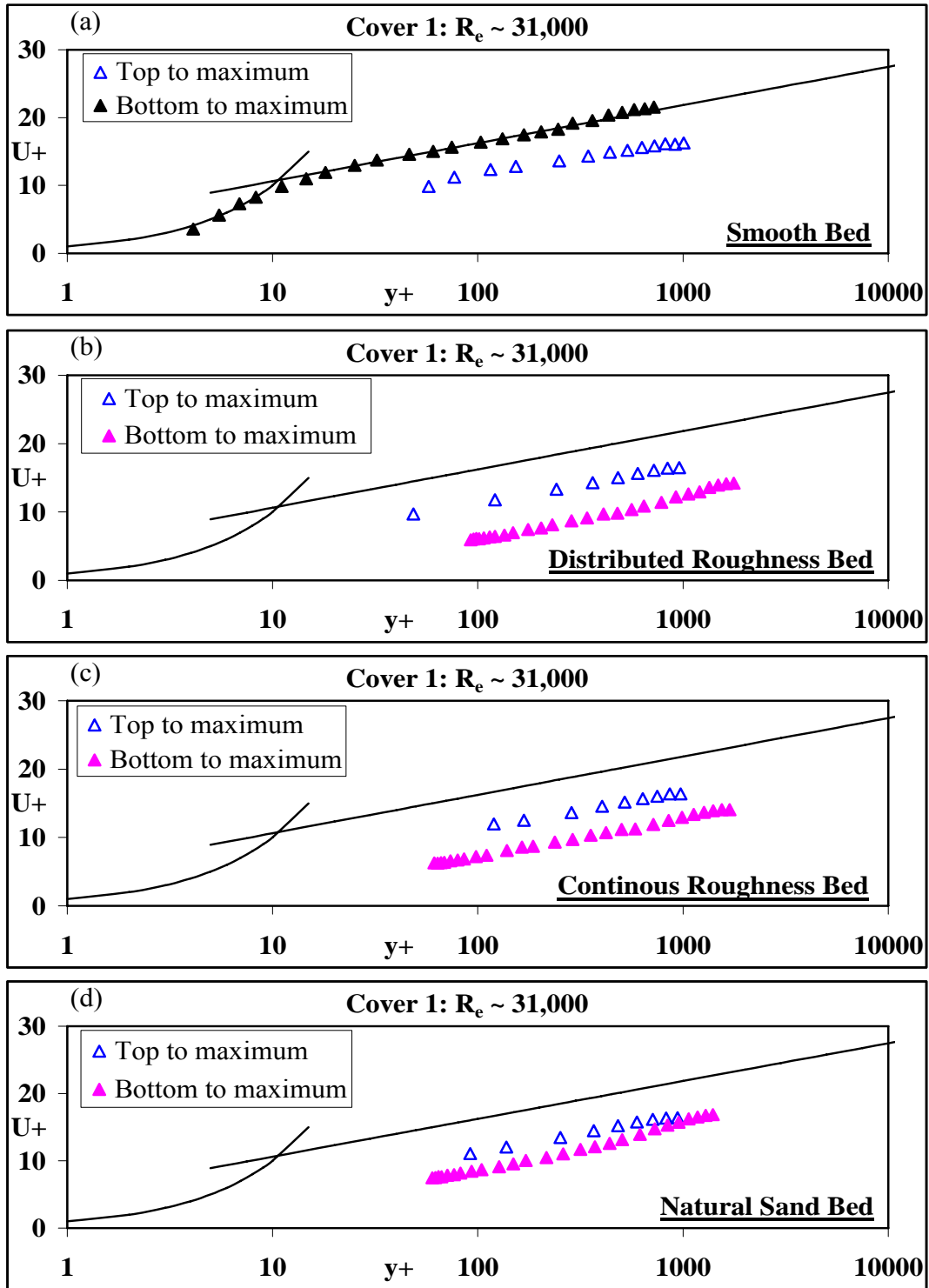


Figure 6.9: Mean velocity profile in inner coordinates with Cover 1 and  $Re \sim 31,000$  for flow over, a) Smooth Bed, b) Distributed Roughness Bed, c) Continuous Roughness Bed, d) Natural Sand Bed

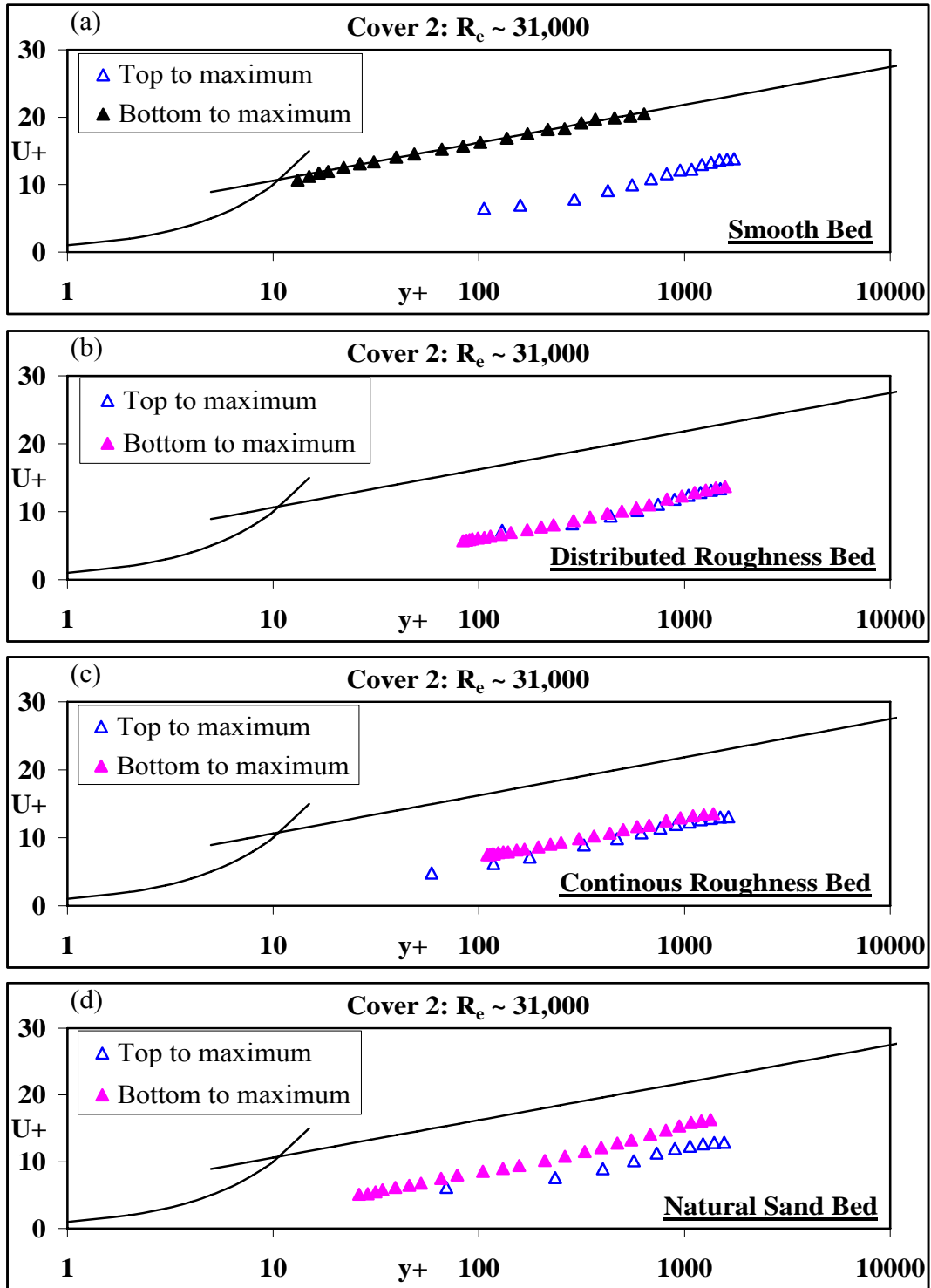


Figure 6.10: Mean velocity profile in inner coordinates with Cover 2 and  $Re \sim 31,000$  for flow over, a) Smooth Bed, b) Distributed Roughness Bed, c) Continuous Roughness Bed, d) Natural Sand Bed

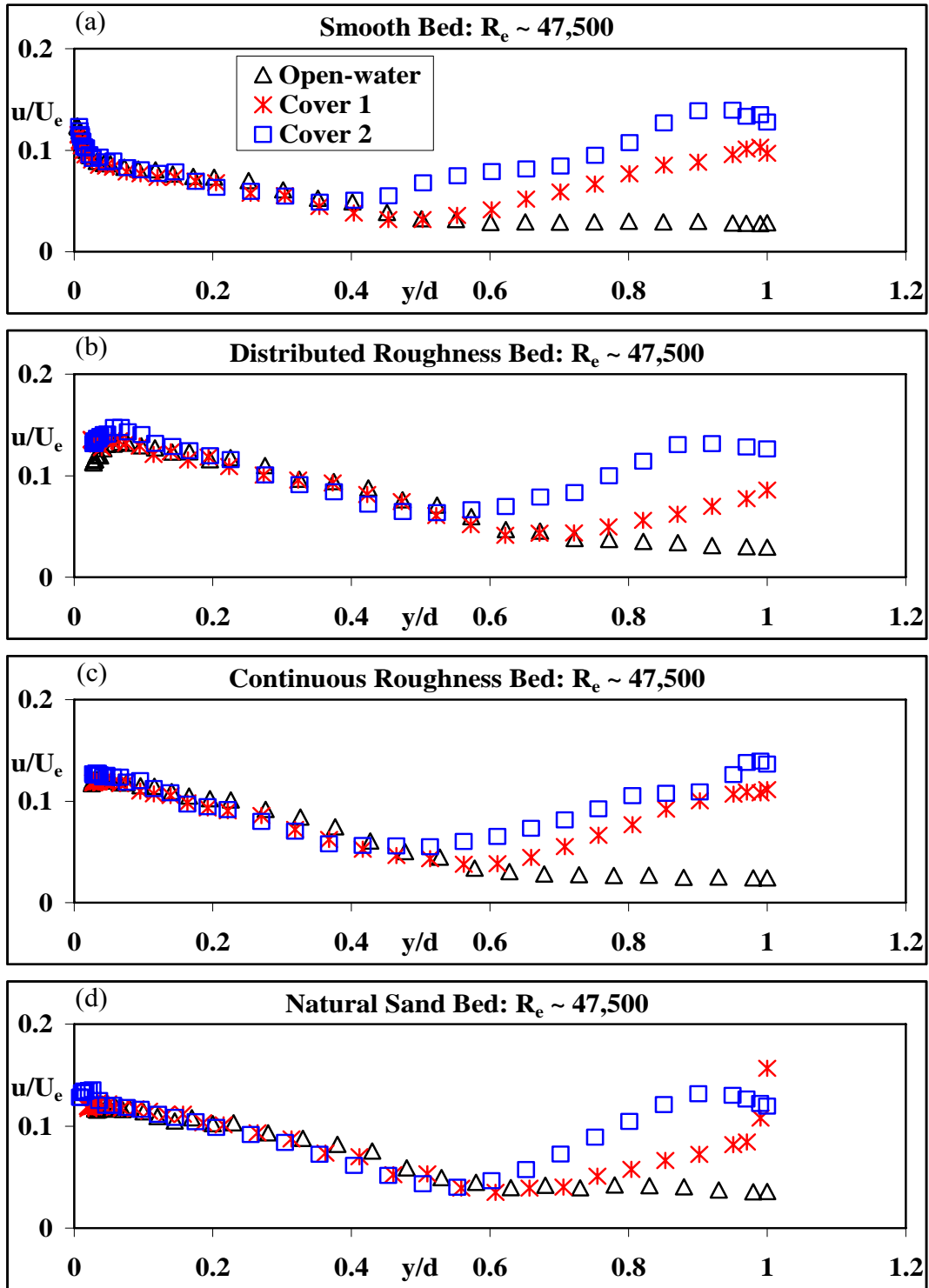


Figure 6.11: Streamwise turbulence intensity for different cover conditions and  $Re \sim 47,500$  for flow over, a) Smooth Bed, b) Distributed Roughness Bed, c) Continuous Roughness Bed, d) Natural Sand Bed

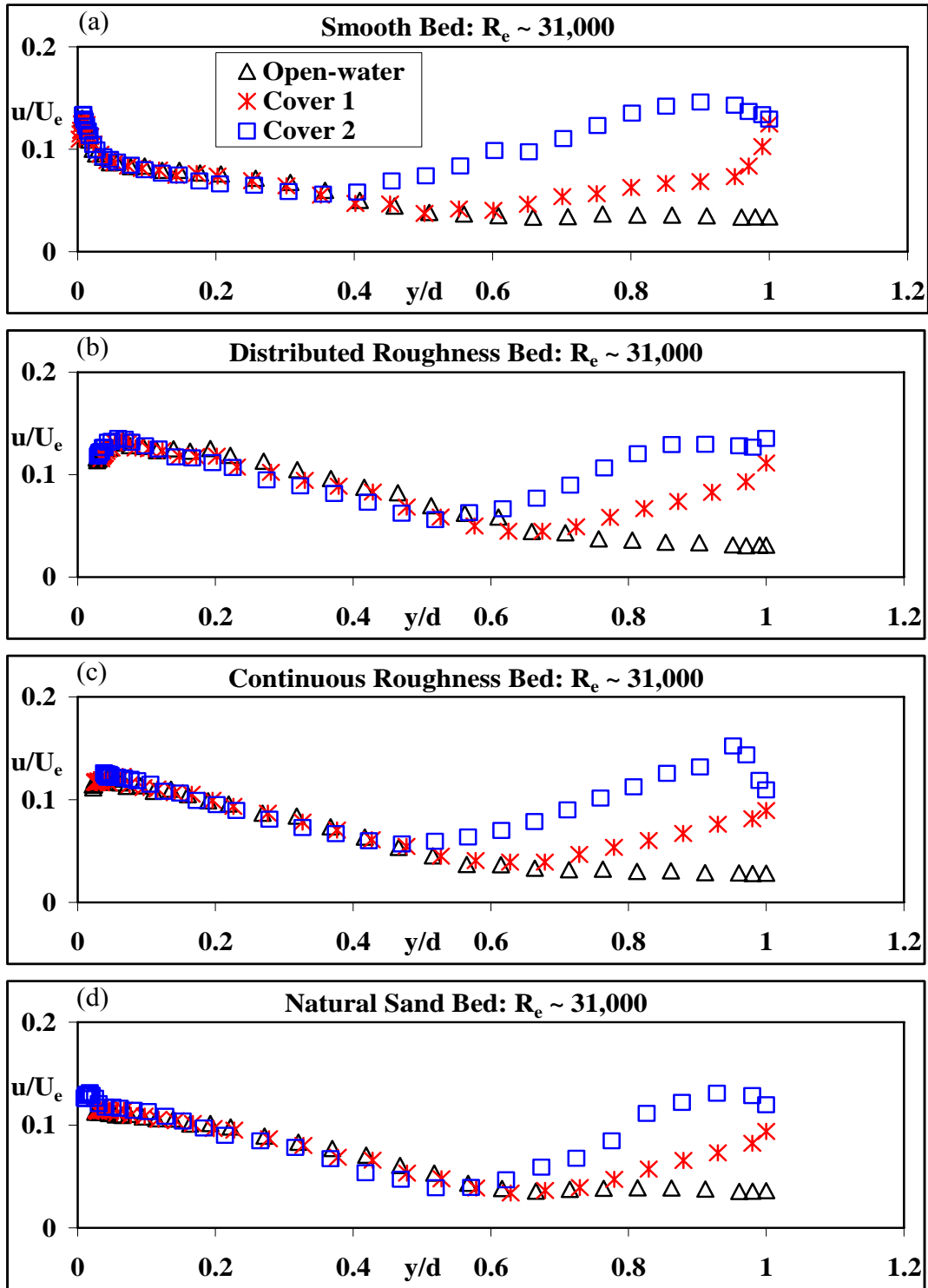


Figure 6.12: Streamwise turbulence intensity for different cover conditions and  $Re \sim 31,000$  for flow over, a) Smooth Bed, b) Distributed Roughness Bed, c) Continuous Roughness Bed, d) Natural Sand Bed

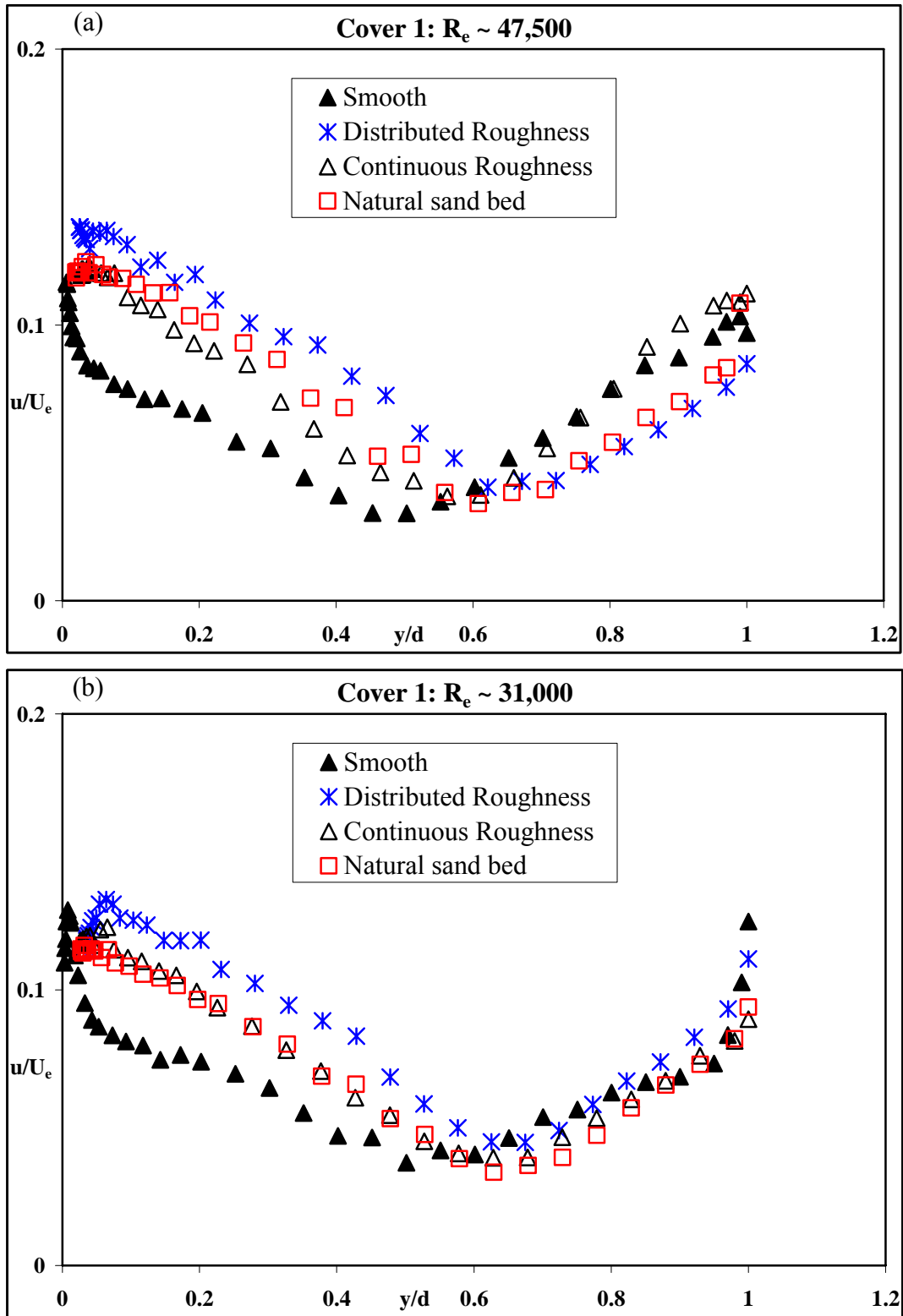


Figure 6.13: Streamwise turbulence intensity for flow over different beds with, a) Cover 1:  $Re \sim 47,500$ , b) Cover 1:  $Re \sim 31,000$

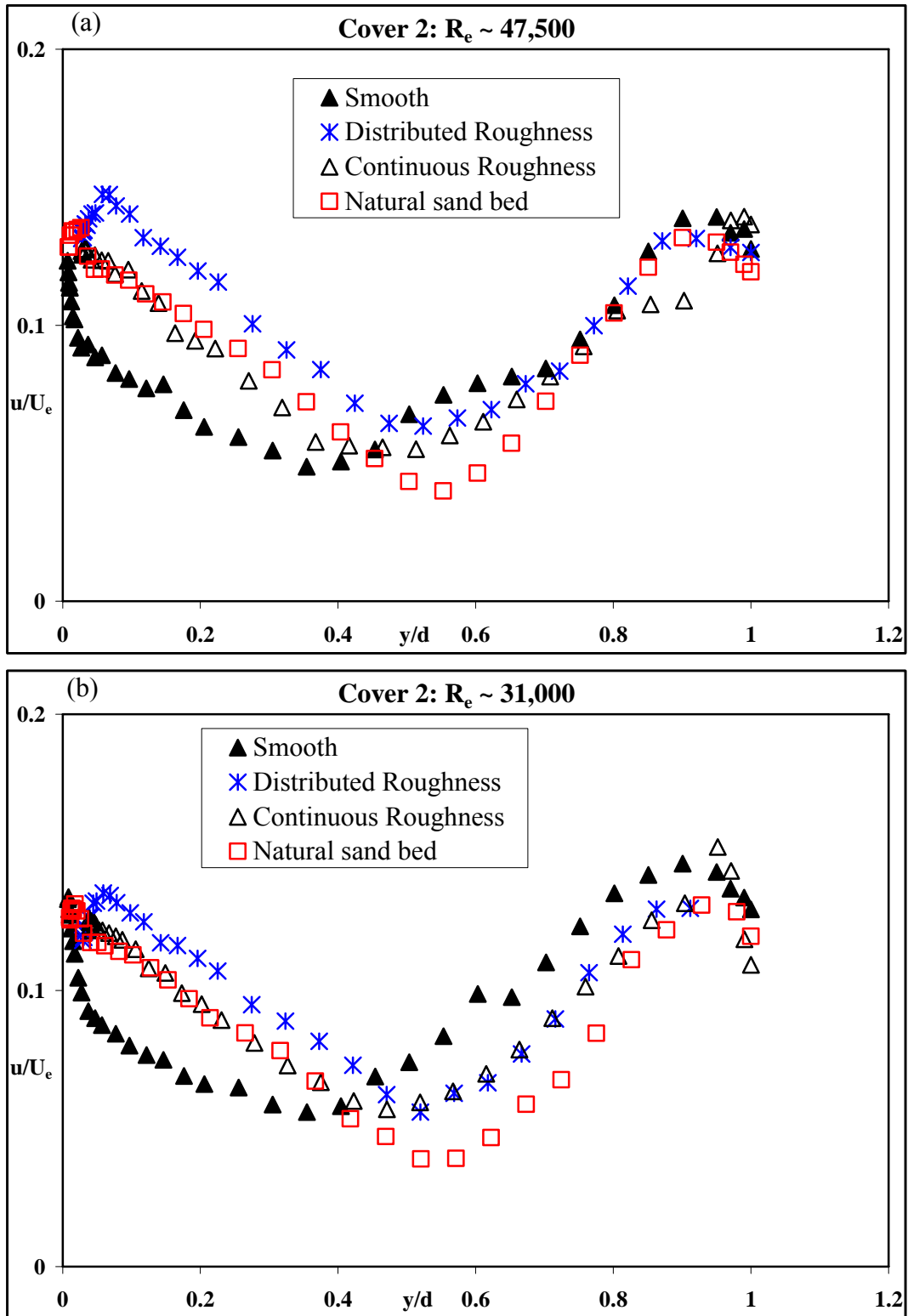


Figure 6.14: Streamwise turbulence intensity for flow over different beds with, a) Cover 2:  $Re \sim 47,500$ , b) Cover 2:  $Re \sim 31,000$

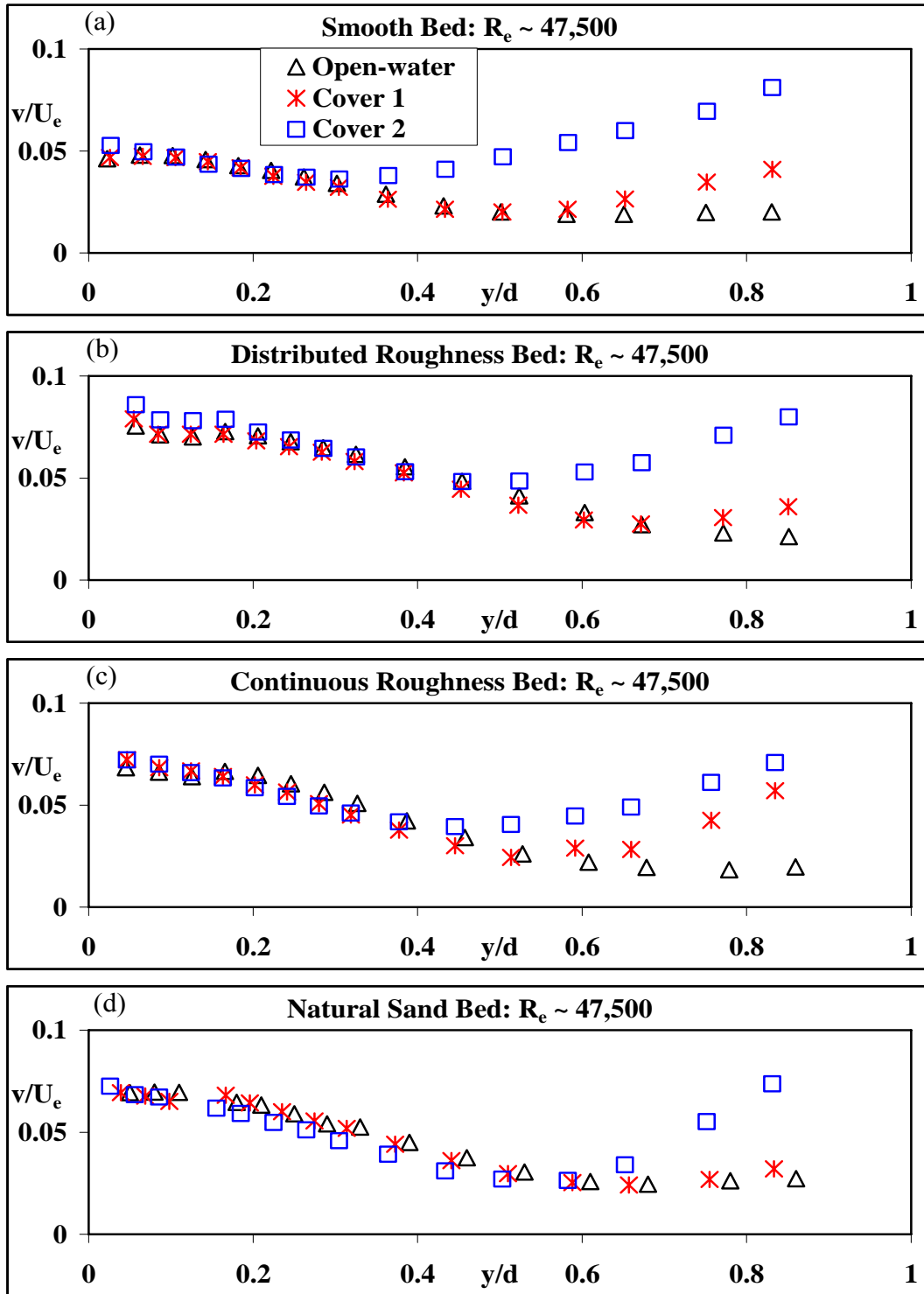


Figure 6.15: Vertical turbulence intensity for different cover conditions and  $R_e \sim 47,500$  for flow over, a) Smooth Bed, b) Distributed Roughness Bed, c) Continuous Roughness Bed, d) Natural Sand Bed

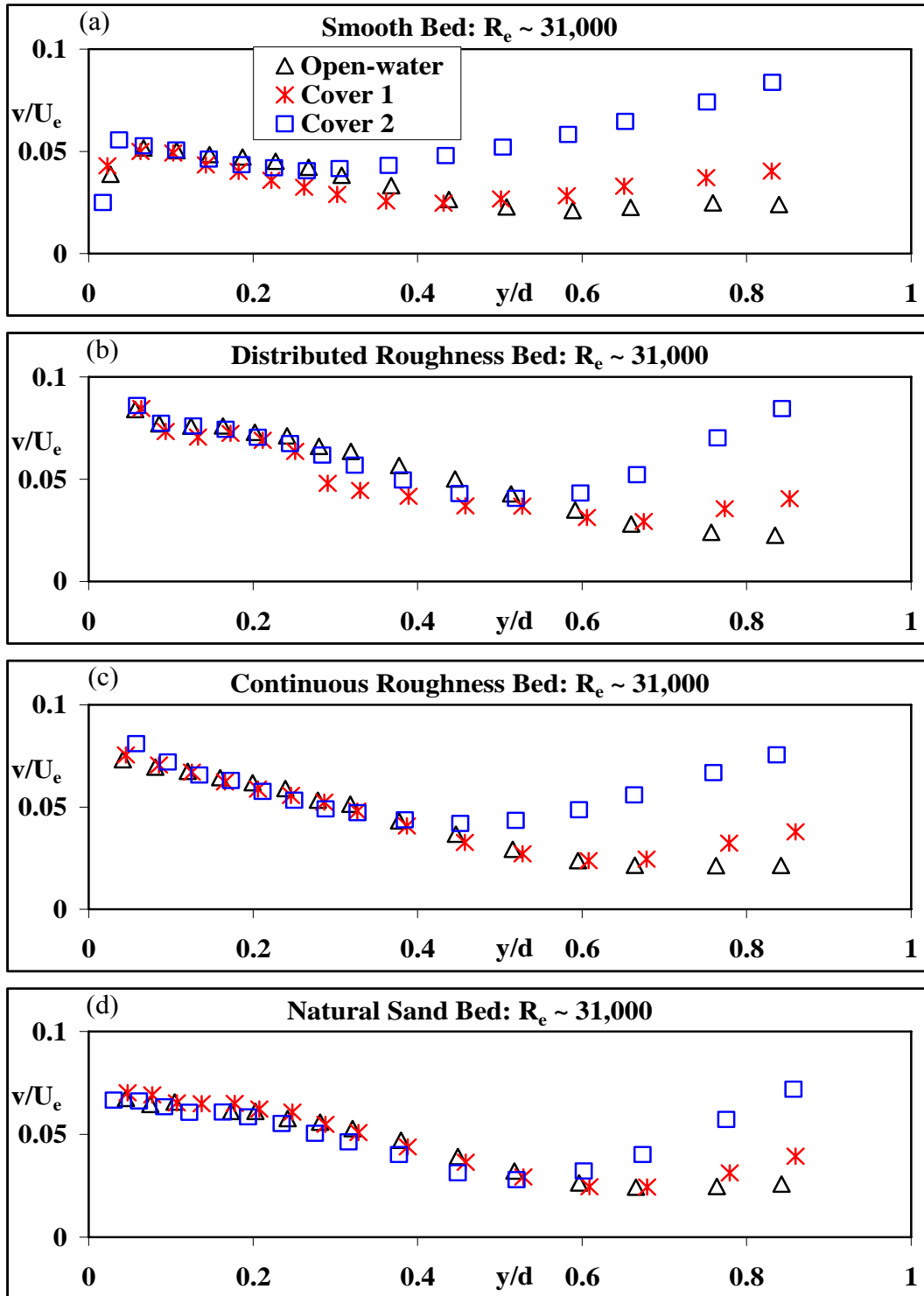


Figure 6.16: Vertical turbulence intensity for different cover conditions and  $R_e \sim 31,000$  for flow over, a) Smooth Bed, b) Distributed Roughness Bed, c) Continuous Roughness Bed, d) Natural Sand Bed



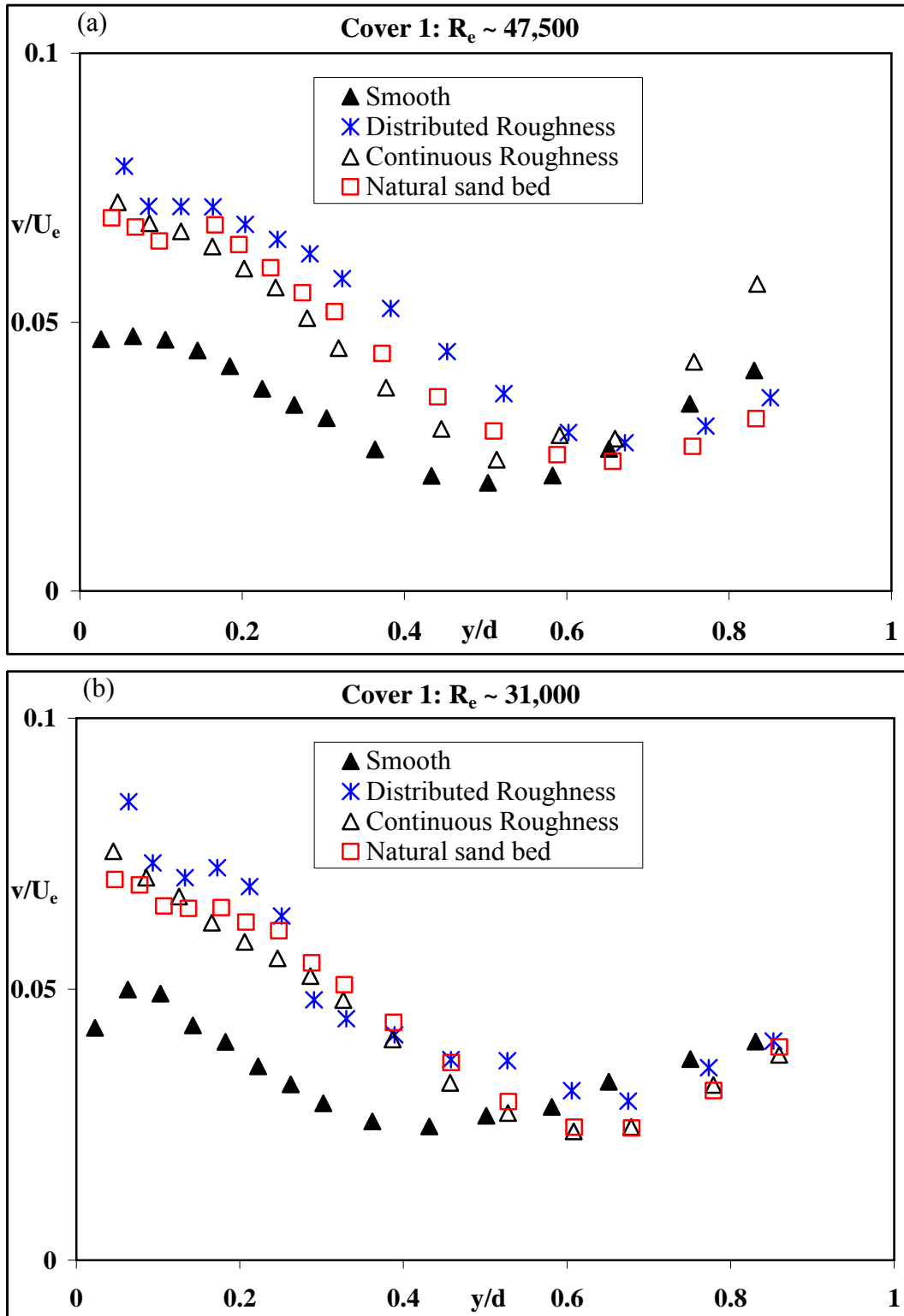


Figure 6.17: Vertical turbulence intensity for flow over different beds with, a) Cover 1:

$Re \sim 47,500$ , b) Cover 1:  $Re \sim 31,000$

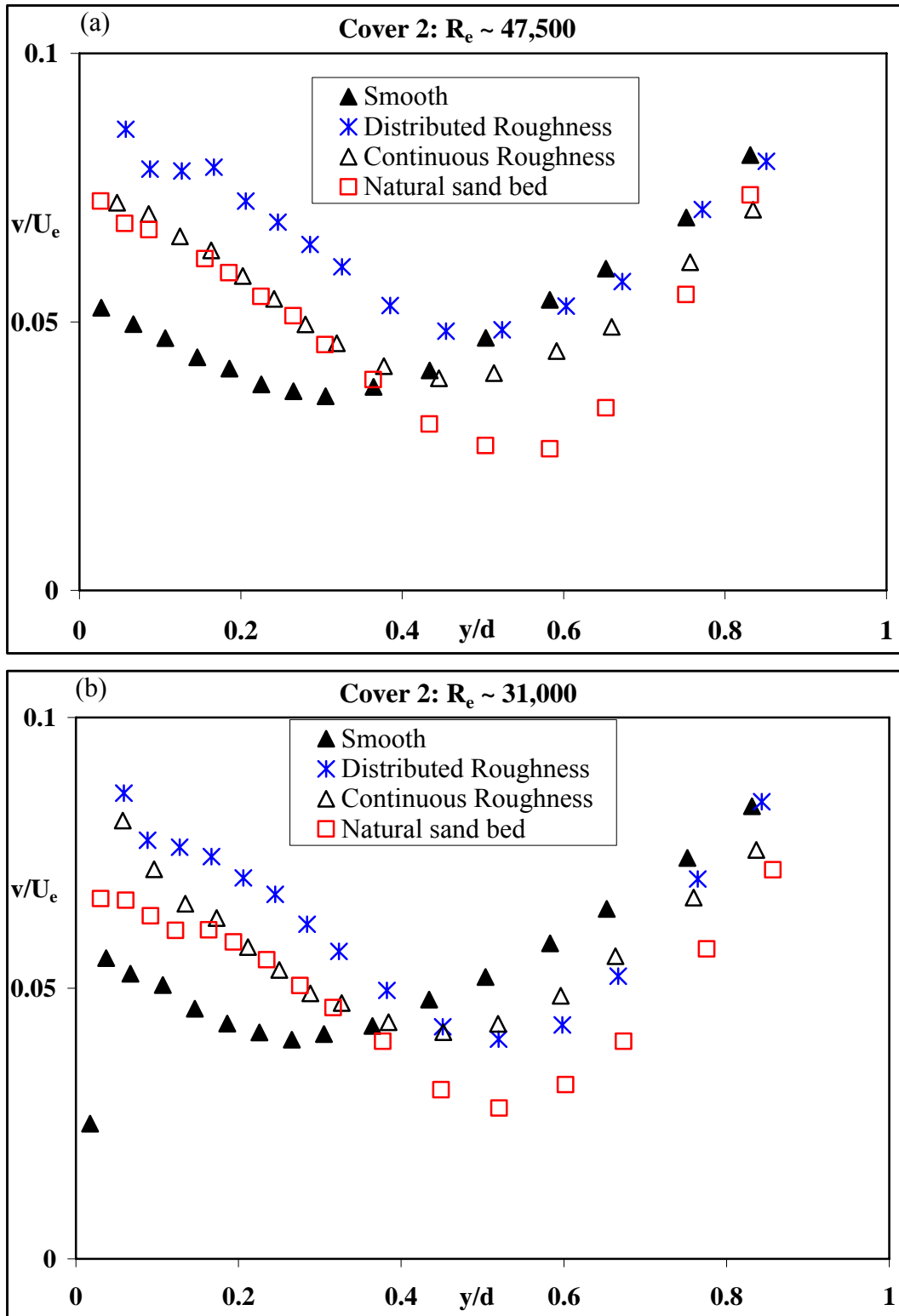


Figure 6.18: Vertical turbulence intensity for flow over different beds with, a) Cover 2:  $R_e \sim 47,500$ , b) Cover 2:  $R_e \sim 31,000$

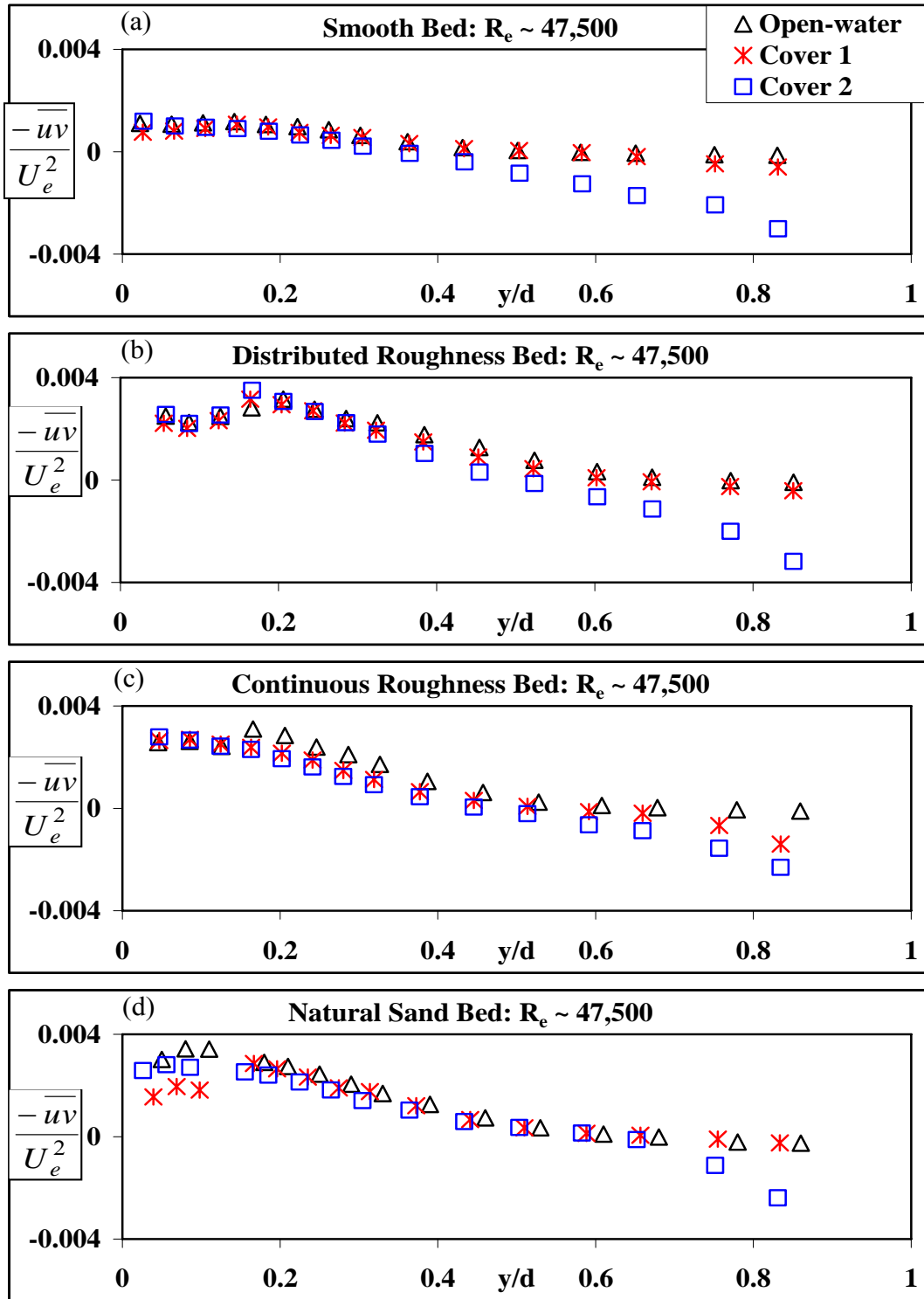


Figure 6.19: Reynolds shear stress for different cover conditions and  $R_e \sim 47,500$  for flow over, a) Smooth Bed, b) Distributed Roughness Bed, c) Continuous Roughness Bed, d) Natural Sand Bed

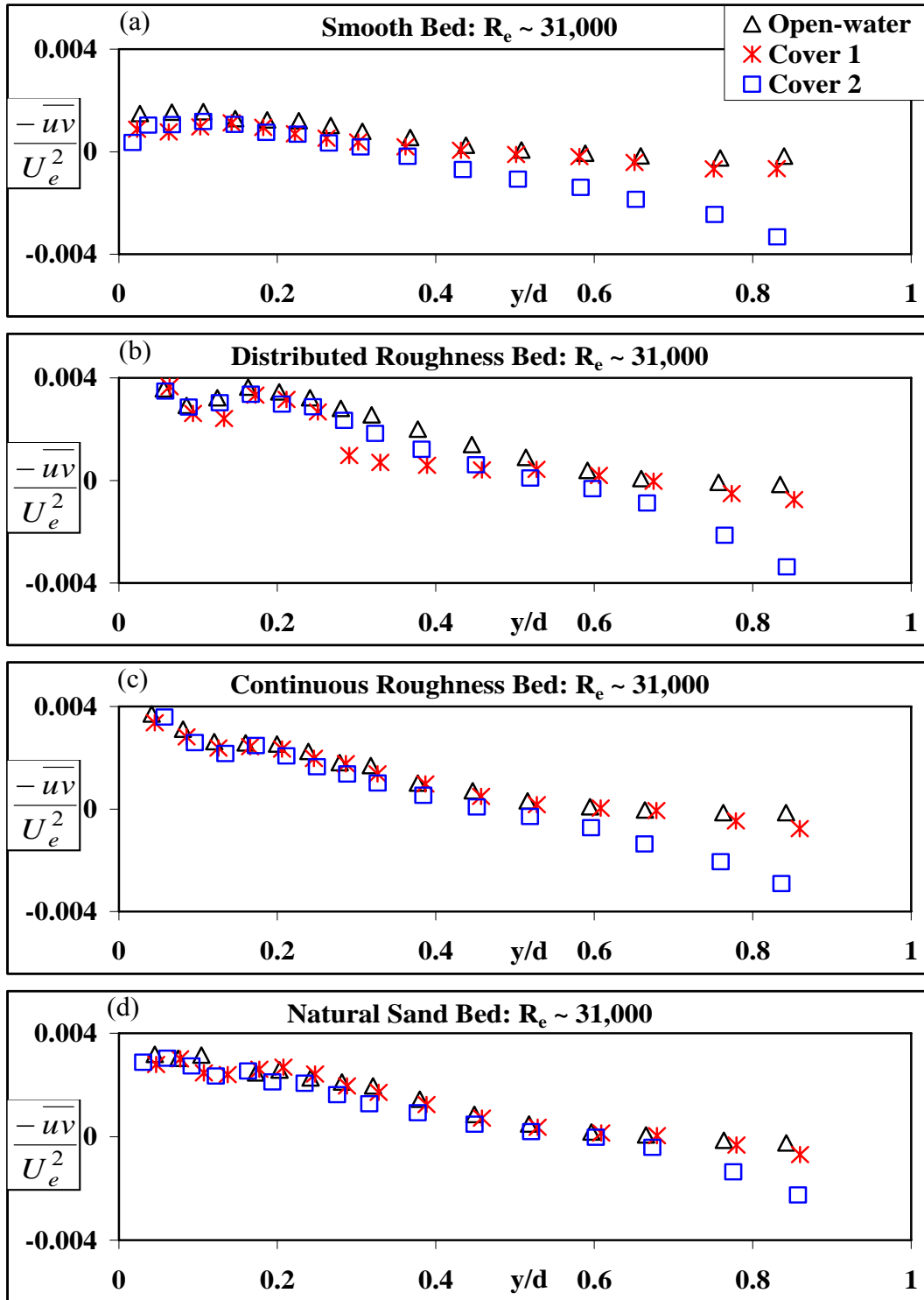


Figure 6.20: Reynolds shear stress for different cover conditions and  $R_e \sim 31,000$  for flow over, a) Smooth Bed, b) Distributed Roughness Bed, c) Continuous Roughness Bed, d) Natural Sand Bed

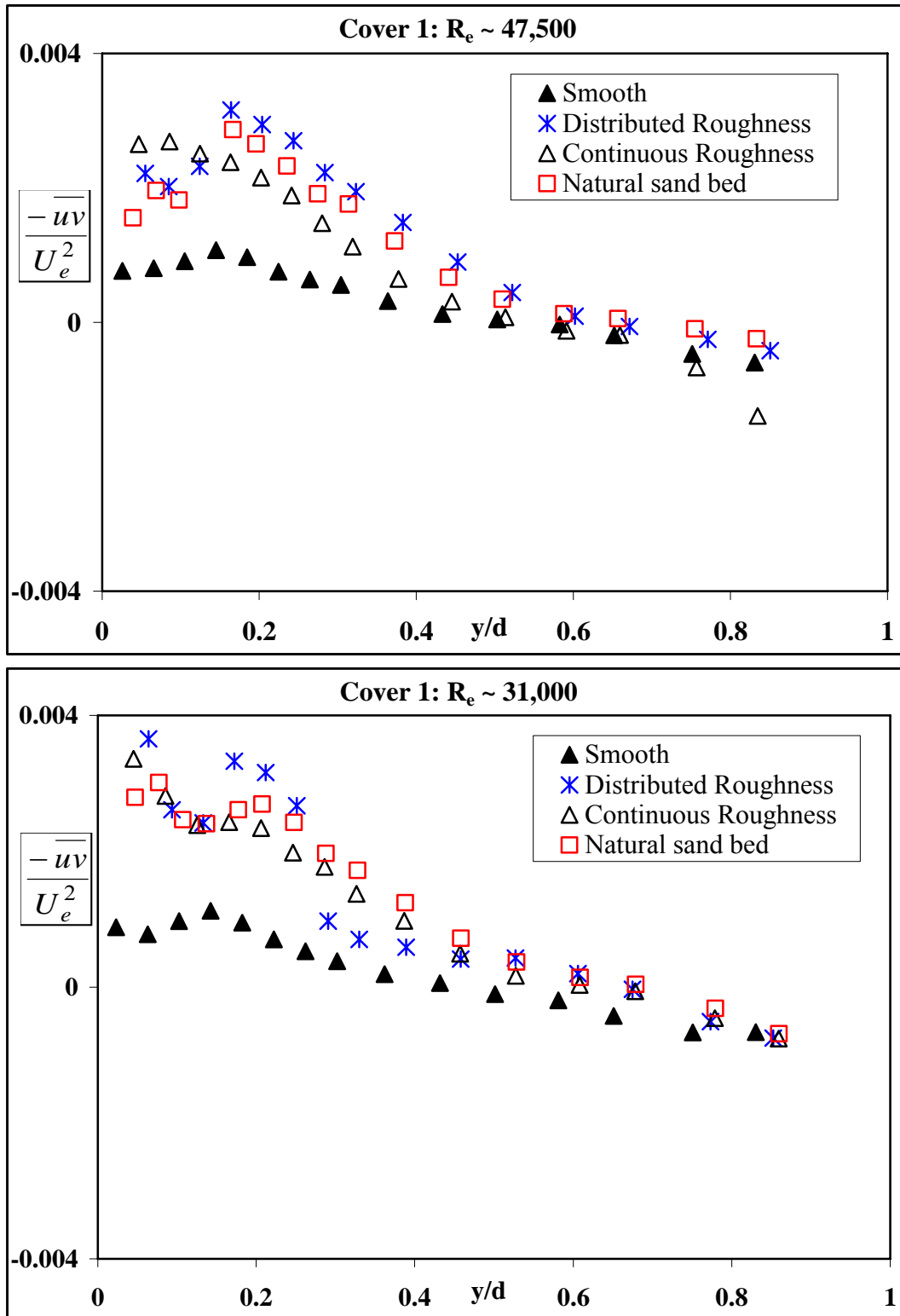


Figure 6.21: Reynolds shear stress for flow over different beds with, a) Cover 1:  $R_e \sim 47,500$ , b) Cover 1:  $R_e \sim 31,000$

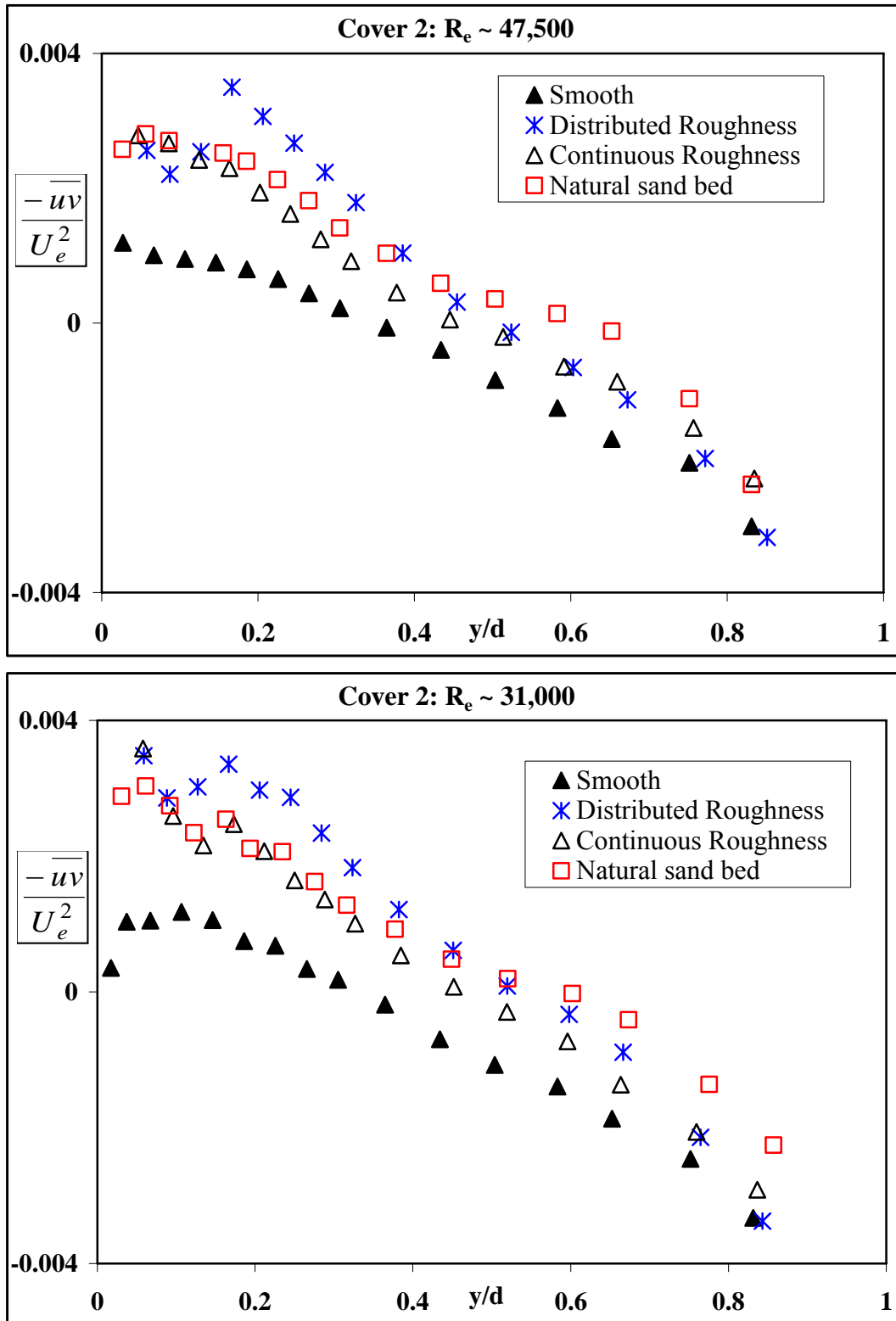


Figure 6.22: Reynolds shear stress for flow over different beds with, a) Cover 2:  $Re \sim 47,500$ , b) Cover 2:  $Re \sim 31,000$

## **CHAPTER 7**

### **Major Conclusions and Future Recommendations**

This thesis dealt with various conditions in open channel flow including the effect of bed roughness, seepage and ice cover. Conclusions related to each one of the above-mentioned effects are presented in the earlier chapters. For brevity, a brief outline of the conclusions is presented below.

#### **7.1 Effect of Roughness**

In this study, the effect of bed roughness on the turbulence characteristics is seen to be prevalent through most of the flow depth. Although the same sand grain is used to create the different rough bed conditions, the differences in turbulence characteristics are an indication that specific geometry of the roughness has an influence. Roughness produces very large instantaneous Reynolds shear stress causing events, which can potentially influence the sediment transport, resuspension of pollutants from the bed and alter the nutrient composition.

#### **7.2 Effect of Seepage**

Introduction of seepage in an open channel flow alters the bed stability. The turbulent characteristics can also be seen to be changed through out the flow depth with the introduction of seepage. Effect of injection on the turbulent characteristics is more evident at the lower flow rate, while the effect of suction seems to be independent of the flow rate. Results from the analysis of turbulent bursting events show clearly the role of seepage well beyond the near-bed region and deep into the outer layer. Injection

eventually increases the magnitude of various turbulent parameters and suction reduces the value in comparison to the no seepage condition.

### **7.3 Effect of Ice Cover**

Significant change in mean velocity profile was observed with the introduction of ice cover. The magnitude of change depends on the roughness of the cover. Changes like the increase of near-bed velocity, decrease in near-surface velocity, increase of maximum mean velocity, downward shift of the location of maximum mean velocity can influence the bed load transport, mixing and erosion. Unlike the mean velocity, the change in turbulent characteristics seems to be bound to the upper half of the flow and the changes can be significant with the rougher cover.

### **7.4 Recommendations for Future Work**

The following recommendations are relevant to future research:

1. Perform a CFD analysis with different bed and surface conditions to enable comparisons with the present results.
2. Study the effect of seepage on open channel flow with different types of sand and flow conditions including both transporting and non-transporting sediment.
3. Study the effect of seepage on incipient motion of bed particles and corresponding changes in turbulence characteristics.
4. Study the effect of ice cover on open channel flow with other types of surface roughness.



5. Study the effect of seepage and ice cover on open channel flow with at different flow depths.
6. Study the coherent structures with the introduction of seepage and ice cover using PIV.

## References

- Afzal, B., Faruque, M. A. A., and Balachandar, R. (2009). "Effect of Reynolds number, near-wall perturbation and turbulence on smooth open channel flows." *Journal of Hydraulic Research*, 47(1), 66-81.
- Agelinchaab, M., and Tachie, M. F. (2006). "Open channel turbulent flow over hemispherical ribs." *International Journal of Heat and Fluid Flow*, 27(6), 1010-1027.
- Antonia, R. A., and Krogstad, P-A. (2001). "Turbulence structure in boundary layers over different types of surface roughness." *Fluid Dynamics Research*, 28(2), 139-157.
- Antonia, R. A., and Zhu, Y. (1995). "Effect of concentrated wall suction on a turbulent boundary layers." *Physics of Fluids*, 7(10), 2465-2474.
- Ashton, G. D. (1986). *River and lake ice engineering*. Water Resources Publications. Littleton. Colo.
- Balachandar, R., and Patel, V. C. (2002). "Rough wall boundary layer on plates in open channels." *Journal of Hydraulic Engineering*, 128(10), 947-951.
- Balachandar, R., and Bhuiyan, F. (2007). "Higher-order moments of velocity fluctuations in an open channel flow with large bottom roughness." *Journal of Hydraulic Engineering*, 133(1), 77-87.
- Balachandar, R., Hyun, B.S., and Patel, V.C. (2007). "Effect of depth on flow over a fixed dune." *Canadian Journal of Civil Engineering*, 34(12), 1587-1599.
- Bey, A., Faruque, M. A. A., and Balachandar, R. (2007). "Two dimensional scour hole problem: Role of fluid structures." *Journal of Hydraulic Engineering*, 133(4), 414-430.

- Bigillon, F., Niño, Y., and Garcia, M. H. (2006). "Measurements of turbulence characteristics in an open-channel flow over a transitionally-rough bed using particle image velocimetry." *Experiments in Fluids*, 41(6), 857-867.
- Chen, X., and Chiew, Y. M. (2004). "Velocity distribution of turbulent open-channel flow with bed suction." *Journal of Hydraulic Engineering*, 130(2), 140-148.
- Chen, X., and Chiew, Y. M. (2007). "Turbulence characteristics of open-channel flow with bed suction." *Journal of Engineering Mechanics*, 133(12), 1388-1393.
- Cheng, N. S., and Chiew, Y. M. (1998a). "Turbulent open-channel flow with upward seepage." *Journal of Hydraulic Research*, 36(3), 415-431.
- Cheng, N. S., and Chiew, Y. M. (1998b). "Modified logarithmic law for velocity distribution subjected to upward seepage." *Journal of Hydraulic Engineering*, 124(12), 1235-1241.
- Cheng, N. S., and Chiew, Y. M. (1999). "Incipient sediment motion with upward seepage." *Journal of Hydraulic Research*, 37(5), 665-681.
- Dancey, C. L., Balakrishnan, M., Diplas, P., and Papanicolaou, A. N. (2000). "The spatial inhomogeneity of turbulence above a fully rough, packed bed in open channel flow." *Experiments in Fluids*, 29(4), 402-410.
- Ettema, R. (2002). "Review of alluvial-channel responses to river ice." *Journal of Cold Regions Engineering*, 16(4), 191-217.
- Faruque, M. A. A., Sarathi, P., and Balachandar, R. (2006). "Clear water local scour by submerged three-dimensional wall jets: Effect of tailwater depth." *Journal of Hydraulic Engineering*, 132(6), 575-580.

- Flack, K. A., Schultz, M. P. and Shapiro, T. A. (2005). "Experimental support for Townsend's Reynolds number similarity hypothesis on rough walls." *Physics of Fluids*, 17(3), 35102-1-9.
- Grass, A. J. (1971) "Structural features of turbulent flow over smooth and rough boundaries." *Journal of Fluid Mechanics*, 50(2), 233-255.
- Harrison, S. S. (1968). "The effect of ground water seepage on stream regimen-a laboratory study." PhD thesis, University of North Dakota, Grand Forks, N.D.
- Helmiö, T. (2001). "Friction measurements of ice cover: Theory and practice in river Pantaneenjoki." *Proceedings of the 2<sup>nd</sup> IAHR symposium on river, coastal and estuarine morphodynamics*, Obihiro, Japan, 10-14 September, 179-187.
- Kaftori, D., Hetsroni, G., and Banerjee, S. (1995). "Particle behavior in the turbulent boundary layer. I. Motion, deposition, and entrainment." *Physics of Fluids*, 7(5), 1095-1106.
- Kirkgöz, M. S., and Ardiçhoğlu, M. (1997). "Velocity profiles of developing and developed open channel flow." *Journal of Hydraulic Engineering*, 123(2), 1099-1105.
- Krogstad, P.-A., Andersson, H. I., Bakken, O. M., and Ashrafian, A. (2005). "An experimental and numerical study of channel flow with rough walls." *Journal of Fluid Mechanics*, 530, 327-352.
- Krogstad, P.-A., Antonia, R., and Browne, L. W. B. (1992) "Comparison between rough and smooth-wall turbulent boundary layers." *Journal of Fluid Mechanics*, 245, 599-617.

- Krogstad, P-A., and Antonia, R. (1999). "Surface roughness effects in turbulent boundary layers." *JExperiments in Fluids*, 27, 450-460.
- Krogstad, P-A., and Kourakine, A. (2000). "Some effects of localized injection on the turbulence structure in a boundary layer." *Physics of Fluids*, 12(11), 2990-2999.
- Lau, Y. L. (1982). "Velocity distribution under floating covers." *Canadian journal of Civil Engineering*, 9, 76-83.
- Lau, Y. L., and Krishnappan, B. G. (1981). "Ice cover effects on stream flows and mixing." *Journal of Hydraulic Division*, 107(10), 1225-1242.
- Lau, Y. L., and Krishnappan, B. G. (1985). "Sediment transport under ice cover." *Journal of Hydraulic Engineering*, 111(6), 934-950.
- Lu, Y., Chiew, Y. M., and Cheng, N. S. (2008). "Review of seepage effects on turbulent open-channel flow and sediment entrainment." *Journal of Hydraulic Research*, 46(4), 476-488.
- Maclean, A. G. (1991). "Open channel velocity profiles over a zone of rapid infiltration." *Journal of Hydraulic Research*, 29(1), 15-27.
- Maclean, A. G., and Willets, B. B. (1986). "Measurement of boundary shear stress in non-uniform open channel flow." *Journal of Hydraulic Research*, 24(1), 39-51.
- Nakagawa, H. and Nezu, I. (1977). "Prediction of the contributions to the Reynolds stress from bursting events in open-channel flows." *Journal of Fluid Mechanics*, 80(1), 99-128.
- Nezu, I. and Nakagawa, H. (1993). *Turbulence in open-channel flows*. IAHR Monograph, A. A. Balkema, The Netherlands.

- Nezu, I. (2005). "Open-channel flow turbulence and its research prospect in the 21<sup>st</sup> century." *Journal of Hydraulic Engineering*, 131(4), 229-246.
- Oldenziel, D. M. and Brink, W. E. (1974). "Influence of suction and blowing on entrainment of sand particles." *Journal of the Hydraulic Division*, 100(HY7), 935-949.
- Parthasarathy, R. N., and Muste, M. (1994). "Numerical model of flow in ice-covered channel." *Journal of Hydraulic Engineering*, 120(9), 1000-1020.
- Patel V. C. (1998). "Perspective: Flow at high Reynolds number and over rough surfaces – Achilles heel of CFD." *Journal of Fluids Engineering*, 120(3), 434-444.
- Prinos, P. (1995). "Bed-suction effects on structure of turbulent open-channel flow." *Journal of Hydraulic Engineering*, 121(5), 404-412.
- Rao, A. R., and Sitaram, N. (1999). "Stability and Mobility of Sand-Bed Channels Affected by Seepage." *Journal of Irrigation and Drainage Engineering*, 125(16), 370-379.
- Rao, A. R., Subrahmanyam, V., Thayumanavan, S., and Damodaran, N. (1994). "Seepage effects on sand-bed channels." *Journal of Irrigation and Drainage Engineering*, 120(1), 60-79.
- Rashidi, M., Hetsroni, G., and Banerjee, S. (1990). "Particle-turbulence interaction in a boundary layer." *International Journal of Multiphase Flow*, 16(6), 935-949.
- Raupach, M. R., Antonia, R. A., Rajagopalan, S. (1991). "Rough wall turbulent boundary layers." *Applied Mechanics Review*, 44 (1), 1-25.
- Richardson, J. R., Abt, S. R., and Richardson, E. V. (1985). "Inflow seepage influence on straight alluvial channels." *Journal of Hydraulic Engineering*, 111(8), 1133-1147.

- Roussinova, V., Biswas, N., and Balachandar, R. (2008). "Revisiting turbulence in smooth uniform open channel flow." *Journal of Hydraulic Research*, 46(Suppl. 1), 36-48.
- Sarathi, P., Faruque, M. A. A., and Balachandar, R. (2008). "Scour by submerged square wall jets at low densimetric Froude numbers." *Journal of Hydraulic Research*, 46(2), 158-175.
- Sarkar, A., and Dey, S. (2007). "Effects of seepage on scour due to submerged jets and resulting flow field." *Journal of Hydraulic Research*, 45(3), 357-364.
- Schlichting, H. (1979). *Boundary-Layer theory*. McGraw-Hill Classic Textbook Reissue Series, McGraw-Hill, Inc., United States of America.
- Schultz, M. P. and Flack, K. A. (2007). "The rough-wall turbulent boundary layer from the hydraulically smooth to the fully rough regime." *Journal of Fluid Mechanics*, 580, 381-405.
- Schultz, M. P. and Flack, K. A. (2005) "Outer layer similarity in fully rough turbulent boundary layers." *Experiments in Fluids*, 38, 328-340.
- Shukla, M. K., and Mishra, G. C. (1994). "Canal discharge and seepage relationship." *Proceeding 6<sup>th</sup> National symposium on Hydro*. 263-274.
- Simons, D. B., and Richardson, E. V. (1966). "Resistance to flow in alluvial channels." *Geological Survey Prof. Paper*, 422-J, U.S. Geological Survey, Washington, D.C.
- Smith, B. T., and Ettema, R. (1997). "Flow resistance in ice-covered alluvial channels." *Journal of Hydraulic Engineering*, 123(7), 592-599.

- Tachie, M. F., Bergstrom, D. J., and Balachandar, R. (2000). "Rough wall turbulent boundary layers in shallow open channel flow." *Journal of Fluids Engineering*, 122, 533-541.
- Tachie, M. F. (2001). "Open-channel turbulent boundary layers and wall jets on rough surfaces." PhD thesis, University of Saskatchewan, Saskatchewan, Canada.
- Tachie, M. F., Bergstrom, D. J., and Balachandar, R. (2003). "Roughness effects in low- $Re_\theta$  open-channel turbulent boundary layers." *Experiments in Fluids*, 35, 338-346.
- Tachie, M. F., Bergstrom, D. J., and Balachandar, R. (2004). "Roughness effects on the mixing properties in open channel turbulent boundary layers." *Journal of Fluids Engineering*, 126, 1025-1032.
- Tan, C. A., Sinha, S. K., and Ettema, R. (1999). "Ice-cover influence on near-field mixing in dune-bed channel: Numerical simulation." *Journal of Cold Regions Engineering*, 13(1), 1-20.
- Teal, M. J., Ettema, R., and Walker, J. F. (1994). "Estimation of mean flow velocity in ice-covered channels." *Journal of Hydraulic Engineering*, 120(12), 1385-1400.
- Townsend, A. A. (1976). "The structure of turbulent shear flow." *Cambridge University Press*.
- Walker, J. F. (1994). "Methods for discharge under ice cover." *Journal of Hydraulic Engineering*, 120(11), 1327-1336.
- Watters, G. Z., and Rao, M. V. P. (1971). "Hydrodynamic effects of seepage on bed particles." *J. Hydr. Div., ASCE*, 101(3), 421-439.
- Willets, B. B. and Drossos, M. E. (1975). "Local erosion caused by rapid forced infiltration." *Journal of the Hydraulic Division*, 101(HY12), 1477-1488.



Yoon, J. Y., Patel, V. C., and Ettema, R. (1996). "Numerical model of flow in ice-covered channel." *Journal of Hydraulic Engineering*, 122(1), 19-26.

Zagni, A. F. E. and Smith, K. V. H. (1976). "Channel flow over permeable beds of graded spheres." *Journal of Hydraulics Division, Proceedings of the ASCE*, 102 (HY2), 207-222.

## APPENDIX A

### UNCERTAINTY ESTIMATES

The uncertainty estimates in the LDA measurements is presented below. At each measurement location, 10000 validated samples were acquired. To avoid errors due to spurious samples, samples outside the three standard deviations from the calculated means were first eliminated. A 95 percent confidence level is assumed in the uncertainty analysis and the variables of interest include the mean velocities, turbulence fluctuations and the Reynolds shear stress.

Based on the methodology outlined by Tachie (2001), the following relationships were used to estimate the uncertainty of various parameters:

$$\text{Streamwise mean velocity: } \frac{\sigma_U}{U} = \left[ (\sigma_o)^2 + \frac{1}{N} \left( \frac{u}{U} \right)^2 \right]^{1/2}$$

$$\text{Vertical mean velocity: } \frac{\sigma_V}{U} = \left[ (\sigma_o)^2 + \frac{1}{N} \left( \frac{v}{U} \right)^2 \right]^{1/2}$$

$$\text{Streamwise turbulence fluctuations: } \frac{\sigma_u}{u} = \left[ (\sigma_o)^2 \left( \frac{\langle uv \rangle}{u^2} \right)^2 + \frac{1}{2N} \right]^{1/2}$$

$$\text{Vertical turbulence fluctuations: } \frac{\sigma_v}{v} = \left[ (\sigma_o)^2 \left( \frac{\langle uv \rangle}{v^2} \right)^2 + \frac{1}{2N} \right]^{1/2}$$

$$\text{Reynolds shear stress: } \frac{\sigma_{\langle uv \rangle}}{\langle uv \rangle} = \left[ (\sigma_o)^2 \left( 1 + \frac{u^2}{\langle uv \rangle} \right)^2 + \frac{1}{N} \left( \frac{2}{R} \right)^2 \right]^{1/2}$$

Here,  $\sigma_o$  is the error due to uncertainty in the determination of the beam-crossing angle.

Following Tachie (2001), a value of 0.4 is considered for  $\sigma_o$ .  $N$  is the number of samples and  $R$  is the shear stress correlation coefficient.

Results of the calculation of uncertainty estimates for different bed conditions and at different distance from bed are shown in Tables A.1 to A.4. The maximum uncertainties in mean velocity, streamwise and vertical turbulence fluctuations and Reynolds shear stress are  $\pm 0.4$ ,  $\pm 7.0$ ,  $\pm 6.0$  and  $\pm 6.1$  percent, respectively.

Table A.1: Uncertainty estimates for tests over smooth bed

Bed	Distance from bed (mm)	U (%)	V (%)	u (%)	v (%)	<uv> (%)
Smooth $R_e \sim 47,500$	3	0.40	0.40	0.65	2.89	2.89
	15	0.40	0.40	0.75	4.11	4.10
	30	0.40	0.40	0.77	4.50	4.48
	50	0.40	0.40	2.08	1.61	1.74
	85	0.40	0.40	0.79	5.87	6.02
Smooth $R_e \sim 31,000$	3	0.40	0.40	0.41	3.47	3.41
	15	0.40	0.40	0.81	2.48	2.46
	30	0.40	0.40	0.66	2.04	2.01
	50	0.40	0.40	0.65	1.60	1.71
	85	0.40	0.40	0.91	1.43	1.57

Table A.2: Uncertainty estimates for tests over distributed roughness bed

Bed	Distance from bed (mm)	U (%)	V (%)	u (%)	v (%)	<uv> (%)
Distributed Roughness $R_e \sim 47,500$	15	0.40	0.40	1.69	3.70	3.69
	30	0.40	0.40	0.86	2.81	2.79
	50	0.40	0.40	0.75	2.03	2.03
	85	0.40	0.40	2.92	1.61	1.75
Distributed Roughness $R_e \sim 31,000$	3	0.40	0.40	6.97	2.06	2.05
	15	0.40	0.40	0.78	1.94	1.92
	30	0.40	0.40	0.98	5.70	5.65
	50	0.40	0.40	0.74	1.88	1.87
	85	0.40	0.40	0.73	3.48	3.64

Table A.3: Uncertainty estimates for tests over continuous roughness bed

Bed	Distance from bed (mm)	U (%)	V (%)	u (%)	v (%)	<uv> (%)
Continuous Roughness $R_e \sim 47,500$	3	0.40	0.40	1.13	2.62	2.61
	15	0.40	0.40	0.98	1.95	1.91
	30	0.40	0.40	0.90	3.32	4.88
	50	0.40	0.40	1.13	3.41	3.46
Continuous Roughness $R_e \sim 31,000$	3	0.40	0.40	0.88	2.22	2.18
	15	0.40	0.40	0.88	2.05	2.02
	30	0.40	0.40	0.68	2.07	2.03
	50	0.40	0.40	0.68	3.84	3.87

Table A.4: Uncertainty estimates for tests over natural sand bed

Bed	Distance from bed (mm)	U (%)	V (%)	u (%)	v (%)	<uv> (%)
Natural Sand Bed $R_e \sim 47,500$	3	0.40	0.40	2.49	2.57	2.53
	15	0.40	0.40	1.03	2.85	2.81
	30	0.40	0.40	0.94	2.52	2.48
	50	0.40	0.40	0.78	2.16	2.21
	85	0.40	0.40	0.85	1.61	1.77
Natural Sand Bed $R_e \sim 31,000$	3	0.40	0.40	0.98	2.62	2.58
	15	0.40	0.40	0.76	2.00	1.97
	30	0.40	0.40	1.50	2.17	2.13
	50	0.40	0.40	0.77	4.03	4.04
	85	0.40	0.40	1.63	1.43	1.59

## VITA AUCTORIS

**Name:** Md Abdullah Al Faruque

**Place of Birth:** Khulna, Bangladesh

**Year of Birth:** 1963

**Education:** Bangladesh University of Engineering and Technology (BUET)  
1981-1986 B.Sc in Civil Engineering  
University of Windsor, Canada  
2003-2004 M.A.Sc in Civil Engineering  
University of Windsor, Canada  
2004-2009 Ph.D. in Civil Engineering

**Awards:** Ontario graduate scholarship in science and technology (OGSST) –  
2008-2009  
Natural sciences and engineering research council (NSERC) – PGS  
D3 – 2005-2007  
Natural sciences and engineering research council (NSERC) –  
PGSM – 2004  
Ontario graduate scholarship (OGS) – 2004 (Declined)  
Ontario graduate scholarship (OGS) – 2005 (Declined)  
University of Windsor, Postgraduate Tuition Scholarship (2004,  
2005-2007)  
BUET, Bangladesh, 1<sup>st</sup> Grade Merit Scholarship (1982-1985)  
BUET, Bangladesh, Technical Scholarship (1981-1985)  
BUET, Bangladesh, Tuition Scholarship (1981-1985)

- Experience:**           **Lecturer** (2008 – to date)  
Civil Engineering Technology, Environmental Management & Safety, Rochester Institute of Technology, New York, USA
- Sessional lecturer & sessional instructor** (2004 – 2008)  
Department of Civil & Environmental Engineering, University of Windsor, Canada
- Consultant, Civil & Structural Engineer** (1996 – 2002)  
KTA Tenaga Sdn Bhd, Kuala Lumpur, Malaysia
- Design & Planning Engineer and Project Coordinator** (1986 – 1996)  
Beximco Engineering Ltd., Dhaka, Bangladesh and Kuala Lumpur, Malaysia
- Membership:**       Registered Professional Engineer (P.Eng), Ontario, Canada (PEO)  
Engineering in training (EIT), Michigan, USA

### **Publications/Reports**

#### **a) Papers in Refereed Journals**

- **Faruque, M.A.A.**, Sarathi, P. and Balachandar, R. (2006). “Clear water local scour by submerged three-dimensional wall jets: Effect of tailwater depth.” *ASCE Journal of Hydraulic Engineering*, 132(6), 575-580.
- Bey, A., **Faruque, M. A. A.**, and Balachandar, R. (2007). “Two dimensional scour hole problem: Role of fluid structures.” *ASCE Journal of Hydraulic Engineering*. 133(4), 414-430.
- Karki, R., **Faruque, M.A.A.** and Balachandar, R. (2007). “Local Scour by submerged offset jets.” *Water Management Journal, Proceedings of the Institution of Civil Engineers, Thomas Telford*, Vol. 160, Issue 3, pp. 169-179.
- Bey, A., **Faruque, M.A.A.** and Balachandar, R. (2008). “Effects of Varying Submergence and Channel Width on Local Scour by Plane Turbulent Wall Jets.” *Journal of Hydraulic Research*, 46(6), 764-776.

- Sui, J., **Faruque, M.A.A.** and Balachandar, R. (2008). “Influence of channel width and tailwater depth on local scour caused by square jets.” *Journal of Hydro-environment Research*, 2(1), 39-45.
- Sarathi, P., **Faruque, M.A.A.** and Balachandar, R. (2008). “Scour by submerged square wall jets at low densimetric Froude numbers.” *Journal of Hydraulic Research*, 46(2), 158-175.
- Afzal, B., **Faruque, M.A.A.** and Balachandar, R. (2009). “Effect of Reynolds number, near-wall perturbation and turbulence.” *Journal of Hydraulic Research*, 47(1), 66-81.
- Sui, J., **Faruque, M.A.A.** and Balachandar, R. (2009). “Local scour caused by submerged square jets under ice cover.” Submitted to the *Journal of Hydraulic Engineering*. **Accepted in August, 2008.**
- Singha, A., **Faruque, M.A.A.** and Balachandar, R. (2009). “Proper orthogonal decomposition analysis of flow structures of seepage effect in open channel flow.” Submitted to the *Journal of Fluids Engineering*.

#### **b) Papers in Conference Proceedings**

- **Faruque, M.A.A.**, Singha, A., Jiahao, T. and Balachandar, R. (2009). “Study on effect of seepage on rough open channel flow through proper orthogonal decomposition (POD).” *The 2009 Joint ASCE-ASME-SES Conference on Mechanics and Materials will be held from June 24<sup>th</sup> to June 27<sup>th</sup>, 2009, Blacksburg, VA, USA.*
- **Faruque, M.A.A.**, Afzal, B., Wolcott, S. and Balachandar, R. (2009). “The effect of the presence of higher background turbulence on smooth open-channel flows.” *22<sup>nd</sup> Canadian Congress of Applied Mechanics, will be held from May 31<sup>st</sup> to June 4<sup>th</sup>, 2009, Dalhousie University, Department of Mechanical Engineering, Halifax, Canada.*

- **Faruque, M.A.A.**, Afzal, B., Bolisetti, T. and Balachandar, R. (2008). “Effect of Reynolds number on smooth open-channel flows.” *2<sup>nd</sup> International Symposium on Shallow Flows, December 10-12, 2008, Hong Kong University of Science and Technology (HKUST), Hong Kong.*
- **Faruque, M.A.A.**, Sui, J., Bolisetti, T. and Balachandar, R. (2008). “Expansion ratio effects on scour by 3D jets.” *4<sup>th</sup> International Conference on Scour and Erosion, November 5-7, 2008, Tokyo, Japan.*
- **Faruque, M.A.A.**, Bey, A. and Balachandar, R. (2007). “Analysis of higher-order velocity moments in a two-dimensional scour hole.” *32<sup>nd</sup> Congress of IAHE, the International Association of Hydraulic Engineering & Research, July 1-6, 2007, Venice, Italy.*
- **Faruque, M.A.A.**, Sarathi, P. and Balachandar, R. (2007). “Scour by submerged square wall jets at low densimetric Froude numbers.” *32<sup>nd</sup> Congress of IAHE, the International Association of Hydraulic Engineering & Research, July 1-6, 2007, Venice, Italy.*
- **Faruque, M.A.A.**, Bey, A. and Balachandar, R. (2007). “Role of channel width and varying tailwater depth on the scour by a plane wall jet.” Paper ID, GC-046. *18th Canadian Hydrotechnical Conference and Symposium Honouring Professor Selim Yalin, August 22-24, 2007, Winnipeg, Manitoba.*
- **Faruque, M.A.A.**, Bey, A., Sui, J. and Balachandar, R. (2006). “Jet Scour: A Revisit of Two-Dimensional and Three-Dimensional Scour Problem.” *International Conference on Application of Fluid Mechanics in Industry and Environment, Organized by Physics and Applied Mathematics Unit, Indian Statistical Institute, Calcutta, August 28-31, 2006, India (Invited presentation).*
- **Faruque, M.A.A.**, Sarathi, P. and Balachandar, R. (2006). “Scour by submerged three-dimensional wall jets.” *Third International Conference on Scour and Erosion, November 1 – 3, 2006, Amsterdam Rai, Netherlands.*
- Bey, A., **Faruque, M.A.A.**, Balachandar, R. and Budkowska, B.B. (2006). “Role of fluid structures in a two-dimensional scour holes.” *Third International Conference on Scour and Erosion, November 1 – 3, 2006, Amsterdam Rai, Netherlands.*



- Sarathi, P., **Faruque, M.A.A.** and Balachandar, R. (2005). “Local scour by three-dimensional wall jets.” *17th Canadian Hydrotechnical Conference, August 17-19, 2005, Edmonton, Alberta, 647-654.*
- **Faruque, M.A.A.**, Sarathi, P. and Balachandar, R. (2004). “Transient local scour by submerged three-dimensional wall jets: Effect of tailwater depth.” Paper ID, 2P-03B-3. *Second International Conference on Scour and Erosion, November 14 - 17 2004, Meritus Mandarin, Singapore, 2, 309-316.*

**c) Technical Reports Relevant to the Academic Field**

- **Faruque, M.A.A.**, Machina, D.W., McCorquodale, J.A. and Balachandar, R. (2004). “Hydraulic model wave studies of open and closed cell cable concrete block mats.” Technical report for International Erosion Control Systems.